REPUBLIQUE DU CAMEROUN
Paix – Travail – Patrie
****
UNIVERSITE DE YAOUNDE I
Faculté des Sciences
DEPARTEMENT DE PHYSIQUE
****
DE MECANIQUE, MATERIAUX ET STRUCTURES

REPUBLIC OF CAMEROUN
Peace – Work – Fatherland
****
UNIVERSITY OF YAOUNDE I
Faculty of Science
DEPARTMENT OF PHYSICS
****
OF MECHANICS, MATERIALS AND STRUCTURES

Control and synchronization of a coupled network of mechanical structures

Thesis submitted and defended in partial fulfillment of the requirements for the awards of a Doctor of Philosophy (Ph. D) degree in Physics

Par : **MBA FEULEFACK Stève Cloriant**
Master of Science in Physics

Sous la direction de
NANA NBENDJO Blaise Roméo
Professor
University of Yaoundé I,
Cameroon
FILATRELLA Giovanni
Associate Professor
University of Sannio, Italy

Année Académique : 2021

UNIVERSITÉ DE YAOUNDÉ I
THE UNIVERSITY OF YAOUNDE I

FACULTÉ DES SCIENCES
FACULTY OF µSCIENCE

DÉPARTEMENT DE PHYSIQUE
DEPARTMENT OF PHYSICS

ATTESTATION DE CORRECTION DE LA THÈSE DE DOCTORAT/PhD

Nous, Professeur **ZEKENG Serge** et Professeur **TCHAWOUA Clément**, respectivement Examinateur et Président du jury de la Thèse de Doctorat/PhD de Monsieur **MBA FEULEFACK Stève Cloriant**, Matricule **08W0306**, préparée sous la direction du Professeur **NANA NBENDJO Blaise Roméo** et du Professeur **WOAFO Paul**, intitulée : « **Control and synchronization of a coupled network of mechanical structures**». soutenue le **Jeudi, 15 Avril 2021**, en vue de l'obtention du grade de Docteur/Ph.D en Physique, Spécialité **Mécanique, Matériaux et Structures,** Option **Mécanique Fondamentale et Systèmes complexes,** attestons que toutes les corrections demandées par le jury de soutenance ont été effectuées.

En foi de quoi, la présente attestation lui est délivrée pour servir et valoir ce que de droit.

Fait à Yaoundé le 29 APR 2021

Examinateur

Pr ZEKENG Serge

Le Chef de Département de Physique

Pr NDJAKA Jean-Marie Bienvenu

Le Président du jury

Pr TCHAWOUA Clément

University of Yaoundé I

Laboratory of Mechanics, Materials and Structures

Thesis

Submitted and defended for the award of

Doctorat/ PhD in Physics

Control and synchronization of a coupled network of mechanical structures

---

by

MBA FEULEFACK Stève Cloriant

Master in Physics

University of Yaoundé I

This thesis is accomplished under the guidance of

NANA NBENDJO	**FILATRELLA**	**WOAFO**
Blaise Roméo	**Giovanni**	**Paul**
Professor	Associate Professor	Professor
University of Yaoundé I	University of Sannio	University of Yaoundé I

Year 2021

Dedication

To my beloved family

Acknowledgments

This thesis is the result of an impassioned and baited work, not only during these years of doctoral work within the Laboratory of Modelling and Simulation in Engineering, Biomimetics and Prototypes (LaMSEBP), at the University of Yaoundé I, but also during my life. Numerous people have contributed to this achievement from my childhood to now. So, there is no better way to me of starting this thesis than by acknowledging their very important support and how grateful I am to them for being part of my life.

- First of all, I am deeply thankful to the **Almighty God**, for His Good gracious towards me.
- I would like to thank Professors **NANA NBENDJO Blaise Roméo** and **WOAFO Paul** for introducing me to the exciting field of nonlinear sciences. I also thank them for providing ideas, valuable help, and support by suggestions and questions regarding my research.
- I would also like to thank Professor **FILATRELLA Giovanni** for the valuable and fruitful exchanges. I have learnt a lot to him about throughout those discussions.
- Special thanks also go out to Professor **NDJAKA Jean-Marie Bienvenu**, Head of the Department of Physics, Faculty of Science, University of Yaoundé I and the teaching staff of his Department for their valuable teachings and their fruitful advices.
- I wish to express my acknowledgments to all the members of the public defence jury who have accepted to discuss and appreciate the results of this thesis, in spite of their numerous duties.
- I am very much in debt to Doctor **UCHECHUKWU Vincent**, for the fruitful collaboration which resulted in many important results for this thesis, for valuable discussions and advices. I hope that we will have more opportunities to share about others attractive scientific issues.
- I would like to thank all my lab elders and mates whose their various questions during my seminars presentations helped me to improve the quality of this document. Once more thank you Dr. **NANA Bonaventure**, Dr. **FOSSI Omer**, the late Dr. **MBOUSSI Aïssatou**, Dr. **SIMO Hervé**, Dr. **NDOUKOUO Ahoudou**, Dr. **TAKOUGANG Sifeu**, Dr. **NANHA Armand** , Dr. **ABOBDA Lejuste**, Dr. **NGUEUTEU Serge**, Dr. **TALLA MBE Jimmy**, Dr. **DJORWE Philippe**, Dr. **GOUNE Geraud**, Dr. **TALLA Francis**, Dr. **METSEBO Jules**, Dr. **NDEMANOU Buris**, Dr. **ANAGUE Lionel**, Dr. **TOKOUE Dianoré**, Dr. **NWAGOUM**

Peguy, Dr. **DONGMO Eric**, Dr. **CHAMGOUE André**, Dr. **NOTUE Arnaud**, Dr. **TCHAKUI Murielle**, Dr. **MAKOUO Lucienne**, Dr. **THEPI Raoul**,Dr. **SONFACK Hervé**, Dr. **FANKEM Raïssa**, Mr. **NGOUNOU Martial**, Mr. **KEMAJOU Issac**, Mr. **KOUEMOU Cédric**.

- Special thank to Professor **DONTSI**, and his wife Mrs. **DONTSI Charlotte**. They have always be there when I was on need of them. They cheerfully encouraged every achievement I made in my life and gave me very crucial advices in my progress.
- I would like to thank Mr. **NGNITEDEM Thierry** for invaluable support and encouragements. He has been there at a very complicated moment of my way and he brought all the support that I was in need.
- I am extremely thankful to my friends from that time ; the ones that grew up together with me. In particular, I thank my dearest and closest friends, Dr. **GHOMSI Nathalie**, Mrs. **TSANE Yolande**, Dr. **NOGNING Philémon**, Mr. **MINKENG Armel**, Mr. **MOUKO Aristide**, Mrs. **KOUDOM Sandra**, Mrs. **VOUKENG Sorele**, and I am also thankful towards each member of **ADAS (Association Des Amis Solidaires)**. If I have achieved so much so far, it has only been because you were always there for me.
- All those whose names have not been mentioned here, but who have contributed in one way or another to the success of this work should hereby receive my sincere gratitude.

Contents

Contents

Abstract

This thesis work deals with the analysis of a control strategy of a network of mechanical structures indirectly coupled through a dynamical environment. Mechanical structures are modelled assuming the Euler-Bernoulli formalism and the dynamic environment is an electrical circuit consisting of piezoelectric patches in parallel conformation with a load resistance.

By means of appropriate mathematical concepts (modal approximation, harmonic balance method, D-subdivision method) and numerical simulation methods (time series, phase portrait, amplitude response curves, bifurcation diagram, Fourier spectrum analysis, root mean square function and standard deviation function) , the dynamical behavior and the synchronization of the network of indirectly coupled mechanical structures are investigated.

The main results of this study show that the increase of the electromechanical coupling parameter leads to a strong reduction of vibration amplitude on a network constituted with only two indirectly coupled structures. An extension of the number of coupled structures allows to explore the occurrence of strong amplitude reduction (SAR) phenomenon and synchronization in the network. SAR phenomenon appears in this system when global synchronization of all beams takes place. The occurrence of global synchronization, which was preceded by dynamical clustering, is dependent on the size of the network as well as on the load resistance of the electrical circuit which indirectly interacts with all the beams. The results further show that the SAR state can be observed for relatively very weak coupling strength and large system-size. Finally, the effect of delay on a network is analyzed. Disturbance-induced by time-delay on the synchronization state and SAR state is also presented. It is conventionally known that delay induces insta-

bility in coupled systems, but we find here that this delay can also contribute to stabilize these systems by synchronizing them.

This work contributes to develop a control strategy which can be applied to the elements of structures of a skyscraper, lamellar structures of an aircraft, several foundations, several nearby bridges, several plates of a airplane or ship, metallic parallel floors, when those structures are subjected to an environmental excitation such as wind, moving loads, tsunami, or earthquake.

Keywords : Strong amplitude reduction, Synchronization, Clustering, Time delay effect, Euler-Bernoulli beam theory, Indirect coupling, Piezoelectric patches.

Résumé

Ce travail de thèse porte sur l'analyse d'une stratégie de contrôle d'un réseau de structures mécaniques couplées indirectement via un environnement dynamique. Les structures mécaniques sont modélisées selon le formalisme d'Euler-Bernoulli et l'environnement dynamique est un circuit électrique constitué de patchs piézoélectriques mis en parallèle avec une résistance de charge.

Au moyen des concepts mathématiques appropriés (approximation modale, méthode de la balance des harmoniques, méthode de D-subdivision) et des méthodes de simulation numérique (évolution temporelle, portrait de phase, courbes d'amplitude, diagramme de bifurcation, analyse du spectre de Fourier, fonction de la moyenne quadratique et fonction de l'écart type), le comportement dynamique et la synchronisation du réseau de structures mécaniques couplées indirectement sont étudiés.

Les principaux résultats de cette étude montrent que l'augmentation du paramètre de couplage électromécanique conduit à une forte réduction de l'amplitude de vibration sur un réseau constitué de seulement deux structures couplées indirectement. Une extension du nombre de structures couplées permet d'explorer l'apparition d'un phénomène de forte réduction d'amplitude et de synchronisation dans le réseau. Ce phénomène de forte réduction d'amplitude apparaît dans ce système lors de la synchronisation globale de toutes les poutres. L'apparition d'une synchronisation globale qui est précédée par un groupement dynamique en clusters, dépend de la taille du réseau ainsi que de la résistance de charge du circuit électrique qui interagit indirectement avec toutes les poutres. Les résultats montrent en outre que l'état de forte réduction d'amplitude peut être observé pour

une intensité de couplage relativement très faible et une taille de réseau de structures couplées importante. Enfin, l'effet du retard sur un réseau est analysé. Les perturbations induites par le retard sur l'état de synchronisation et l'état de forte réduction d'amplitude sont également présentées. On sait classiquement que le retard induit une instabilité dans les systèmes couplés, mais on constate ici que ce retard peut également contribuer à stabiliser ces systèmes en les synchronisant.

Ce travail contribue à développer une stratégie de contrôle qui peut être appliquée aux éléments de structures d'un gratte-ciel, aux structures lamellaires de la coque d'un aéronef, aux différents piliers d'un pont, à plusieurs ponts proches, à plusieurs plaques d'un avion ou d'un navire, à des plaques parallèles métalliques, lorsque ces structures sont soumises à une excitation environnementale telle que le vent, des charges mobiles, un tsunami ou un tremblement de terre.

Mots Clés : Forte réduction d'amplitude, Synchronisation, Groupement, Effet du retard, Théorie des poutres d'Euler-Bernoulli, Couplage indirect, Patchs piézoélectriques.

List of Abbreviations

AD : Amplitude Death
AC : Alternative current
DC : Direct Current
DOF : Degree Of Freedom
DDE : Delay Differential Equation
DVA : Dynamic Vibration Absorber
ER : Electro-Rheological
MR : Magneto-Rheological
MENS : Micro-ElectroMechanical Systems
NDT :Non-Destructive Testing
OD : Oscillation Death
ODE : Ordinary Differential Equation
PDE : Partial Differential Equation
RK4 : Fourth order Runge-Kutta
RMS : Root Mean Square
SAR : Strong Amplitude Reduction
SHM : Structural Health Monitoring
SMA : Shape Memory Alloys
SDOF : Single Degree Of Freedom
TLD : Tuned Liquid Damper
TLCD : Tuned Liquid Column Damper
TMD : Tuned Mass Damper

List of Figures

List of Figures

General Introduction

The evolution of techniques and means of construction leads humans being to embark on adventures of building structures, mega-structures as well as man-made devices much impressive than others. The current technological challenges call for the construction of lightweight and environmentally friendly structures, among others. These structures are subjected to various environmental stresses such as winds, moving loads, explosions, earthquakes, tsunamis, etc., which generate vibrations on them. Though less impressive, man-made devices also experienced vibrations expressing generally a malfunctioning. The problem posed by these vibrations remains very current in the scientific community and also in the industrial world. Indeed, vibrations can be a source of discomfort, noise, or disrupt the functioning of certain systems. Therefore vibrations induced by diverse sources are a particular type of pollution which can be heard as a noise if the frequencies that characterize the phenomenon lie within the audible range, or perceived directly as vibration. On the other hand, the presence of unwanted vibrations within both mechanical and civil structures is a handicap for them as they can lead to fatigue and, in the worst case, to the short- or long-term destruction of those structures. Indeed, many structural failures can be raised such as the famous Tacoma narrow bridge collapse on 1940 in United States due to dynamical interactions with the wind, or the Rana Plaza collapse which was a structural failure due to the weight and vibration of heavy machinery, and occurred on $24th$ April 2013 in Bangladesh, where an eight-story commercial and factory building named Rana Plaza collapsed. Such a catastrophic scenarios can lead to numerous losses in human life, as well as substantial material and economic damage. Researchers and engineers are therefore working hard to propose solutions to minimize or even eliminate the impact that these vibrations can have on structures. It should be noted that this problem of vibrations

on structures arises on a large scale ; among others we can list the field of civil engineering, mechanical engineering, aeronautics, automotive, on platforms on shore and offshore and many others.

In order to cope and to attain higher performance levels demanded in almost all dynamic systems under vibration control, many control techniques have been developed stretching from the basic solutions to more sophisticated ones depending of the technological stake and the base period. The most trivial technique is to transfer structure from a region where it is exposed to vibrations for another much healthier, but this technique is not easily feasible in tremendous cases. In a general manner, there are two main ways to solve the problem of vibrations : passive and active control methods. Passive control which is a traditional approach for reducing dynamic stressing by changing (usually increasing) of the mass, the stiffness or the damping of the structure with respect to the initial scheme in order to increase the damping effect. The modification may take the form of basic structural changes or the addition of 'passive' elements such as masses (which can be chunks of concrete), springs (such as vibration isolators), fluid dampers or damped rubbers. Passive control devices do not require any external energy supply. Whereas active control devices make used of an external source of power, aimed at supplying the control energy and modulated by the control system using the information supplied by the sensors. The energy source is used to drive active elements under control through the electromechanical, hydroelectric and electro-pneumatic actuators installed across the structure [1, 2, 3, 4].

Vibration analysis and control of dynamical systems is a fascinating topic for scientists and for engineers since vibrations occur in almost all real systems around us and they are commonly harmful. Thus, many works have been done in our research group dealing with the problems of vibrations ; numerous techniques and devices to reduce those vibrations on structures were presented. The present thesis is an extension of the previous ones to the case a network of mechanical structures coupled through a dynamical environment. Thus throughout this thesis, we intend to achieve the following objectives :

– Modelling a network of Euler's beams indirectly coupled via piezoelectric patches in parallel conformation, in order to induce an environmental coupling.
– Study the strong amplitude reduction phenomenon in the case of two and a network of indirectly coupled Euler's beams and the effect of the parameters of the system on the occurrence of this phenomenon.
– Analyze the effect of the time delay on the stability of the network of indirectly coupled Euler's beams and the occurrence of SAR phenomenon.
– The synchronization phenomenon both in the cases without and with time delay on the network of indirectly coupled Euler's beams is also highlighted.

The present work is therefore organized into three chapters. In ***chapter one***, we present a literature review on Euler's beams theory, vibration control techniques, complex network dynamics and the problem of the thesis is also stated a this level. ***Chapter two*** deals with the methodology, we describe the mathematical formalisms, numerical methods used to characterize the dynamical and synchronization states of the physical systems studied. ***Chapter three*** is devoted to the presentation and discussion of the results of mathematical analysis and numerical simulations. We end with a ***general conclusion*** where we summarize the main results obtained, and perspectives related to our future investigations are suggested.

CHAPITRE 1

LITERATURE REVIEW

1.1 Introduction

This chapter presents a non-exhaustive bibliographic review with regard to the subject of Euler-Bernoulli beam theory, vibrations as well as control techniques used to mitigate these vibrations. Flexible civil and mechanical systems experience undesirable vibrations in response to environmental and operational forces. The presence of those vibrations can limit the accuracy of sensitive instruments or cause significant errors in applications where high-precision positioning is essential. Then, the concept of complex networks will be introduced which includes the network topologies, application domains of networks, diverse dynamics exhibited by those networks and especially the amplitude death phenomenon.

1.2 Generalities on the Euler-Bernoulli beam theory

The Euler-Bernoulli beam model is one of the first mathematical descriptions of the motion of a vibrating beam.

During the mid-1700s, mechanical engineering was not considered a science, and it was not considered that the work of a mathematics academy could have practical applications, and the construction of bridges and buildings continued empirically. During this time, the Euler-Bernoulli model (also know as classical beam theory) was developed. Jacob Bernoulli first discovered that the curvature of an elastic beam at any point is proportional to the bending moment at that point. Daniel Bernoulli, nephew of Jacob, was the first one who formulated the differential equation governing the motion of a vibrating beam. Later, Jacob Bernoulli's theory was accepted by Leonhard Euler in his study of the shape of elastic beams

under various loading conditions [5].

Though, the Euler-Bernoulli model tends to slightly overestimate the natural frequencies, this theory is still commonly used because it is simple and provides reasonable engineering approximations for many problems.

Depending on boundary conditions, different types of equations modelling the dynamics of Euler's beams. Throughout this thesis, we are interested in the case of a beam articulated at both ends.

1.2.1 Boundary conditions

An element of structure is connected to the outside world by a certain number of links. Depending on the use of a structure, the beams and other elements of the structures constituting this one are connected at their ends in different configurations, which lead to rich dynamics.

The way the beam is supported translates into conditions on the function $w(L,t)$ and its derivatives. These conditions are collectively referred to as boundary conditions. It is a general mathematical principle that the number of boundary conditions necessary to determine a solution to a differential equation matches the order of the differential equation. Those conditions are necessary in order to reduce the partial differential equations to ordinary differential ones. There are thus several boundary conditions among which,

– **Hinged at both ends** : with the transversal displacement and the bending moment which are nulls at each end.

$$\begin{cases} w(0,t) = w(L,t) = 0 \\ \frac{\partial^2 w(0,t)}{\partial x^2} = \frac{\partial^2 w(L,t)}{\partial x^2} = 0 \end{cases} \tag{1}$$

– **Free at both ends** : with the bending moment and the shear force which are constrained to zero at both ends.

$$\begin{cases} \frac{\partial^2 w(0,t)}{\partial x^2} = \frac{\partial^2 w(L,t)}{\partial x^2} = 0 \\ \frac{\partial^3 w(0,t)}{\partial x^3} = \frac{\partial^3 w(L,t)}{\partial x^3} = 0 \end{cases} \tag{2}$$

– **Clamped at both ends** : with the transversal displacement and the slope which are nulls at each end.

$$\begin{cases} w(0,t) = \frac{\partial w(0,t)}{\partial x} = 0 \\ w(L,t) = \frac{\partial w(L,t)}{\partial x} = 0 \end{cases} \tag{3}$$

– **Cantilever beam** : defined by one end which is clamped and the other one is free, and the boundary conditions are as follows :

$$\begin{cases} w(0,t) = \frac{\partial w(0,t)}{\partial x} = 0 \\ \frac{\partial^2 w(L,t)}{\partial x^2} = \frac{\partial^3 w(L,t)}{\partial x^3} = 0 \end{cases} \tag{4}$$

1.2.2 Beams with supported ends

We first consider the nonlinear transverse vibrations of uniform beams supported in such a way as to restrict the movement at the ends and hence produce mid-plane stretching.

Let us consider an infinitesimal length of beam shows in figure 1, with ends label by M and N in the undeformed position and M' and N' in the deformed position. We limit our analysis in case the movement of the beam is in the plane ; this approximation is valid when the stresses inducing the lateral deformations have a privileged direction.

In order to establish the equations governing the dynamics of the beam, the dynamics of the beam is constrained in a two-dimensional reference frame having as base vector $\vec{i}$ and $\vec{j}$. Consider u and w as the longitudinal and transverse displacement respectively.

The displacement of M is given by

$$\overrightarrow{\Delta M} = \overrightarrow{MM'} = u(x,t)\,\vec{i} + w(x,t)\,\vec{j} \tag{5}$$

and the displacement of N is defined as

$$\overrightarrow{\Delta N} = \overrightarrow{NN'} = \left(u + \frac{\partial u}{\partial x}dx\right)\vec{i} + \left(w + \frac{\partial w}{\partial x}dx\right)\vec{j} \tag{6}$$

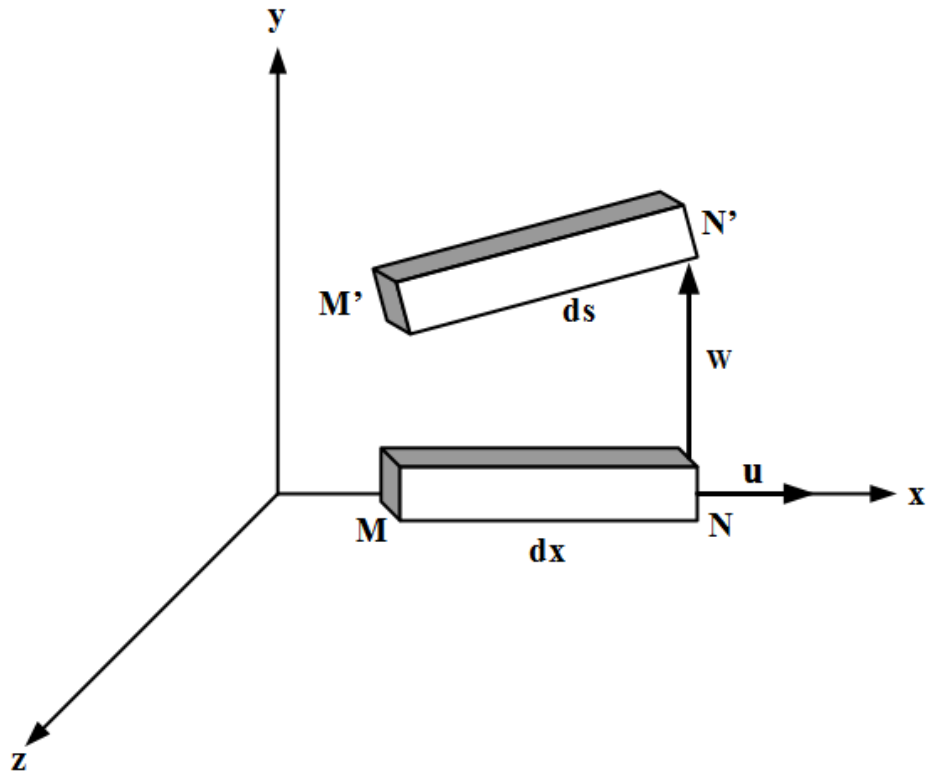

FIGURE 1 – *Element of beam in the deflected and undeflected positions*

It appears from figure 1 that,

$$\overrightarrow{\Delta M} + \overrightarrow{M'N'} = \overrightarrow{\Delta N} + dx\vec{i} \tag{7}$$

where $\overrightarrow{M'N'}$ is the vector giving the position N' relative to M'. The length of the deformed segment is defined as

$$\left|\overrightarrow{M'N'}\right| = ds = \left[\left(1+\frac{\partial u}{\partial x}\right)^2 + \left(\frac{\partial w}{\partial x}\right)^2\right]^{1/2} dx \tag{8}$$

and the unit vector parallel to the deformed segment is defined as

$$\vec{\delta} = \frac{\overrightarrow{M'N'}}{\left|\overrightarrow{M'N'}\right|} = \left[\left(1+\frac{\partial u}{\partial x}\right)\vec{i} + \left(\frac{\partial w}{\partial x}\right)\vec{j}\right]\frac{dx}{ds} \tag{9}$$

When the beam is in motion, its length changes and simultaneously the tension in the

beam also change. The instantaneous value of the tension is defined as

$$N = \frac{EA(ds - dx)}{dx} \tag{10}$$

where E and A are respectively the Young's modulus and the cross-sectional area in the rest.

The dynamical equation of motion resulting from the vibration of the element of beam is thus given as [6]

$$\begin{cases} m\frac{\partial^2 u}{\partial t^2} = \frac{\partial}{\partial x}\left(N\vec{\delta}\right)\vec{i} \\ m\frac{\partial^2 w}{\partial t^2} + \frac{\partial V}{\partial x} + \gamma\frac{\partial w}{\partial t} = \frac{\partial}{\partial x}\left(N\vec{\delta}\right)\vec{j} + f(t) \end{cases} \tag{11}$$

where $m = \rho A$ is the mass per unit of length, ρ is the mass density, $f(t)$ is the transversal load per unit of length applied to the beam and V is the shear force.

For a bending beam, the following relations exist between the shear force and the bending moment $V - \frac{\partial M}{\partial x} = 0$ and also between the bending moment and the deflection of the beam $M = EI\frac{\partial^2 w}{\partial x^2}$; where I is the moment of inertia. Thus, the set of equations (11) becomes,

$$\begin{cases} m\frac{\partial^2 u}{\partial t^2} = \frac{\partial}{\partial x}\left(N\vec{\delta}\right)\vec{i} \\ m\frac{\partial^2 w}{\partial t^2} + EI\frac{\partial^4 w}{\partial x^4} + \gamma\frac{\partial w}{\partial t} = \frac{\partial}{\partial x}\left(N\vec{\delta}\right)\vec{j} + f(t) \end{cases} \tag{12}$$

In modeling, we will limit ourselves to the first-order limited development of dx/ds, and we get

$$\frac{dx}{ds} = 1 - \frac{1}{2}\left(2\frac{\partial u}{\partial x} + \left(\frac{\partial u}{\partial x}\right)^2 + \left(\frac{\partial w}{\partial x}\right)^2\right) \tag{13}$$

Inserting equations (9), (10) and (13) in equation (12), we obtain

$$\begin{cases} m\frac{\partial^2 u}{\partial t^2} - EA\frac{\partial^2 u}{\partial x^2} = \frac{1}{2}EA\frac{\partial}{\partial x}\left(\left(\frac{\partial w}{\partial x}\right)^2 - 2\frac{\partial u}{\partial x}\left(\frac{\partial w}{\partial x}\right)^2\right) \\ m\frac{\partial^2 w}{\partial t^2} + EI\frac{\partial^4 w}{\partial x^4} + \gamma\frac{\partial w}{\partial t} = EA\frac{\partial}{\partial x}\left(e\frac{\partial w}{\partial x}\right) + f(t) \end{cases} \tag{14}$$

with

$$e = \frac{\partial u}{\partial x} - \left(\frac{\partial u}{\partial x}\right)^2 + \frac{1}{2}\left(\frac{\partial w}{\partial x}\right)^2 \tag{15}$$

In the set of equations (14) and (15), it appears the first, the second, the third and the fourth order of u resulting from the longitudinal motion of the beam. Here, only the first order approximation of u is considered. Due to the fact that the transversal displacement is more important than the longitudinal displacement. From this approximation, equation (15) becomes

$$e = \frac{\partial u}{\partial x} + \frac{1}{2}\left(\frac{\partial w}{\partial x}\right)^2. \tag{16}$$

Taking into account the fact that the radius of gyration r of the beam , the longitudinal inertial term is neglected in equation (14). Therefore $u = O\left(w^2\right)$, and after some simplifications, it becomes the following equation

$$e = \frac{1}{2l}\int_0^l \left(\frac{\partial w}{\partial x}\right)^2 dx \tag{17}$$

Inserting this expression in equation (14), the general equation governing the behaviour of the beam with articulated ends is given by

$$m\frac{\partial^2 w}{\partial t^2} + \gamma\frac{\partial w}{\partial t} + EI\frac{\partial^4 w}{\partial x^4} - EA\left[\frac{1}{2l}\int_0^l \left(\frac{\partial w}{\partial x}\right)^2 dx\right]\frac{\partial^2 w}{\partial x^2} = f(t) \tag{18}$$

1.3 An overview on vibration and control techniques

1.3.1 Effect of vibrations on human body

The interest granted by the community to the concept of vibration starts with the discovery of the first musical instruments (probably whistles and drums). From that moment, many works were carried out in order to better understand the physical phenomena and also establish mathematical properties proceeding from this concept [4].

Almost all human activities involve in vibrations in one form or others. Even our own bodies experience vibrations through the quasi-periodic motion of some organs and members which belong to them. For example, our vital functions are maintained by the beat at low frequencies of the heart or lungs when we are breathing, and we see because light waves undergo vibration. We hear because of vibrations at high frequencies of eardrums and we speak due to the oscillatory motion of larynges (tongue). We can also mention the fact that walking involves the oscillatory motion of hands and legs [7]. It should be noted that an exposure of the human body to certain intensities and frequency of vibrations can lead to irreversible damages of some organs. The effects that are felt also depend both on the exposure time and the part of the body exposed to vibrations. Thus, the standards and laws for the amount of vibration generates by any machineries or devices on service are increasingly stringent. The maximum root mean square (r.m.s.) values or peak values of acceleration that cause reduced proficiency when applied for a stated time in a vertical direction to a sitting subject are plotted as a function of frequency in figure 2. The figure, taken from the ISO 2631 – 1978 standard, deals with a field from 1 to 80 Hz and with daily exposure times from 1 min to 24 h. The exposure limits can be obtained by multiplying the values reported in figure 2 by 2, while the reduced comfort boundary is obtained by dividing the same values by 3.15 (i.e., by decreasing the r.m.s. value by 10 dB) [2].

An attempt to classify the different vibration frequencies on certain parts of the body has been done by R.E.D. Bishop [7] and the result of this classification is presented in figure 3. Note that there is a range of resonance frequencies for which each organ vibrates with a large amplitude. Thus, depending on individuals the resonance frequency of the thorax (abdomen) varies between 3-6 Hz.

1.3.2 Effect of vibrations on mechanical and civil structures

Progress involves the challenge of building structures, machines and other devices that are increasing lighter and more faster for machines. But the fact of lightening the elements which constitute these structures and machines that are mainly the beams, the plates, the shells among others, makes these more sensitive to the various stresses of their environ-

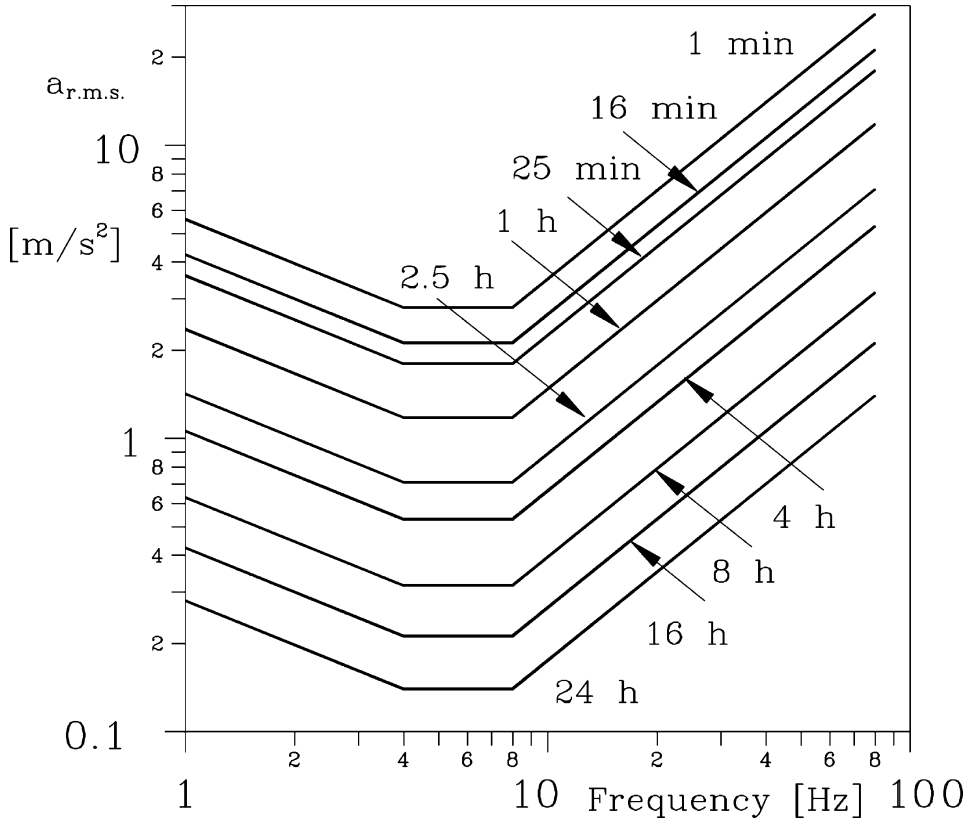

FIGURE 2 – *Vertical vibration exposure criteria curves defining the 'fatigue-decreased proficiency boundary' (ISO* 2631 – 1978 *standard).*

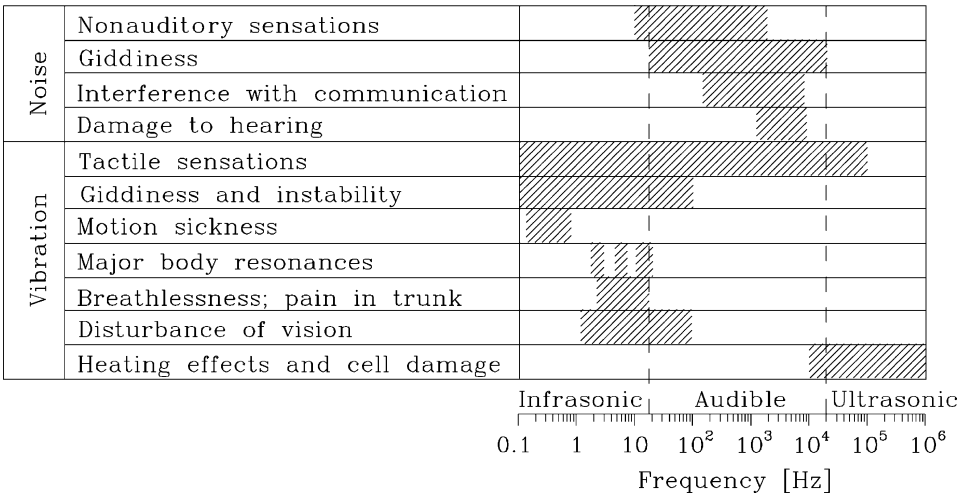

FIGURE 3 – *Effects of vibration and noise (intended as airborne vibration) on the human body as functions of frequency (R.E.D. Bishop, Vibration, Cambridge Univ. Press, Cambridge, 1979).*

ment (due to their high flexibility) and leads to give rise to nonlinear behaviors. As result, the presence of those vibrations will generate undesirable effects such as mechanical or

structural failure, frequent expensive maintenance of machines and discomfort for users.

The causes that can induce vibrations on a mechanical or civil structure are numerous. We can list among other things :

- Construction activities such as blasting,compaction of soil, and operation of heavy engines on the construction site induce ground and structure vibrations. Ground vibrations may affect adjacent or remote structures. Their effects range from nuisance to local population and disturbance of working conditions for sensitive devices, to diminution of structure serviceability and durability, which may induce damages on them [8].
- Basically, no civil engineering structures is safe from wind loading effects. Thus, wind-induced vibrations may affect structures as building, towers, pylons, suspension and cable-stayed bridges among others. Wind manifests itself in many forms such as gusts actions, buffeting, vortex shedding, galloping and so on. Wind-induced vibrations may strongly affect either the serviceability or the fatigue behaviour and safety of structures or both, depending on the type of structure [9].
- Machinery equipment permanently fixed at a place (which means all machinery, components or installations working continuously) can also induced structural vibrations. Machinery can affect many different parts of civil engineering structures such as foundations, pedestals or structural members (slabs and beams), and even whole buildings in several ways with quite different types of dynamic forces. Waves induced by machines may be transmitted into neighbouring buildings or adjacent rooms in the form of vibrations and special attention has to be paid to these problems [10].
- Vibrations induced by people may strongly affect the serviceability and, in rare cases, the fatigue behaviour and safety of structures. Most important vibrations are induced by rhythmical body motions such as walking, dancing, running, jumping, handclapping with body bouncing while standing among others. Structures affected by pedestrians are predominantly footbridges and floors in buildings, but there are similar problems associated with stairways and ship gangways [10].

1.3.3 Vibration control techniques

The quenching of vibrations has for long been a problem of primary importance in many engineering fields. In the past, the classic methods used to attain an acceptable level of vibration are pursued by increasing the stiffness and the mass of the structure with respect to the initial scheme in order to increase the damping effect.

Detection and control of unwanted vibrations are increasingly crucial in a range of engineering applications. The control devices are particularly used on structures such as aircraft, satellites, bridges, sports stadia and other tall/slender structures (earthquake- and wind-excited buildings), passive ship stabilizers, helicopters, power transmission lines, hand-held electric hair-clippers, etc. There are also applications in the areas of robotics, mechatronics, micro-electromechanical systems (MEMS) and non-destructive testing (NDT) and related disciplines such as structural health monitoring (SHM) [11, 3, 12]. Therefore there is a need to add control forces through specific devices to a vibrating system, that will oppose or resist external solicitations.

From these observations, numerous control techniques have been setted up both in the scientific community and in the industrial domain, in order to reduce the degree of nuisance of these vibrations.

a. Passive vibration control

Passive vibration controllers use either hydraulic or mechanic devices to mitigate the vibration of a structure. As hydraulic passive devices, Tuned Liquid Column Damper (TLCD) and Tuned Liquid Damper (TLD) can be listed.

A hydraulic form of the vibration control device was first proposed in 1883 [13] as a passive ship stabilizer to reduce the rolling motion of ships at sea, and was actually used in 1902. Tuned Liquid Column Damper (TLCD) was first proposed by Sakai et al. [14] ; it uses water-sloshing motion to mitigate the vibration [15, 16, 17]. In other words, the TLCD mitigates vibration energy by combined actions of involving the movement of the liquid mass in device container and a damping force generated by an orifice (Fig. 4 (a)). Tuned

Liquid Damper (TLD) uses a similar strategy to suppress dynamic responses (Fig. 4 (b)). Both dampers can work as a vibration absorber during a severe wind or an earthquake event, and furthermore, they can be used as a daily water supplier facility at the top of structure [16].

On other hand, mechanic passive devices work either by isolation or absorption. A vibration isolator consisted of a spring and viscous damper is placed between the mass and the excitation and try to minimise the transmission of a support excitation $f(t)$ to the structure (Fig. 4 (c)). Whereas a vibration absorber or Tuned Mass Damper (TMD) first proposed by Frahm in 1909 was consisted of a simple mass-spring-damper device attached to the main vibrating system [18], but the theoretical study was first presented by Ormondroyd and Den Hartog in 1928 [19]. It is based on simple idea of transferring the kinetic energy of the vibrating structure to a properly tuned and specially designed single d.o.f. oscillator, where it is dissipated (Fig. 4 (d)).

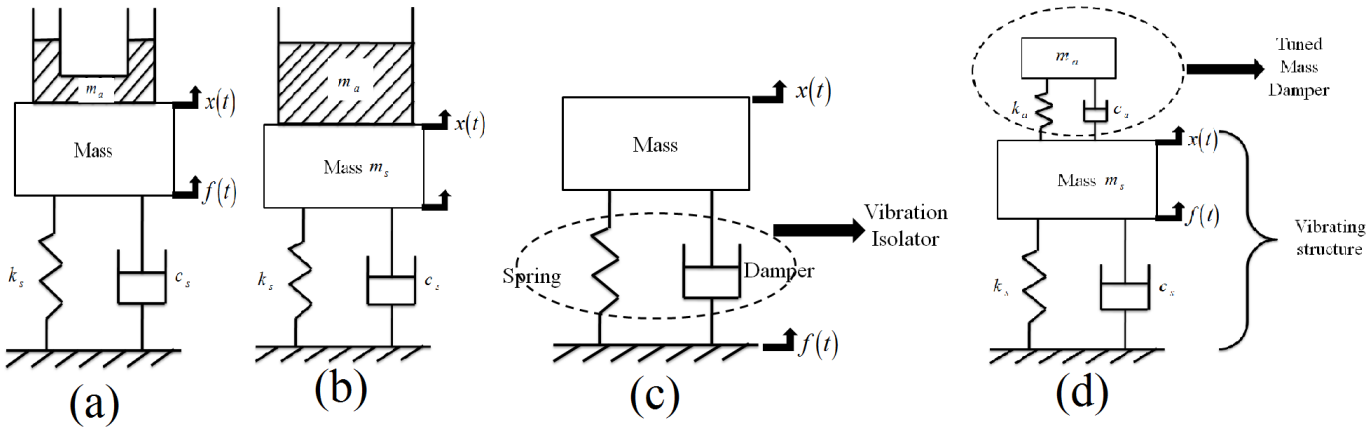

FIGURE 4 – *Schematic diagram of passive vibration control devices : (a) TLCD, (b) TLD, (c) vibration isolator and (d) vibration absorber.*

Depending on the application, it can also be called Dynamic Vibration Absorber (DVA). TMD systems have been installed on tall buildings and towers in the world, and their performances were considerably successful. Examples include the Citicorp Center in New York City, the John Hancock Building in Boston, Sydney tower in Sydney, Crystal Tower Building in Osaka and Taipei 101 building in Taiwan (Figure 5).

Passive devices act in many cases as dampers. For example, if a piezoelectric material

FIGURE 5 – *Dynamic Vibration Absorber (DVA) of the Taipei 101 building. The DVA consists of a pendulum with a mass of* 730 $tons$ *suspended with* 4 *cables extending over* 4 *floors.*

is simply shunted by a resistor, a sort of electric damper is obtained. And the same effect can be obtained with any other transducers. Thus, Nanha Djanan et al. [20] dealt with the enhancement of a passive electromechanical control of vibration on a thin plate submitted to non-ideal excitation. They used Routh-Hurwitz criteria to obtain the stability condition of the controlled system and some dynamics exploration leading to the condition for which the amplitude of vibration is reduced in the mechanical structure. Kitio Kwuimy et al. [21] investigated the dynamic and the electromechanical control of an Euler's beam. They found using the mode expansion formalism adequate electrical parameters to reduce the vibration amplitude, to control the snap through instability and horseshoe chaos. An extension of this work to the case of a plate has been done by Nwagoum et al. [22].

b. Active vibration control

Active control puts together sensors, actuators, controllers and power amplifiers (Fig. 6). Actuators are used to generate motion in a way that the vibration generated by external disturbances is cancelled (and so can put energy into the system), while sensors mounted

on the structure give information about the vibratory state of this one.

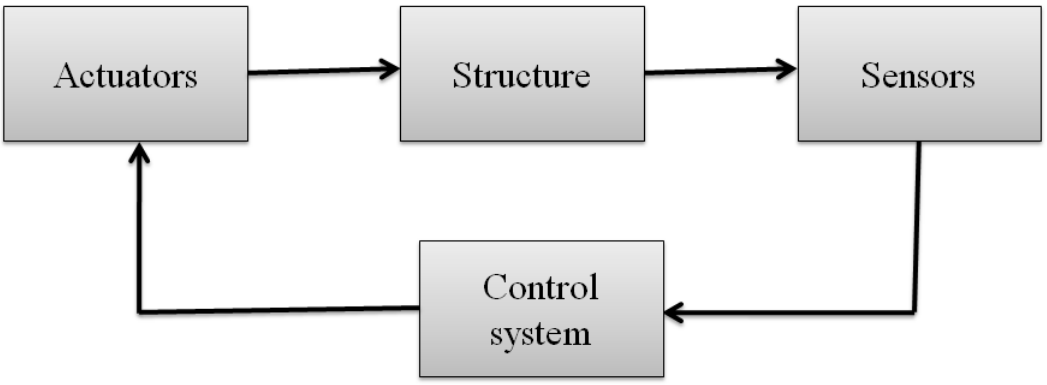

FIGURE 6 – *Block diagram of a smart structure.*

It is increasingly common for structures to integrate a set of actuators and sensors coupled by a controller, in order to cope with unwanted vibrations. These types of structures have become known as smart structures (sometimes called adaptive or intelligent structures). They often use new composite materials known as smart materials or multifunctional materials, because they can perform several tasks. For example, the same material can be used both as sensor or actuator according to the desired use. Piezoelectric, magnetostrictive, Magneto-Rheological (MR), Electro-Rheological (ER) materials and Shape Memory Alloys (SMA) are some examples of smart materials.

Nevertheless, not all active control devices use intelligent materials, so electromechanical transducers are also available. Thus, Nana Nbendjo [23] dealt with the control of a single non-linear Euler's beam using piezoelectric actuator, different voltage sources were considered. It has been shown that for some appropriate amplitude of alternative external voltage source, vibrations of the system can be damped. Nanha Djanan et al. [24] used a system with electric transducer to control the vibration of a beam supporting a DC motor (non-ideal system), through numerical and mathematical approach they showed that the system is found to present saturation phenomenon, leading to the effective control of vibration amplitudes of the mechanical structure.

c. Semi-active vibration control

The interest in semi-active control devices lies in the fact that these devices unlike active devices use much lower amounts of energy to supply the actuators. Indeed, semi-active controller can be broadly defined as a passive controller in which some parameters (stiffness, damper, etc.) can be varied with low cost energy. Another important difference between these two types of control is that the semi-active control can not add energy to the system, but only resists to vibrations (contrary to the active device), thus the system cannot be destabilised by a semi-active control. This type of control is therefore less vulnerable to power failure.

An example of a semi-active vibration control acting on single-degree-of-freedom (SDOF) oscillator constituted of a mass-spring-damper oscillator is shown in figure 7. To decide how to select the variable damping coefficient c_s, information is needed about the relative displacement of the mass and the input, this can be achieved by using sensors.

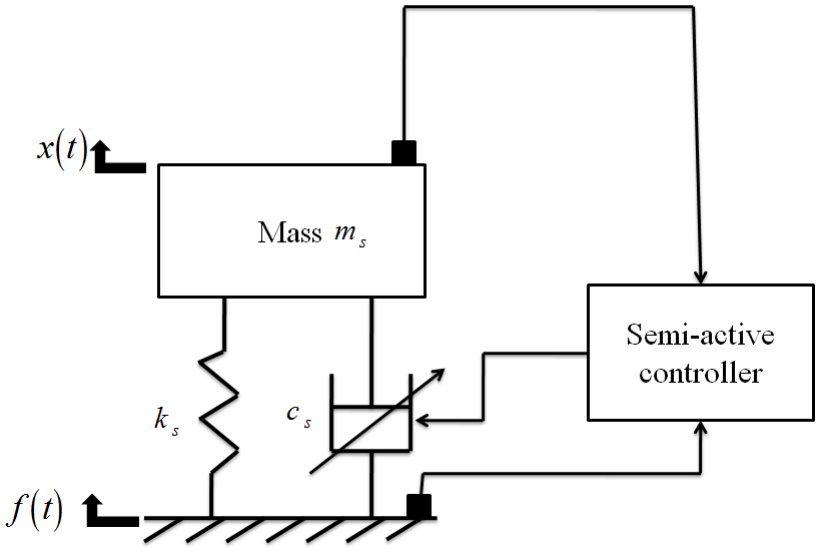

FIGURE 7 – *Semi-active vibration control acting on a SDOF oscillator.*

One of the best way to implement a semi-active element is to switch between a high and a low damping value. Usually, the high damping is selected when the damper force is resisting the direction of motion of the mass, and the low damping force is used when this is not the case. Practically, this can be achieved in various ways, for example one of the most com-

mon is by switching between high and low viscosity in a magneto-rheological (MR) damper [11]. Ndemanou et al. dealt with the control of dynamics of a cantilever Timoshenko beam subjected to earthquake loads using a MR damper. They also derived condition of stability of the controlled system using the Routh–Hurwitz criterion [25].

Nevertheless, vibration can exhibit useful features profitably in several industrial and domestic applications. For instance, vibration is put to work in oscillatory conveyors, hoppers, sieves, washing machines, compactors, shakers and mixers. Vibration has been found to improve the efficiency of certain machining, forging and welding process. Vibrating machines also find applications in medicine, curing human diseases. Another useful applications of vibration can be found in measuring tool like accelerometers, in vibratory testing materials and also in the field of energy harvesting [26, 27, 28, 29, 30].

1.3.4 Concept of piezoelectricity

As piezoelectric materials are mainly concerned in this thesis, a brief description of those materials is given in this subsection. A piezoelectric material is defined depending on the way we use it :

An electrical voltage is generated on a piezoelectric material when an external mechanical force is applied on it, this material experience the direct piezoelectric effect (Figure 8 (a)). In this case, the piezoelectric materials are usually used as sensors.

On other hand, when an electrical field parallel to the direction of polarization is applied to a piezoelectric material, it is deformed. This is called inverse piezoelectric effect (Figure 8 (b)). In this other case, the piezoelectric materials are used as actuators.

Piezoelectricity was discovered in 1880 by French physicists Jacques and Pierre Curie. However, The inverse effect was mathematically deduced from fundamental thermodynamic principles by Gabriel Lippmann in 1881. The first applications were for laboratory measuring devices (precision balance and charge generator using the direct and indirect piezoelectric effect, respectively) [31]. Nowadays, piezoelectricity is exploited in a number of useful applications, such as the production and detection of sound, piezoelectric ink-jet printing, piezoelectric motors, generation of high voltages, electronic frequency genera-

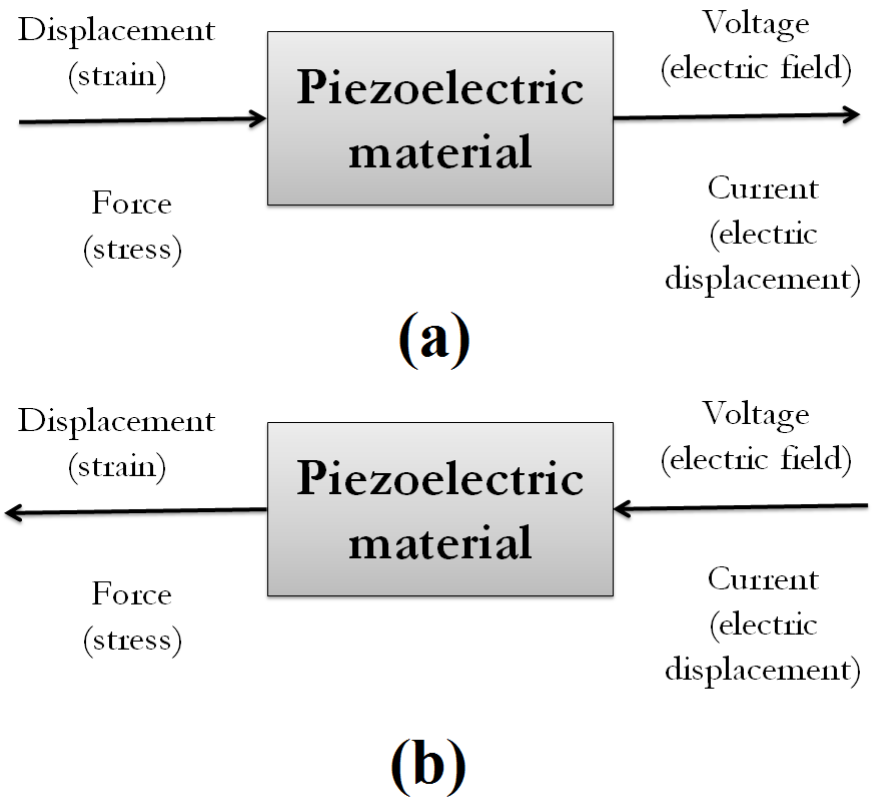

FIGURE 8 – *Block diagram of a piezoelectric principle : (a) direct piezoelectric effect, (b) inverse piezoelectric effect.*

tion, microbalances, to drive an ultrasonic nozzle, and ultrafine focusing of optical assemblies, energy harvesting [28, 32, 33, 34].

As far as the control of structures is concerned, piezoelectric materials have been enormously used since the last decades. It has been shown throughout the literature that piezoelectric materials can be used as passive, semi-active, active or hybrid electromechanical vibration absorbers when shunted by electrical networks. Note that piezoelectric active control was introduced in 1985 by Bailey et al. in order to actively damp the vibrations of distributed-parameter systems. They defined a piezoelectric actuator as distributed-parameter actuator [35]. Morgan et al. presented an efficient active-passive hybrid piezoelectric absorber concept. The control strategy developed by them was able to achieve high performance and were more robust than passive and semi-active absorbers [36, 37]. In another way, an analysis of divers shunt circuits employed in piezoelectric passive vibration

damping of an elastic structure has been done by Caruso. This study presented the optimal value of the electric components belonging to each shunt circuit and the performance of these shunts circuits has also be compared [38].

1.4 Complex network dynamics

The network science was introduced by the mathematician Leonhard Euler in 1741 through the Königsberg problem. He faced and solved the problem to know if it was possible to find a path that crosses each of the seven bridges of Königsberg once and only once. By describing the islands as nodes and the bridges as links connecting the nodes he found an abstract representation of the problem and laid the foundation of graph theory, the mathematical theory describing the structure of networks [39].

Since the introductive work of Euler, the network science has known an important growth in very different scientific domains with a large number of theories established to understand implied problems. Nowadays, the complex dynamics of interacting or coupled nonlinear systems have attracted great attention of researchers from various fields such as physics, chemistry, biology, economics, and social sciences [40]. The dynamics of many complex systems can be understood as the collective behavior of a large number of dynamical units coupled via their mutual interactions. The dynamical behavior of such connected systems has been an interesting topic of study especially due to its relevance in understanding a large variety of natural systems. The interaction between the subsystems may exhibit rich forms of emergent phenomena such as synchronization, hysteresis, phase locking, riddling, amplitude death, and oscillation death [41, 42, 43, 44]. As synchronization and oscillation quenching mainly are concerned in this thesis, a brief description of these phenomena is given in the subsections below.

In order to model and understand the phenomena resulting from the dynamical behaviors of a network of N coupled nonlinear oscillators, the dynamics on a network can

generally be described by a set of differential equations,

$$\dot{\mathbf{X}}_i = \mathbf{F}_i \left[\mathbf{X}_i \left(t\right), t\right] + \epsilon \mathbf{G}_i \left(\mathbf{X}\right) \qquad i = 1, \ldots, N. \tag{19}$$

where

$$\mathbf{G}_i \left(\mathbf{X}\right) = \sum_{j=1}^{N} \mathbf{A}_{ij} \mathbf{H}\left(\mathbf{X}_i, \mathbf{X}_j, \tau\right) \qquad i = 1, \ldots, N. \tag{20}$$

Here $\mathbf{X}_i$ represents m_i-dimensional vector of dynamical variables for the ith oscillator, and $\mathbf{F}_i$ the local dynamics which describes the uncoupled oscillator. ε is the coupling strength between the oscillators. The oscillators may be identical or distinct, and are coupled to the others, as specified via the coupling function $\mathbf{G}_i$. $\mathbf{A}$ is a matrix $(m \times m)$ with elements 0 and 1 and defines the components of the oscillators i and j that are coupled each other or not. The actual coupling is specified by the term $\mathbf{H}\left(\mathbf{X}_i, \mathbf{X}_j, \tau\right)$ which is a function of $\mathbf{X}_i \left(t\right)$ and $\mathbf{X}_j \left(t - \tau\right)$. The time-delay τ can be constant, discrete or distributed.

Based on the nature of interacting subsystems, they can be coupled mainly in two ways : direct or indirect coupling.

- **Direct coupling**

  It is known that when two systems are coupled directly, they can synchronize under suitable conditions. Different types of direct coupling configuration can be found in literature such as as diffusive, replacement, and synaptic couplings, etc.

  An example of a direct coupling is the linear and diffuse one, defined as

$$\dot{\mathbf{X}}_i = \mathbf{F}_i \left[\mathbf{X}_i \left(t\right), t\right] + \epsilon \sum_{j=1}^{N} \mathbf{A}_{ij} \mathbf{H}\left(\mathbf{X}_i - \mathbf{X}_j\right) \qquad i = 1, \ldots, N. \tag{21}$$

- **Indirect coupling via an environment**

  Often and throughout this thesis, it is assumed that the oscillators are coupled via a dynamical environment that possesses its own dynamics and which in turn is modulated by the interaction with the oscillators. In this case, the state of each element in the system influences the environment, and the state of the environment in turn affects the elements. Since the elements are not directly interacting with each other but through a common medium, this configuration has also been called environmental

coupling [45] or relay coupling [46] or bath coupling [47]. Indirectly coupled systems through an environment may exhibit a large variety of dynamical behaviors such as antisynchronization [49], non-trivial collective behavior, dynamical clustering [50] and amplitude death [51].

Consider a network of N nonlinear oscillators coupled indirectly through a dynamic environment. The dynamics of such systems coupled through an environment y is given as,

$$\dot{\mathbf{X}}_i = \mathbf{F}_i\left[\mathbf{X}_i\left(t\right), t\right] + \epsilon\gamma\mathbf{y} \tag{22a}$$

$$\dot{\mathbf{y}} = -\kappa\mathbf{y} - \frac{\epsilon}{N}\sum_{j=1}^{N}\gamma^T\mathbf{X}_j \tag{22b}$$

where the subscript $i = 1,\ldots,N$ in $\mathbf{X}_i$ and $\mathbf{F}_i$ represents ith oscillator. Here, ϵ is the coupling strength. The intrinsic dynamics of the environment decays with damping parameter κ in the absence of feedback from the nonlinear oscillators. The environment is kept active by feedback from coupled subsystems as given by the last term in Eq. (22b). Each subsystem also gets feedback from y [the last term in Eq. (22a)]. γ is a column matrix ($m \times 1$), with elements 0 or 1, and it decides the components of $\mathbf{X}_i$ that get feedback from the environment. γ^T is the transpose of γ and it decides the components of $\mathbf{X}_i$ that give feedback to the environment.

1.4.1 Synchronization phenomenon in networks

In 1665, the mathematician and physicist, Christiaan Huygens discovered an antiphase synchronization of two pendulum clocks suspended side by side of each other on the same beam. This was the beginning of nonlinear science and one of the first observations of the phenomenon of coupled harmonic oscillators, which has been since used to model various systems in nearly all branches of science. Synchronization has become a basic concept of

the interdisciplinary field of nonlinear and complex systems science [52, 53].

According to Pikovsky et al., synchronization can be simply understood as an adjustment of rhythms of oscillating objects due to their weak interaction[41]. Synchronization processes are ubiquitous in nature and play a very important role in technology. Many types of synchronization have been identified. Among them, it is worth mentioning complete synchronization, phase synchronization, antiphase synchronization, lag synchronization, anticipating synchronization, and generalized synchronization.

In biology and in neuroscience, networks are present at almost all scales and the synchronization is encountered at different levels. Indeed, synchronization is a crucial phenomenon in these domains and is an useful tool to understand the molecular interactions up to population dynamics, passing through biological systems. In neuroscience, applications are offered mainly at two different levels, one for the synchronization of individual spiking neurons and the other for the coupling between the cortical areas in the brain [52, 54, 55, 56].

In communication, synchronization is used to extract a message (between a transmitter and a receiver) from the mask. This demand in secure communication, especially in military applications, was one of the primary motivations for studying the synchronization of chaotic systems. The preliminary work of Pecora and Caroll simulated many researchers in developing new increasingly sophisticated methods to improve communication security [57, 58].

In electrical engineering, synchronization in power grids for example is necessary for a stable and robust operation, and failure may result in cascading power breakdown [59, 60, 61]. Another instance is the use of self-sustained oscillators to model a parallel operating system of microwave oscillators [30, 62].

In electromechanical engineering, a wide variety of electromechanical systems have been developed in order to optimize and increase the productivity of these systems. Thus several types of coupling (electrical, magnetic, piezoelectric and others) and electrical oscillators (both self-sustained and non-autonomous) have been experimented and this according to the objective [26, 63, 64, 65].

1.4.2 Oscillation quenching phenomena

In strong coupling regime of a network of dynamical systems, one of the major self-organized behaviors, oscillation quenching refers to a suppression of oscillation under various types of interaction or intentional control. This phenomenon was first observed by Rayleigh during the dynamical study of two organ pipes standing side by side. Rayleigh observed not only mutual synchronization between the two pipes when they began to sound in unison, but also the effect of quenching (oscillation death) when the coupling results in suppression of oscillations of interacting systems. Later, Bar-Eli [66] described this aspect in coupled chemical oscillators, and since then, this notable collective behavior has been extensively studied in theories and experiments.

Two kinds of oscillation quenching including amplitude death (AD) and oscillation death (OD) have been extensively studied in many real-world applications, such as vibration suppression in mechanical engineering [67, 68, 69, 70, 71], synthetic genetic networks [72, 73], and laser systems [74, 75]. Amplitude death corresponds to the case where the coupled oscillators arrive at a common stable steady state in autonomous networks. It has been shown that the occurrence of amplitude death in coupled nonlinear systems is highly dependent on both the characteristics of individual oscillators and the nature of coupling between oscillators. Early researches [76, 77, 78] deemed that amplitude death only occurred in mismatched oscillators under strong coupling. Further, Reddy et al. [79] reported that a transmission delay in the mutual connections could also induce amplitude death even if the subsystems are identical. Karnatak et al. [80] investigated the dynamics of oscillators that are mutually coupled by dissimilar (or conjugate) variables, where the systems are not coupled via same variables, and also found that AD could occur in identical oscillators even if there was no delay in the interaction. Another type of coupling-inducing amplitude death in the identical oscillators even in the absence of time delay is the dynamical coupling, which was first proposed by Konishi [81]. Resmi et al. in their work presented the appearance of amplitude death on a system of coupled oscillators through competing between the indirect or environmental coupling and diverse types of direct coupling as diffusive, re-

placement, and synaptic couplings [49]. Apart from the above linear coupling, Prasad et al. [82] found that a nonlinear coupling could arouse an amplitude death through the creation of new fixed point and the stabilization of the coupled systems, that in the absence of parameter mismatch or time delay. In addition to above-discussed scenarios which give rise to AD in nonlinear systems, there exist other strategies such as asymmetric coupling [83], through a linear augmentation of oscillatory dynamical system [84], attractive and repulsive coupling [85], and so on.

For non-autonomous coupled systems with external excitations, there is no equilibrium solution so that the concept of amplitude death state is modified [86]. So recently, Resmi et al. have introduced AD in non-autonomous coupled systems especially in two driven van der Pol systems with direct diffusive coupling and indirect coupling through an environment. In this case, amplitude death phenomenon is interpreted as the suppression of amplitude of oscillations of coupled systems at a very low value around their fixed point [49]. Further, a similar phenomenon is observed in Duffing systems with the same coupling form. Pisarchik investigated the occurrence of oscillation death phenomenon in coupled non-autonomous systems excited by a parametric excitation. The study was made theoretically with two Duffing oscilators, and a relation of the death effect with the Hopf bifurcation of the whole system and crisis of coexisting attractors are demonstrated[87]. Sekikawa et al. also reported the oscillation death in the Bonhoeffer–van der Pol oscillator under weak periodic perturbations [88]. Yamapi analyzed the dynamics of an electromechanical damping device, which consist of an electrical system coupled magnetically to a mechanical structure, and found quenching of vibration of mechanical part with appropriate coupling parameter [89]. Recently, Zhang et al. investigated the onset of the phenomenon of amplitude death for non-autonomous network model constituted of a number of floating modules serially coupled by flexible connectors. Playing on the strength of connectors, they obtained the state of amplitude death [67]. Further, Xu et al. investigated the analytical criterion for the boundary of the amplitude death by using the average method, with the same model configuration [86]. Though, non-autonomous systems extensively exist in physical, biological, and engineering systems in real life, studies for amplitude death in such systems

seem scarce and insufficient in comparison with the abundant results from autonomous systems.

Although most research reports on quenching phenomenon in coupled systems have been mainly focused on the suppression of the dynamics of two interacting oscillators using different coupling processes [49, 90] ; quenching of oscillations has been investigated in a large number of coupled robust-chaos oscillators [91], in which globally coupled systems exhibit amplitude death beyond a threshold of the coupling parameter. Moreover, the introduction of heterogeneity in the local parameters of coupled oscillators could drive the system to oscillation death state, with coexisting clusters of oscillators in different steady states. In addition, quenching phenomenon in a variety of network topologies such as global connection topology [92, 78] ; networks with complex topologies for instance small-world networks [93] ; the ring topology [94] ; scale-free networks [95] had been investigated and reported.

1.4.3 Delayed-network systems

In recent years, a great deal of interest has been devoted on exploring the complex behaviors generated from time delayed nonlinear oscillators. This great attention is due to the fact that delay is ubiquitous in a large number of dynamical systems and in different fields of application. It is well-known that in the presence of time delay can induce complex phenomena on certain simple systems which do not occur in its absence. This delay can influence either negatively or positively the stability and dynamics of a system. Therefore, time delay can alter the stability of an equilibrium point, gives birth to a limit cycle, leads to bifurcation, chaos [96, 97, 98, 99].

In the collective behaviour of real life systems, time delay is usually associated with finite propagation velocities of information signals, finite reaction times of chemicals, transportation of matter or information of electrical signals on transmission lines and so on. Time-delayed coupled dynamical oscillators can induce a large variety of dynamical phenomena such as synchronization, clustered chimera states, oscillation quenching and so on [41, 100].

In structural control engineering, it is particularly important to take into account the effect of the delay in the active control of structures because its origin and influence have been shown both theoretically and experimentally. Indeed, the delay can be generated either by the time interval between the detection of the vibration by the control device and the application of the force necessary to attenuate it, or the time taken to calculate the force necessary to quench the vibration [101, 102]. It seems therefore natural to include time delay in the modelling of mechanical and civil structures under control.

1.4.4 Networks on mechanical and civil structures

Putting together several elementary structures for the construction of a civil or mechanical structure can push during the modelling and the study of the stability of the final structure to consider this one as a network of elementary structures which can be coupled or not. This consideration can be justified through various structures as :

– ***A multi-module floating airport*** : The floating airport consists of a number of floating modules serially coupled by flexible connectors. The idea of building floating airport was born in the 1930s. It was abandoned at first and in the 1970s and 1980s that researchers and engineers launched the challenge to design technologies related to very large floating structures (VLFS). For the floating airport, each floating module can be viewed as an oscillator in waves, and by combining all the modules in a certain topological form with flexible connectors, the integrated system becomes a huge dynamic network. Due to mutual interaction among coupled oscillating modules, the collective behavior of coupled VLFS is of a great interest to scientists and engineers in developing a floating airport [67].

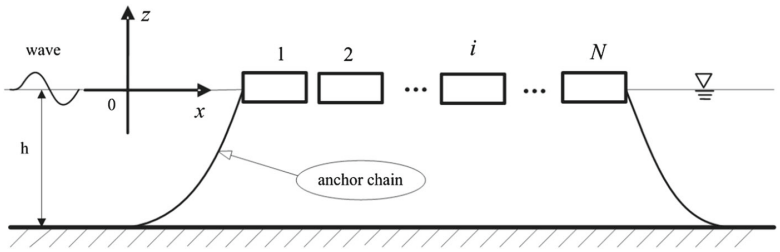

FIGURE 9 – *Model sketch for N serially connected floating modules [67].*

– ***Multi-floor buildings*** : The skeleton of a building made of concrete or with different types of aggregates consists essentially of beams and the different floors are separated by slabs that can be likened to plates. Indeed, Luongo and Zulli analysed the parametric, external and self-excited tower under turbulent wind flow. The tower was considered as a square section building, constituted by a multi story shear-type frame, subjected to unsteady wind flow, uniformly distributed all along its height. The cross-wind transversal displacement of the i-th story of the tower is materialized by $v_i(x)$ as show in the figure bellow

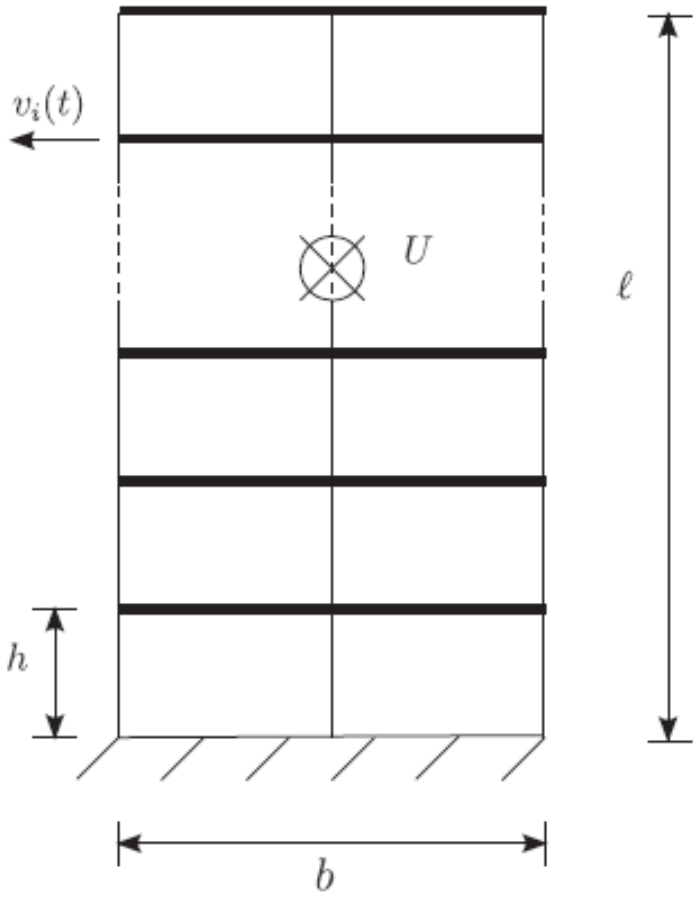

FIGURE 10 – *Frontal view of the tower subjected to the wind flow* [103].

These mechanical and civil structures are very often subjected to different types of external stresses such as the loads to bear, the weight of the structure, the weight of the snow, traffic, support reactions, etc. ; while their pieces are subject to internal forces from neighboring pieces. It is therefore essential to conceive, on the one hand, structures with the

capacity to support the loads applied to them without destroying or deforming them appreciably, and on the other hand to design vibration control devices that take into account the presence of different structural elements in some cases.

1.5 Problem of the thesis

Essential works on vibration control of various mechanical structures have been carried out in our research group and some of those works have been listed above. It should be noted that the theoretical control techniques used on those works deal with the problem of vibration reduction on idealized or isolated structures (beams, plates, etc). But it is necessary to note that the external action characterized by the different types of known forces can act on a structure or directly on the various structural elements. Thus, the approximation made when a structure is assumed ideal, can be harmful during the effective control of the structure as we do not know how the considered control strategy impacts the dynamic each structural element of the structure.

On other hand, in engineering applications, undesirable vibrations constitute a major concern in controlled structures. Persistent irregular vibrations can induce damage after a long time, which could lead to the reduction of the performance of the structures.

Taking inspiration from the phenomenon of amplitude death highlighted in the autonomous systems and more recently in the non-autonomous systems, we intent to solve the problem of quenching the vibrations on a network of mechanical structures indirectly coupled via a dynamical environment.

1.6 Conclusion

This chapter has given an overview on the generalities concerning the vibrations and the effects induced by those vibrations on civil and mechanical structures. Different control strategies used to mitigate those vibrations have been also presented. Then, an introduction to the complex network dynamics has been presented. Different network topologies

have been highlighted and the rich dynamic phenomena exhibited by those network have been discussed, especially the synchronization state and quenching of vibrations. The following chapter will be devoted to the description of mathematical tools used to model a network of coupled beams indirectly coupled via an dynamic environment. Analytical and numerical formalisms used to solve the problem of the thesis are presented.

CHAPITRE 2

METHODOLOGY : MATHEMATICAL FORMALISMS AND NUMERICAL METHODS

2.1 Introduction

This chapter presents the analytical and numerical methods used to solve the problem statement of the thesis. Section 2.2 deals with the mathematical formalisms and numerical simulation processes used to investigate the dynamical states resulting from ordinary differential equations as well as the hardware and software used. In section 2.3, the analysis tools used to characterize the dynamical states such as strong amplitude reduction and synchronization are presented. In section 2.4, whole mathematical models used to get different results of the thesis are presented. The conclusion of the chapter appears in section 2.5.

2.2 Mathematical formalisms and numerical methods

In order to propose solutions to the equations resulting from the modelling of the differential systems of this thesis, it is interesting to propose a set of mathematical and numerical methods allowing first to simplify the PDEs and to solve them afterwards.

2.2.1 Mathematical formalisms

In this subsection, different theories and mathematical methods used to propose solutions to the systems of differential equations of this thesis are stated.

a. Galerkin approximation for partial differential equations

Vibrations of continuous systems (strings, rods, beams, plates and shells) are governed by PDEs. Galerkin decomposition method is used to simplify the problems of vibrating structures through the reduction of the PDEs into ODEs [21, 104, 105].

Lets $w(x,t)$ describes the displacement of a structure at the time t and spatial location x. Any sufficiently smooth deflection field $w(x,t)$ satisfying any fixed boundary conditions can then be represented as a weighted sum of mode shapes :

$$w(x,t) = \sum_{n=1}^{N} q_n(t)\,\phi_n(x) \tag{23}$$

where N represents the number of modes used in the approximation, $q_n(t)$ represents the amplitude of vibrations of the structure associated with the nth mode and $\phi_n(x)$ represents the modal function solution of the $n-$th mode of the beam linear natural equation with the associated boundary conditions.

b. Harmonic balance method

Harmonic balance method is usually used to determine exact or approximate periodic solutions of ODEs (linear or nonlinear) subjected to sinusoidal periodic excitations [6, 106].

Consider the following differential equation :

$$\ddot{x} + x = f(x, \dot{x}, t) \tag{24}$$

where the dot over the x refers to the differentiation with respect to time t and the function f satisfies the following condition $f(x,\dot{x},t) = f(x,\dot{x},t+T)$.

The basic idea is to find the periodic solution of equation 24 in the form :

$$x = A\cos\left(\omega t + \varphi\right) \tag{25}$$

where A is the amplitude of oscillations, ω the pulsation of the sinusoidal excitation and φ the phase at the origin. Inserting equation 25 into equation 24 and equating separately

the coefficient of sine and cosine terms which have the same harmonics, one obtains after neglecting harmonics order greater than first harmonic, a system of algebraic equations which are the amplitude equations.

c. Linear stability of delay differential equations

The question of stability for delayed nonlinear equations near their steady-state solutions or fixed points is particularly important when the dynamical states of any system are investigated, as it is the case in this thesis. Indeed, the study of the stability makes possible to realize what happens if a system is disturbed slightly near an equilibrium condition.

– **Linearization near an equilibrium solution**

Let consider a set of autonomous DDEs of first order defined as [106]

$$\frac{d\mathbf{X}(t)}{dt} = \mathbf{H}\left[\mathbf{X}(t), \mathbf{X}(t-\tau), \alpha\right] \tag{26}$$

where $\mathbf{X}(t) = (x_1(t), x_2(t), \ldots, x_n(t))$ is the vector of n-dynamical variables of the system, $\mathbf{X}(t-\tau) = (x_1(t-\tau), x_2(t-\tau), \ldots, x_n(t-\tau))$ is the delayed vector of n-dynamical variables, $\mathbf{H} = (h_1(t), h_2(t), \ldots, h_n(t))$ is a n-dimensional vectorial function and $\alpha = (\alpha_1, \alpha_2, \ldots, \alpha_p)$ is a set of control parameters of the system.

Let us denote an equilibrium point $\mathbf{X}_0$ and consider small variations $\delta\mathbf{X}$ of the system around this equilibrium point, defined by

$$\mathbf{X}(t) = \mathbf{X}_0 + \delta\mathbf{X}(t) \tag{27}$$

Substituting Eq. 27 into 26 and expanding this equation in a Taylor series about $\mathbf{X}_0$, and discarding terms of order higher than the first in the $\delta\mathbf{X}$'s leads to the variational equation

$$\frac{d\delta\mathbf{X}(t)}{dt} = \mathbf{J}_0(\alpha)\,\delta\mathbf{X}(t) + \mathbf{J}_1(\alpha)\,\delta\mathbf{X}(t-\tau) \tag{28}$$

where $\mathbf{J}_0$ and $\mathbf{J}_1$ are matrix $(n \times n)$ of partial derivatives at the equilibrium point $\mathbf{X}_0$ and are called Jacobian matrix.

– **D-subdivision algorithm**

The eigenvalues of the linear set of the equations 28 can be found from the characteristic equation of the system. In that case, the characteristic equation becomes

$$G(s;\alpha) = \det\left(s\mathbf{I} - \mathbf{J}_0(\alpha) - \mathbf{J}_1(\alpha)\, e^{-s\tau}\right) \tag{29}$$

where $\mathbf{I}$ is the unit matrix and s are the eigenvalues of the system 29 and roots of the characteristic equation.

The algorithm of the D-subdivision method can be summarized as follows [107] :

1. First, solve the equation

$$G\left(j\omega;\alpha\right) = 0 \tag{30}$$

for s as a function of $j\omega$ (including the origin of the complex plane) in order to find (stability crossing) surfaces in the parameter space $\mathbb{R}^{n_p}$ such that for each s on such a surface, there exists at least one characteristic root on the imaginary axis.

2. Second, these surfaces divide the parameter space into several regions and sometimes it is possible to conclude, by using appropriate additional arguments, for which region the stability is guaranteed. As additional arguments, we can find, for example, a particular point (on some of the axis of the parameter space) for which the stability analysis becomes easier to perform (finite-dimensional systems, eventually). Each region derived in this way is characterized by the same number of strictly unstable characteristic roots for all the points of the corresponding domain.

2.2.2 Numerical methods

Numerical analysis deals with many problems of physical, biological, technological sciences or problems resulting from economic and social models. It is involved in the deve-

lopment of computer codes (meteorology, particle physics, etc.), but also in the problems of simulations (aeronautics, nuclear industry, etc.) or mathematical experiments. It has close links with computer sciences. His methods are based both on the search for exact solutions as in the case of matrix analysis or algebraic calculus, on approximate solutions that most often result from discretization processes as in the treatment of differential equations [108].

The following subsections give a non-exhaustive description of numerical methods and tools used to solve some problems throughout this thesis.

a. Fourth-order Runge-Kutta method for ordinary differential equations

In numerical analysis, Runge-Kutta methods are an important family of implicit and explicit iterative methods for approximating solutions of Ordinary Differential Equations (ODEs). These techniques were developed in the 1901s by German mathematicians Carle Runge and Martin W. Kutta, and modernized in 1960 by John Butcher.

Let us consider a vectorial variable $\mathbf{X}(t) = (x_1(t), x_2(t), ..., x_n(t))$ with $n-$dimensional vectorial flow $\mathbf{F} = (F_1, F_2, ..., F_n)$, the ODE can be written as

$$\frac{d\mathbf{X}(t)}{dt} = \mathbf{F}(t, \mathbf{X}(t)) \quad \text{with} \quad \mathbf{X}(t_0) = \mathbf{X}_0 \,. \tag{31}$$

The fourth order Runge-Kutta (RK4) iterative scheme for the case of Eq. (31) can be given by [109, 110]

$$\begin{aligned} x_{i+1,j} &= x_{i,j} + h\left(L_{1,j} + 2L_{2,j} + 2L_{3,j} + L_{4,j}\right)/6 \\ t &= t + h\,, \end{aligned} \tag{32}$$

where

$$\begin{aligned} L_{1,j} &= \mathbf{F}(t_i, x_{i,j}) \\ L_{2,j} &= \mathbf{F}(t_i + h/2, x_{i,j} + hL_{1,j}/2) \\ L_{3,j} &= \mathbf{F}(t_i + h/2, x_{i,j} + hL_{2,j}/2) \\ L_{4,j} &= \mathbf{F}(t_i + h, x_{i,j} + hL_{3,j}), \end{aligned} \tag{33}$$

where i represents the time incrementation and j labels the variables related to x_j. $L_{1,j}$, $L_{2,j}$, $L_{3,j}$, $L_{4,j}$ are intermediate variables and h represents the time step.

b. Fourth-order Runge-Kutta method for delay differential equations

In the case of delay differential equations (DDEs), the dynamical state of a system at each time t depends both on the value of the vector of n-dynamical variables $\mathbf{X}$ at time t, and also on the value of $\mathbf{X}$ at a prior time $t-\tau$, with $\tau > 0$ [111, 112]. Taking into account the delayed variable $\mathbf{X}(t-\tau) = (x_1(t-\tau), x_2(t-\tau), ..., x_n(t-\tau))$ with $n-$dimensional vectorial flow $\mathbf{F} = (F_1, F_2, ..., F_n)$, a DDE can be written as

$$\begin{aligned} \frac{d\mathbf{X}(t)}{dt} &= \mathbf{F}(t, \mathbf{X}(t), \mathbf{X}(t-\tau)) \\ \text{with } \mathbf{X}(t) &= \mathbf{f}(t) \text{ for } t \in [-\tau, 0], \end{aligned} \tag{34}$$

where $\mathbf{f}$ is a $n-$dimensional vector which depends of the time t, $\mathbf{X}(t) = [x_1(t), x_2(t), ..., x_n(t)]$ and $\mathbf{X}(t-\tau) = (x_1(t-\tau), x_2(t-\tau), ..., x_n(t-\tau))$ are unknown vectorial variables. At the difference of ODEs where the initial conditions were given by a discrete and finite set of value, initial conditions in DDEs should be indicated (through the use of a function) for all the values contained into the continuous interval $[-\tau, 0]$, so an infinity of values should be known to characterize the system. The RK4 iterative scheme for the case DDEs defined by Eq. (34) can be given by

$$
\begin{aligned}
x_{i+1,j} &= x_{i,j} + h\left(L_{1,j} + 2L_{2,j} + 2L_{3,j} + L_{4,j}\right)/6 \\
t &= t + h\,,
\end{aligned}
\tag{35}
$$

where

$$
\begin{aligned}
L_{1,j} &= \mathbf{F}(t_i, x_{\tau,i,j}, x_{i,j}) \\
L_{2,j} &= \mathbf{F}(t_i + h/2, x_{\tau,i,j}, x_{i,j} + hL_{1,j}/2) \\
L_{3,j} &= \mathbf{F}(t_i + h/2, x_{\tau,i,j}, x_{i,j} + hL_{2,j}/2) \\
L_{4,j} &= \mathbf{F}(t_i + h, x_{\tau,i,j}, x_{i,j} + hL_{3,j})\,,
\end{aligned}
\tag{36}
$$

where i represents the time incrementation and j labels the variables related to x_j. $L_{1,j}$, $L_{2,j}$, $L_{3,j}$, $L_{4,j}$ are intermediate variables and h represents the time step.

c. Hardware and software

Throughout this thesis, we used a Laptop having Window 7 as operating system. For mathematical expansions and numerical simulations, the following software were used : Matlab, Fortran and Maple. These software are enormously used in scientific research and engineering.

2.3 Numerical techniques for the characterization of the dynamical and synchronization states of nonlinear systems

There are many differential equations, especially nonlinear ones, that are not susceptible to be solved analytically in any reasonably convenient manner. Numerical methods provide one means of dealing with these equations. In this section, some numerical techniques allow to a qualitative understanding of the solutions rather than to detailed quantitative informations.

2.3.1 Tools for the characterization of the dynamical states

a. Phase portrait

A phase portrait is a geometric representation of the trajectories of a dynamic system in the phase space : at each set of initial conditions corresponds a curve or a point. Phase portraits are a valuable tool for the study of dynamical systems, they consist of a set of standard trajectories in the state space. This makes it possible to characterize the presence of an attractor, a repellor or a limit cycle for the chosen parameter values. However the drawback of this computational tool is that it can be sometimes hard to distinguish the quasi-periodicity and chaos phenomena by using the phase portrait diagram.

b. Fourier spectrum analysis of nonlinear equations

This method is a traditional tool for decomposing both periodic and non-periodic motions into an infinite number of harmonic functions. It has the distinguishing characteristic of generating a periodic approximations.

If $y(t)$ represents the response of some system as a function of time, $Y(\omega)$ is a spectral function that measures the amount of frequency ω making up this response. By sampling a nonperiodic function at N times (for functions that are known only for a finite number of times t_k), we can determine N values of the Fourier transform of this function (N independent $y(t)$ values can produce N independent $Y(\omega)$ values).

Assuming that the function $y(t)$ we wish to transform is measured or sampled at a discrete number $N+1$ of times (N time intervals)

$$y_k = y(t_k) \quad \text{for} \quad t_k = kh \quad \text{with} \quad k = 0, 1, 2, \ldots, N. \tag{37}$$

The discrete Fourier transform is evaluated from the Fourier transform and is obtained

after applying a trapezoid rule. It is defined as

$$Y(\omega_n) = \frac{1}{\sqrt{2\pi}} \int_{-\infty}^{\infty} e^{-i\omega_n t} y(t)\, dt = \frac{h}{\sqrt{2\pi}} \sum_{k=1}^{N} e^{-i\frac{2\pi kn}{N}} y_k \tag{38}$$

The Fourier spectrum analysis gives the relative strengths of various frequency components of a time series.

c. Bifurcation diagram

Bifurcations are important scientifically, they provide models of transitions and instabilities as some control parameter is varied [110].The dynamical behavior of a system can change qualitatively as the control parameters are varied. In particular, fixed points can be created or destroyed, or their stability can change. If the phase portrait changes its topological structure as a parameter is varied, we say that a bifurcation has occurred. The bifurcation diagram is plotted by computing time series of a dynamical variable for different value of the control parameter and by saving the consecutive maxima of the variable. Thus, bifurcation diagram is helpful to understand how the long term behavior of a model changes as parameter values change. Bifurcation diagram is very important for the study of the route to chaos. This diagram is also a helpful tool to identify different dynamical transitions such as the steady states, periodic and/or quasi-periodic orbits, or chaotic attractors.

2.3.2 Tools for the characterization of the synchronization state

a. Root mean square function

The root mean square value of a set of values (or a continuous-time waveform) is the square root of the arithmetic mean of the squares of the values, or the square of the function that defines the continuous waveform.

For a discrete set of values $(x_1(t), x_2(t), \ldots, x_N(t))$ defining the dynamical states of dif-

ferent variables, the RMS at a time t is described as follows

$$\eta(t) = \left[\frac{1}{N} \sum_{i=1}^{N} x_i(t)^2 \right]^{1/2} \tag{39}$$

The synchronization state is numerically characterized by the asymptotic time-average $\langle \eta \rangle$ of the instantaneous root-mean-square function $\eta(t)$ of the distribution of state variables $x_i(t)$ with $i = 0, 1, \ldots, N$.

Global synchronization for a system of coupled dynamical variables $x_i(t)$ which describes the collective dynamics is attained when $\langle \eta \rangle = 0$.

b. Standard deviation function

The standard deviation is a quantity whose invention goes back to the nineteenth century period when statistics were developed in the United Kingdom. Abraham de Moivre is credited with discovering the concept of measure of dispersion that appears in his book "The Doctrine of Chances" in 1718. But the term standard deviation has been used to the first time by Karl Pearson in 1893 in front of the Royal Society.

For a discrete set of values $(x_1(t), x_2(t), \ldots, x_N(t))$ defining the dynamical states of different variables, the standard deviation at a time t is given the following expression

$$\sigma(t) = \left[\frac{1}{N} \sum_{i=1}^{N} (x_i(t) - \bar{x}(t))^2 \right]^{1/2} \tag{40}$$

with the mean value $\bar{x}(t)$ defined as

$$\bar{x}(t) = \frac{1}{N} \sum_{i=1}^{N} x_i(t) \tag{41}$$

The occurrence of stable synchronization in a network of coupled systems can be numerically characterized by the asymptotic time-average $\langle \sigma \rangle$ of the instantaneous standard deviations of the distribution of state variables $x_i(t)$ with $i = 0, 1, \ldots, N$.

Global synchronization for a system of coupled dynamical variables $x_i(t)$ which describes a collective dynamic of the system, corresponds to the value $\langle \sigma \rangle = 0$.

A relationship exists between the RMS and a standard deviation and can be defined as

$$\eta(t)^2 = \bar{x}(t)^2 + \sigma(t)^2 \tag{42}$$

2.4 Nonlinear modelling of the network of indirectly coupled mechanical structures

2.4.1 Model description of a system of two indirectly coupled structures

a. Description of the system

Figure 11 presents a system of two hinged-hinged Euler's beams coupled indirectly through piezoelectric patches. The piezoelectric patches are laminated on both sides of each beam ; and they are all mounted together in parallel with a load resistance and a current source.

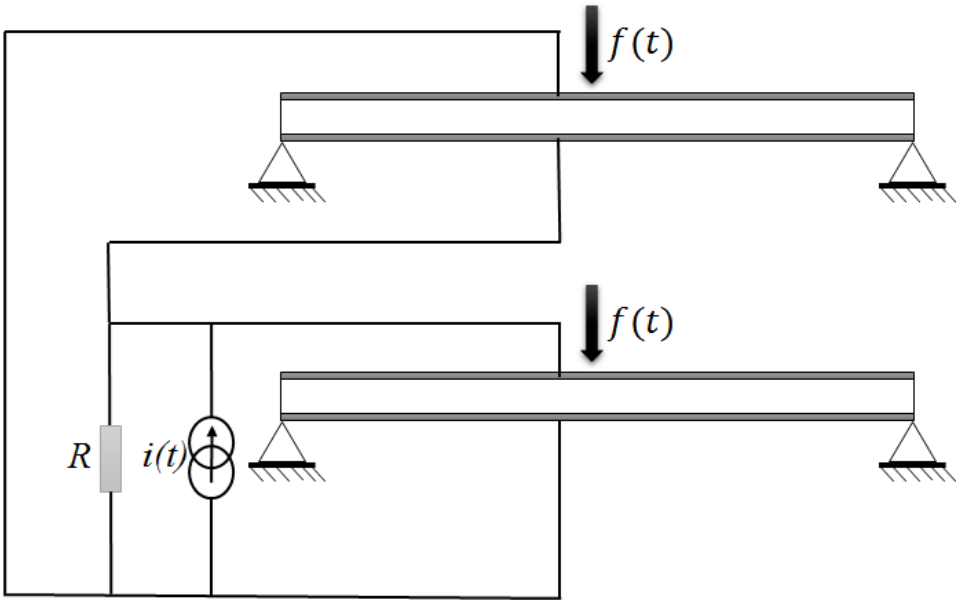

FIGURE 11 – *Schematic of two hinged-hinged beams indirectly coupled through a dynamic environment constituted of piezoelectric patches (Dark grey colour) in parallel conformation with a load resistance and a current source.*

In this coupling configuration, the electrical part is kept active by feedback from the

vibrations of each beam and simultaneously, the state of electrical part influences or regulates the dynamics of each beam. This kind of coupling configuration is particularly important in modern research of coupled oscillators, and it is known in the literature as indirect coupling [51] or environmental coupling [45] or relay coupling [46] or bath coupling [47]. In a such configuration, the mechanical energy is converted to an electrical one through the piezoelectric transduction principle and this electrical energy is dissipated through the load resistance.

The mechanical part of the system is constituted of two isotropic, uniform and flexible Euler's beams of length l with a cross section area A, and those beams are excited by a common external load $f(t)$ with an amplitude f_0 and an external frequency ω. Applying both the mechanical and the Kirchhoff's laws, the equations of motion of the mechanical and electrical parts are modelled as follows :

$$m_1\frac{\partial^2 w_1}{\partial t^2}+\delta\frac{\partial w_1}{\partial t}+EI\frac{\partial^4 w_1}{\partial x^4}-EA\left[\frac{1}{2l}\int_0^l\left(\frac{\partial w_1}{\partial x}\right)^2 dx\right]\frac{\partial^2 w_1}{\partial x^2} +\tilde{\alpha}v(t)=f_0\cos\omega t \tag{43a}$$

$$m_2\frac{\partial^2 w_2}{\partial t^2}+\delta\frac{\partial w_2}{\partial t}+EI\frac{\partial^4 w_2}{\partial x^4}-EA\left[\frac{1}{2l}\int_0^l\left(\frac{\partial w_2}{\partial x}\right)^2 dx\right]\frac{\partial^2 w_2}{\partial x^2} +\tilde{\alpha}v(t)=f_0\cos\omega t \tag{43b}$$

$$C_p\frac{dv}{dt}+\frac{v}{R}=-\tilde{\alpha}\int_0^l\left(\frac{\partial^3 w_1}{\partial x^2\partial t}+\frac{\partial^3 w_2}{\partial x^2\partial t}\right)dx+i(t) \tag{43c}$$

where $w_i(x,t)$ represents the transversal displacement, $m_i=\rho_i A_i$ is the mass per unit of volume, E the Young's modulus, I the quadratic moment, and δ is a common damping coefficient to each beam, with $i=1,2$. The fifth term of Eqs.(43a) and (43b) traduces the coupling between beams and piezoelectric patches, $\tilde{\alpha}$ is the electromechanical coupling parameter and $v(t)$ is the voltage across the load resistance. $C_p=2\varepsilon_{33}^S bl/t_p$ is the net clamped (i.e. constant strain) capacitance of the piezoelectric layers, ε_{33}^S is the permittivity, t_p is the

thickness of piezoelectric layers, b is the base of the beam, R the value of the passive load resistance, the subscript 3 indicates the direction corresponding to y [48]. $i(t) = i_0 \cos \omega_e t$ is an external current source which supplies the piezoelectric patches. The presence of the current source is to study the effects of an external source on the dynamics of the system.

The associated hinged-hinged boundary conditions are given by

$$w_i|_{x=0,l} = 0 \qquad \text{and} \qquad \left.\frac{\partial^2 w_i}{\partial x^2}\right|_{x=0,l} = 0 \tag{44}$$

b. Modal equations of the system

To deal with the analysis of this system, it is convenient to transform the partial differential equations into ordinary differential equations by using the Galerkin decomposition method [6]. The following set of dimensionless variables is introduced :

$$W_1 = \frac{w_1}{r}; W_2 = \frac{w_2}{r}; \tau = \frac{t}{T}; X = \frac{x}{l}; V = \frac{v}{V_0} \tag{45}$$

where T is a reference time and its value will be defined later ; V_0 is a reference voltage.

According to boundary conditions, the transversal displacement of beams is decomposed as follow :

$$W_1(X,\tau) = \sum_n Z_{n1}(\tau)\,\Phi(X) \tag{46a}$$

$$W_2(X,\tau) = \sum_n Z_{n2}(\tau)\,\Phi(X) \tag{46b}$$

where $Z_i(\tau)$ is the time-dependent function of each mode and $\Phi(X)$ is the shape function obtained from the mechanical part. Taking into account the boundary conditions of both beams in the system, $\Phi(X)$ is expressed as $\Phi(X) = \sin(n\pi X)$. Substituting Eqs. (46) in Eq. (43) and projecting back on the nth mode (assuming single-mode dynamics), yields the

TABLE 1 – *Values of physical parameters of the system*

Element	Notation	value
beams		
length	l	10 m
Young's modulus	E	200×10^9 N/m^2
mass density	ρ	7985 kg/m^3
width of beams	b	0.2 m
thickness of beams	h	0.1 m
Piezoelectric patches properties		
Permittivity	e_{33}	15.91 nFm^{-1}
load resistance	R	29.3 $k\Omega$

following dimensionless modal equations :

$$\frac{d^2Z_{n1}}{d\tau^2}+\lambda\frac{dZ_{n1}}{d\tau}+Z_{n1}+\frac{1}{4}Z_{n1}^3+\chi V=F_0\cos\Omega\tau \tag{47a}$$

$$\mu\frac{d^2Z_{n2}}{d\tau^2}+\lambda\frac{dZ_{n2}}{d\tau}+Z_{n2}+\frac{1}{4}Z_{n2}^3+\chi V=F_0\cos\Omega\tau \tag{47b}$$

$$\frac{dV}{d\tau}+\beta V=a\chi\left(\frac{dZ_{n1}}{d\tau}+\frac{dZ_{n2}}{d\tau}\right)+I_0\cos\Omega_e\tau \tag{47c}$$

with

$$\begin{aligned}&\lambda=\left(\frac{l}{n\pi}\right)^2\frac{\delta}{\sqrt{E\mathrm{Im}_1}};\chi=\frac{2\tilde{\alpha}V_0l^4}{EIr(n\pi)^5}\left(1-(-1)^n\right);r=\sqrt{\frac{I}{A}};\\&F_0=\frac{2f_0l^4}{EIr(n\pi)^5}\left(1-(-1)^n\right);\mu=\frac{m_2}{m_1};T=\left(\frac{l}{n\pi}\right)^2\sqrt{\frac{m_1}{EI}};\\&\Omega=\omega T;\Omega_e=\omega_eT;\beta=\frac{T}{RC_p};I_0=\frac{i_0T}{C_pV_0};a=\frac{EIr^2(n\pi)^6}{2C_pV_0^2l^5}\end{aligned} \tag{48}$$

The parameters of the beams and those of the piezoelectric patches used in numerical simulation are given in table 1. A precision will be done in text if one of these values is modified.

2.4.2 Model description of a network of indirectly coupled Euler's beams

a. Model description

Figure 12 shows a system of N number of hinged-hinged Euler's beams and the electrical circuit which is consisting of piezoelectric patches. In this subsection, we assume that in the network, the beams are identical Euler's beams with length l and that they are exci-

ted by a common force of amplitude f_0 and frequency ω. The same assumptions done in subsection 2.4.1 are taken into account in this subsection, and the model equation for a network indirectly coupled Euler's beams is then given by :

$$m\frac{\partial^2 w_i}{\partial t^2} + \delta\frac{\partial w_i}{\partial t} + EI\frac{\partial^4 w_i}{\partial x^4} - EA\left[\frac{1}{2l}\int_0^l \left(\frac{\partial w_i}{\partial x}\right)^2 dx\right]\frac{\partial^2 w_i}{\partial x^2} + \tilde{\alpha}\, v(t) = f_0 \cos\omega t \tag{49a}$$

$$C_p\frac{dv}{dt} + \frac{v}{R_p} = -\tilde{\alpha}\sum_{i=1}^{N}\int_0^l \frac{\partial^3 w_i}{\partial x^2 \partial t} \tag{49b}$$

where in Eq. (49a), $w_i(t)$ represents transversal displacement of the beam i ($i = 1, 2, ..., N$) at time t ; $v(t)$ is the voltage across the resistance load ; $\tilde{\alpha}$ is the electromechanical coupling parameter, measuring the strength of the global coupling between piezoelectric patches and beams. m, E, I, δ are the mass per unit length, Young's modulus, quadratic moment and transversal damping coefficient of each beam respectively. The equation of the electrical part can be obtained applying Kirchhoff's laws to all the coupled piezoelectric patches, and it is given by Eq.(49b), with $C_p = \sum_{i=1}^{N} c_{p_i}$ and R_p which are the resultant capacitance of the piezoelectric patches and load resistance, respectively. The term on the right hand side of the electrical equation (Eq.(49b)) represents the influence of the motion of each beam on the electrical part, and mutually the resultant voltage $v(t)$ from this electrical part influences the dynamics of each beam.

b. Modal equations of the system

In order to proceed with numerical analysis of the system of Eqs. (49a) and (49b), we first introduce the following dimensionless variables :

$$W_i = \frac{w_i}{r}; X = \frac{x}{l}; \tau = \frac{t}{T}; V = \frac{v}{V_0} \tag{50}$$

where r is the radius of gyration of the cross section A, T is a dimensionless time variable and V_0 is a reference voltage. The value of T will be given later. It is convenient to

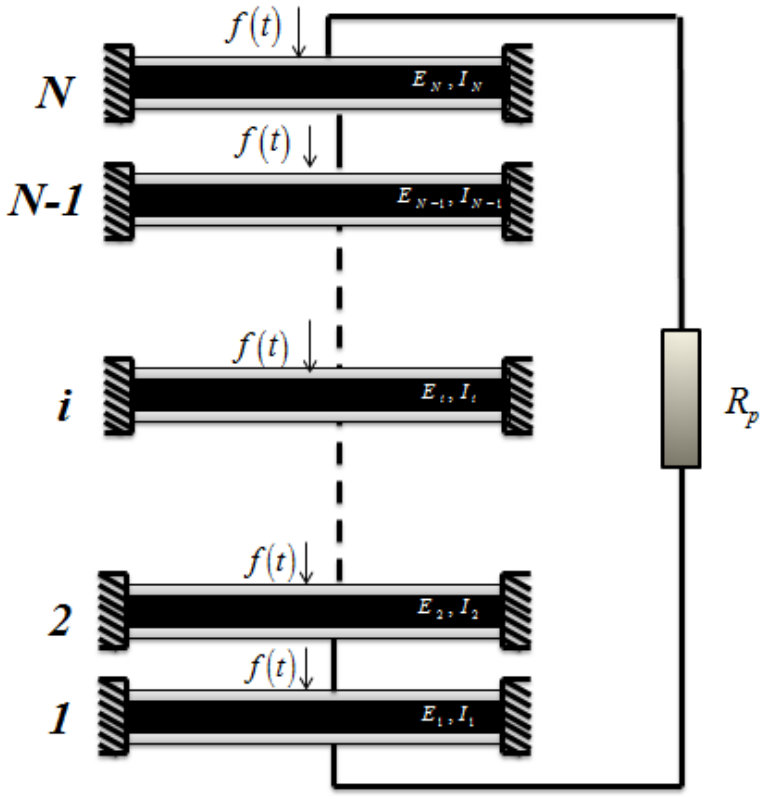

FIGURE 12 – *Schematic of a network of N hinged-hinged beams indirectly coupled via piezoelectric patches.*

transform the dimensionless partial differential equations into ordinary differential equations by using the Galerkin decomposition method [23].

According to the boundary conditions of a hinged-hinged beam defined by Eq. (51) :

$$W_i|_{X=0,1} = 0 \text{ and } \left.\frac{\partial^2 W_i}{\partial X^2}\right|_{X=0,1} = 0, \tag{51}$$

The transversal displacement of the i^{th} beam is defined as follows :

$$W_i(X,\tau) = \sum_n Z_{ni}(\tau)\,\Phi_n(X) \tag{52}$$

where $Z_{ni}(\tau)$ is the time dependent function of the mode n for each beam i and $\Phi_n(X) = \sin(n\pi X)$ is the shape function. After some mathematical manipulations, we obtain the fol-

lowing modal equations :

$$\frac{d^2 Z_{ni}}{d\tau^2} + \lambda \frac{dZ_{ni}}{d\tau} + Z_{ni} + \frac{1}{4} Z_{ni}^3 + \chi V = F_0 \cos(\Omega\tau) \tag{53a}$$

$$\frac{dV}{d\tau} + \beta V = a\chi \sum_{i=1}^{N} \frac{dZ_{ni}}{d\tau} \tag{53b}$$

with

$$\begin{gathered} \lambda = \left(\frac{l}{n\pi}\right)^2 \frac{\delta}{\sqrt{E\mathrm{Im}}}; \chi = \frac{2\tilde{\alpha} V_0 l^4}{EIr(n\pi)^5} \left(1-(-1)^n\right); F_0 = \frac{2 f_0 l^4}{EIr(n\pi)^5} \left(1-(-1)^n\right) \\ T = \left(\frac{l}{n\pi}\right)^2 \sqrt{\frac{m}{EI}}; \Omega = \omega T; \beta = \frac{T}{R_p C_p}; a = \frac{EIr^2 (n\pi)^6}{2 C_p V_0^2 l^5} \end{gathered} \tag{54}$$

2.4.3 Description and nonlinear model of the delayed network of indirectly coupled beams

a. System description

The system consists with a network of N simple supported beams as shown in figure 13. Each beam is assumed isotropic, uniform and flexible. We assume that all beams are identical Euler's beams and that they are excited by a common force of amplitude f_0 and frequency ω. The network of beams are interconnected indirectly through an electrical circuit as described in the previous subsection. The electrical part integrates a load resistance and the capacitance of the piezoelectric patches. The piezoelectric layers are laminated along each side of both beam.

Prior experimental and analytical studies in the area of structural control have investigated the effects of time delays on the system under control. A time delay occurs on a controlled system during the computation time or the actuation of the control force [102].

In our model, the value of the load resistance used to dissipate the electrical energy is adjusted through the computation unit, after the evaluation of the total voltage delivered by the piezoelectric patches. This process generates the birth of a time delay.

b. Modal equations of the system

Applying both continuous mechanical principles to the mechanical part and the Kirchhoff's laws to the electrical part as done in the previous subsection, the system of delayed indirectly coupled beams can be defined by the following set of equations

$$\frac{d^2 Z_i}{dt^2} + \lambda \frac{dZ_i}{dt} + Z_i + \alpha Z_i^3 + \chi V = f_0 \cos(\omega t) \tag{55a}$$

$$\frac{dV}{dt} + \beta V = a\chi \sum_{i=1}^{N} \frac{d}{dt}(Z_i(t-\tau)) \tag{55b}$$

where the variables Z_i and V represent the dimensionless variable of the displacement for the ith beam and the voltage across the load resistance, respectively with $i = 1, 2, ..., N$. χ which represents the strength of the electromechanical coupling parameter, τ which is the time delay between the detection of vibrations and the actuation feedback action of the controller, and other parameters in Eq.(55) are assumed positive throughout this work.

In this part of the work, the simulations will be carried out for $\lambda = 0.39$, $\alpha = 0.25$, $\beta = 1.24$, $a = 318.26$, $\omega = 0.3$, $f_0 = 5.0$, $N = 20$, otherwise if the values are changed, the new values will be specified.

Equation (55) is obtained assuming the Euler-Bernoulli formalism with the requirements that the beam is thin and relatively long and that the torsional and axial vibrations are negligible compared to the flexural vibration. The equations modelling such a system have been established for a network of beams indirectly interconnected to an electrical circuit, without time delay consideration [113].

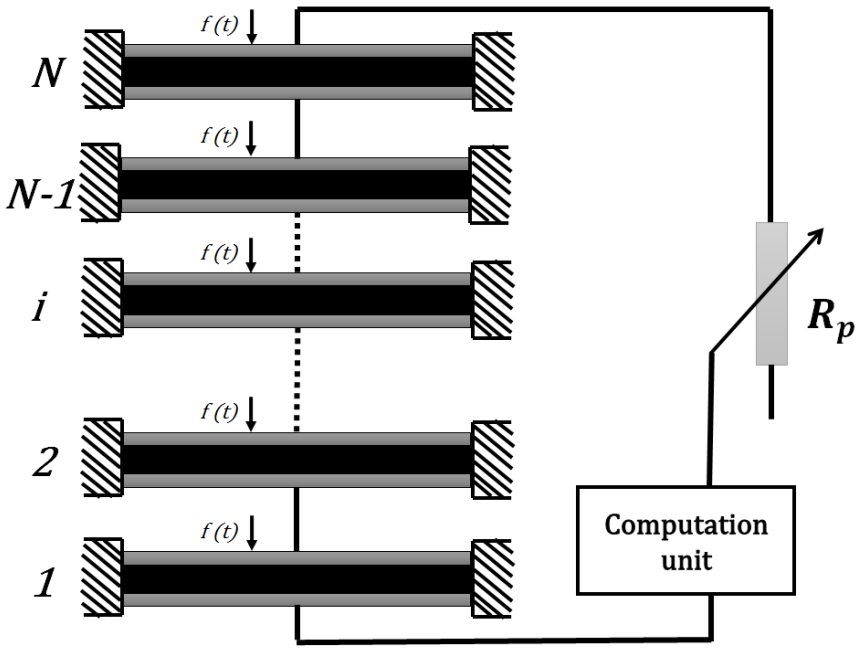

FIGURE 13 – *Schematic diagram of a feedback time delay indirectly coupled network of beams.*

2.5 Conclusion

In this chapter, we have described the mathematical formalisms and numerical methods used to solve the problem of this thesis. We started by the presentation of the Galerkin decomposition method used to reduce the problem of the PDEs into ODEs. We also presented the harmonic balance method to solve the nonlinear ODEs obtained from the model of this thesis and the stability criteria for DDEs is also investigated. Then we have provided to the readers the tools that will be used for characterization of the dynamical and synchronization states of dynamical systems under consideration in the thesis. At last, nonlinear modelling of electromechanical systems constituted of a network of beams indirectly connected to piezoelectric patches, with different consideration have been presented. The next chapter will be focused on the dynamical analysis and the investigation of the occurrence of strong amplitude reduction (SAR) on a network of Euler's beams indirectly connected to a dynamical environment. Synchronization state and the effect of time delay will also be investigated.

CHAPITRE 3

RESULTS AND DISCUSSIONS

3.1 Introduction

This chapter is devoted to the presentation and discussions of the results from mathematical analysis and numerical simulations. Therefore, the chapter is organized as follows. The first section deals with the analysis of a strong amplitude reduction phenomenon taking into account two indirectly coupled Euler's beams through a dynamic environment. In the second section, an extension of this study is done for a case of a network of indirectly coupled beams, and the synchronization state of the network is also highlighted. The third section presents the effect of the time delay on the occurrence of SAR phenomenon and synchronization state for a network of indirectly coupled beams. The last section is devoted to the conclusion of the chapter.

3.2 Strong amplitude reduction of vibration on two beams indirectly interconnected using a piezoelectric damper

3.2.1 Influence of different current sources on the control strategy

a. Effect of an AC source

The vibration amplitude of the first beam Z_1 (for the first mode) is plotted as function of the external frequency Ω for different values of current amplitude I_0 (Fig. 14). This figure shows that the vibration amplitude of the beam increases as current amplitude increases. So we conclude that the use of an AC source is harmful for the system of coupled beams under control, it alters the efficiency of the control strategy as it increases the vibration

amplitude of the beams with the increase of its amplitude I_0. The observations done for the first beam are the same for the second one.

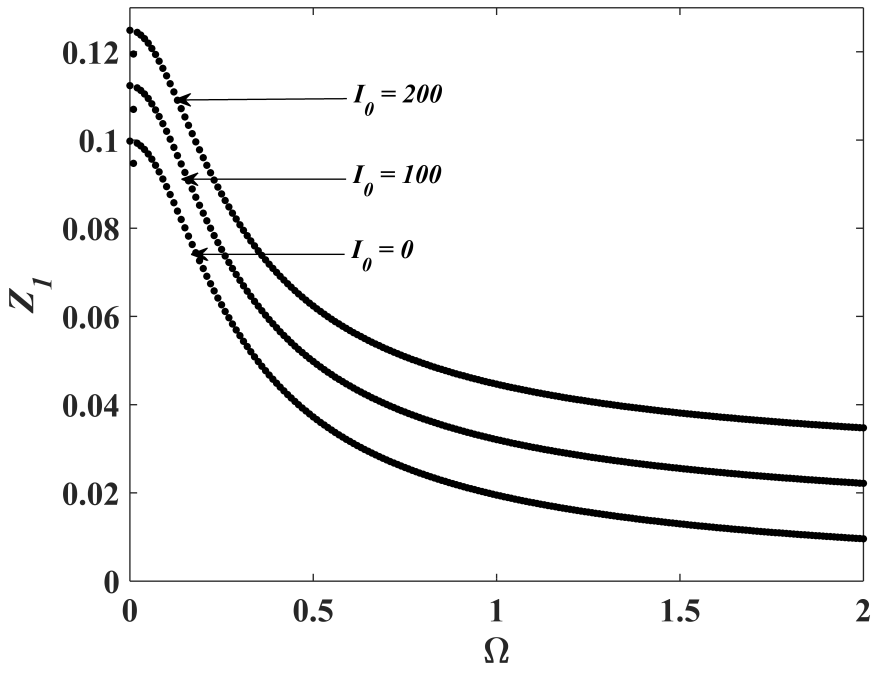

FIGURE 14 – *Effect of an AC source on vibration amplitude of the first beam Z_1 as function of the external load frequency* Ω*, for current amplitudes* $I_0 = 0.0$, $I_0 = 100$, $I_0 = 200$. *The others parameters are :* $F_0 = 0.1$, $\mu = 1.0$, $\chi = 0.1$, $\Omega_a = 5.03$

b. Effect of a DC source

By using a DC source, the vibration amplitude of the displacement Z_1 is plotted as function of the amplitude of the intensity of the direct current I_0 (Fig. 15). As the intensity I_0 increases the vibration amplitude of the displacement Z_1 decreases slightly. Thus, one realizes that DC source contributes to decrease vibration the amplitude of the beams, and it is clear that its use will be benefit for the control, nevertheless this reduction is very weak. So in the rest of this section, the effect of current supply source will be neglect in the following analysis.

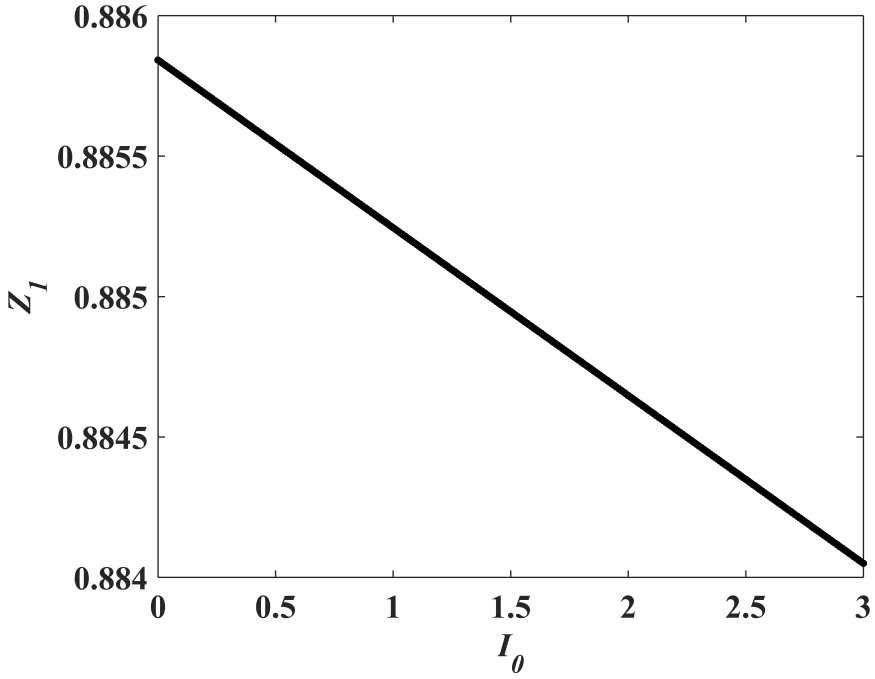

FIGURE 15 – *Effect of a DC source on vibration amplitude of the first beam Z_1 as function of the intensity of the direct current I_0, for $\chi = 0.03$, $\mu = 1.0$, $F_0 = 1.0$.*

3.2.2 General analysis of oscillations quenching mechanism on the system

The steady-state response of the set of equations (47) are determined by applying the harmonic balance method [106, 6] by setting :

$$Z(\tau) = A_1 \cos(\Omega\tau) + A_2 \sin(\Omega\tau) \tag{56a}$$

$$V(\tau) = B_1 \cos(\Omega\tau) + B_2 \sin(\Omega\tau) \tag{56b}$$

Inserting Equations (56) into Equations (47) and equating the coefficients in $\sin(\Omega\tau)$ and $\cos(\Omega\tau)$ (assuming that the terms due to higher frequencies can be neglected), the

following set of equations is obtained :

$$\begin{aligned}
&\left(1-\Omega^2+\tfrac{3}{16}A^2\right)A_1+\lambda\Omega A_2+\chi B_1=F_0\\
&-\lambda\Omega A_1+\left(1-\Omega^2+\tfrac{3}{16}A^2\right)A_2+\chi B_2=0\\
&\beta B_1+\Omega B_2=2a\chi\Omega A_2\\
&-\Omega B_1+\beta B_2=-2a\chi\Omega A_1
\end{aligned} \tag{57}$$

After some mathematical algebraic manipulations, we obtain the amplitude of the both beams that satisfies the following non-linear algebraic equation :

$$\left[\left(1-\Omega^2+\frac{2a\chi^2\Omega^2}{\Delta}+\frac{3}{16}A^2\right)^2+\left(\lambda\Omega+\frac{2a\chi^2\beta\Omega}{\Delta}\right)^2\right]A^2=F_0^2 \tag{58}$$

With $\Delta=\beta^2+\Omega^2$ and $A^2=A_1^2+A_2^2$. We notice that this result is obtained for the shift mass parameter $\mu=1.0$, meaning the masses of the beams are equals.

a. Effect of the electromechanical coupling parameter on the dynamical behavior of the beams

The frequency response curve is plotted in term of the amplitude of displacement of the beams Z_1 and Z_2 as function of the external frequency of excitation Ω for different strengths of the electromechanical coupling parameter (Fig. 16). This figure shows that the vibration amplitudes of both beams decrease as the strength of the electromechanical coupling parameter increases, meaning a vibration reduction of both beams with the increase of the coupling parameter. Moreover the increase of the coupling parameter leads to a disappearance of the sub-harmonic resonance, and a suppression of the amplitude jump is also observed. A similar result has been highlighted by Nwagoum et al., when they were analysing the vibration control of a thin plate with an RL electromechanical controller [22].

In order to complement this analysis, the bifurcation diagram is plotted for different values of the electromechanical coupling parameter. Figure 17 presents the effects of the coupling parameter on the bifurcation diagrams of the beams. It is observed a progressive deterioration and disappearance of complex motions of the beams as the strength of the coupling parameter increases, even for the large value of the external load. This observation

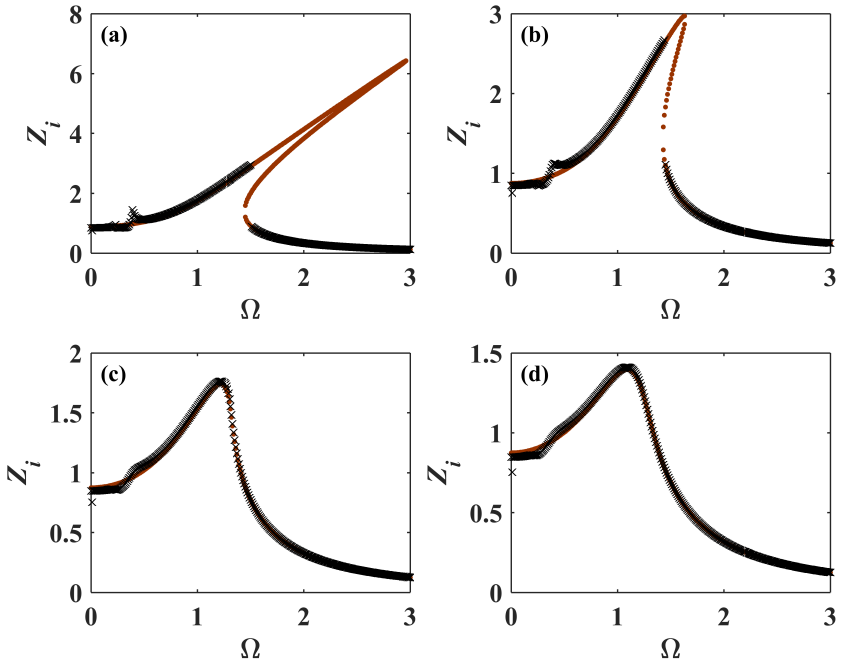

FIGURE 16 – *Amplitude response curve of Z_i as function of frequency external excitation* Ω, $i = 1,2$. *Showing the effects of the electromechanical coupling parameter on vibration amplitude of both beams, for* $F_0 = 1.0$, $E_0 = 0.0$, $\mu = 1.0$. *Analytical curves* $(\cdots)$, *numerical curves* $(\times\times\times)$.

was also made on an electromechanical damping device with magnetic coupling used to quench chaotic vibrations on a mechanical structure [89].

b. Strong amplitude reduction via indirect coupling

Nana Nbendjo [23] dealt with the control of a single non-linear Euler's beam using piezoelectric actuator, different voltage sources were considered. For the case of a passive piezoelectric control, it has been shown that the vibrations can not be completely damped but only reduced. Figure 18 (a) displays the amplitude variation in oscillatory responses of both beams Z_i as function of the electromechanical coupling parameter χ where the mass ratio is set at $\mu = 1.0$. Firstly, there is a small decrease of the vibration amplitude of both beams in the interval $[0.0;0.06]$, followed by an almost negligible decrease thereof in the range $[0.06;0.16]$. Around the value of the coupling parameter $\chi = 0.16$, the vibration amplitude drop abruptly and tends to low amplitude values which characterizes the state

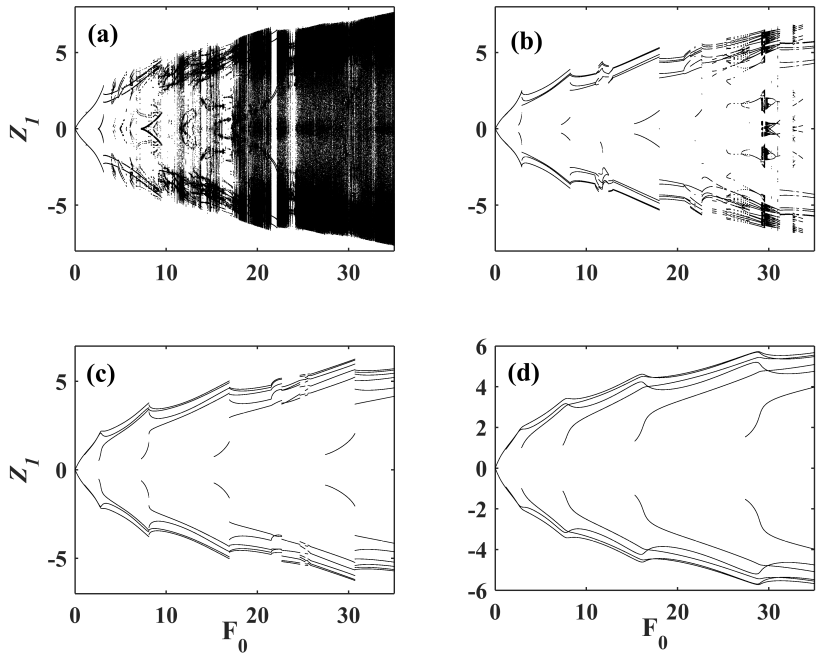

FIGURE 17 – *Bifurcation diagram of dimensionless displacement Z_1 of one beam as function of the amplitude of the external excitation F_0 : (a) $\chi = 0.0$, (b) $\chi = 0.01$, (c) $\chi = 0.015$, (d) $\chi = 0.02$. Showing the disappearance of the complex motions as the coupling parameter increases. The others parameters are $\Omega = 0.3$, $E_0 = 0.0$, $\mu = 1.0$.*

of strong amplitude reduction (SAR). Although the different transitions described above are not observed on the analytic curve, there is nevertheless a very good coincidence between these two results. An extension is made through the analyze of the bifurcation diagram, the displacement of both beams Z_i undergoes the n-periodic motions sequence to one-cycle then move to SAR state as shows in Fig.18 (b), therefore the complex movements of the beams are quenched as the coupling parameter increases, followed by periodic motions then SAR state appears [89, 67, 113].

c. Effect of the parameters of the system on the vibratory states of the beams

From the previous analysis, it has been found that the amplitude of complex motions (multi-periodic and chaotic motions) is always greater than those of the period-1 motions. In order to analyze the parameters that contribute to the reduction of the amplitude of the vibrations on mechanical and civil engineering structures, we investigate in this subsec-

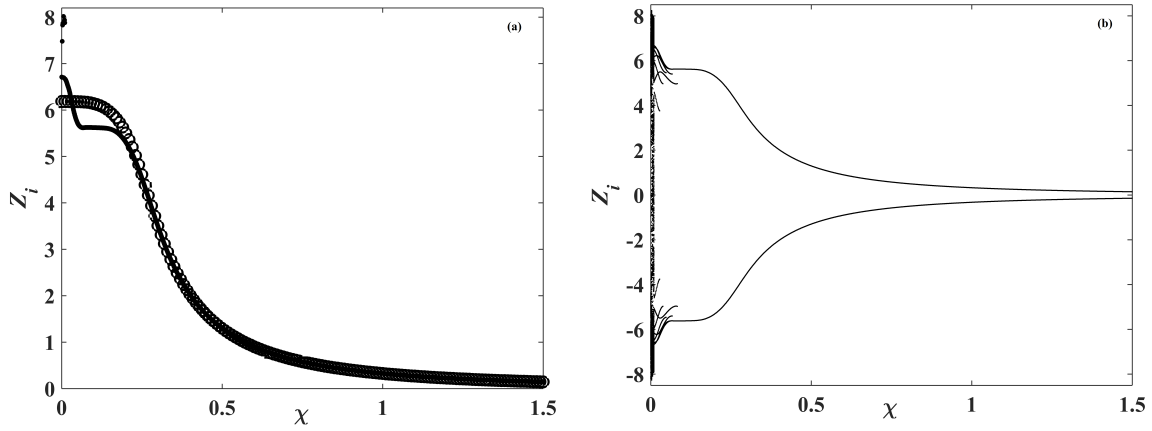

FIGURE 18 – *(a) Amplitude and (b) bifurcation diagram of dimensionless displacement Z_i of the beams as function of the electromechanical coupling parameter χ, for $F_0 = 50.0$, $i = 1,2$. Others parameters are defined in Fig. 17. Analytical curves (**ooo**), numerical curves ($\cdots$) (On fig. 13 (a).*

tion, the effect of the mass shift between both beams and also the effect of the variation of a load resistance on the occurrence of SAR state.

Figure 19 displays the frequency response curves of the displacement of both beams for different values of shift mass μ and the same value of the coupling parameter $\chi = 0.03$. The beams exhibit exactly the same dynamical motions for $\mu = 1.0$ as the external frequency of the load increases, meaning that they are in a synchronization state. But for all other values of the shift mass, each beam presents its own dynamics and the amplitude of vibrations is more large in these cases.

Figure 20 shows the amplitude of displacement of both beams Z_i with $i = 1,2$, as function of the coupling parameter χ for $\mu = 1.0$ and different values of the load resistance R. It is shown that the vibration amplitude of the beams stays important for small values of the load resistance ($R_p = 29.3 \times 10^2\ \Omega$), in spite of the values of the coupling parameter taking in a certain domain. Meanwhile, the strong amplitude reduction state is attained as the load resistance value is increased, and the value of the coupling parameter for which the phenomenon occurs is progressively reduced. We conclude that the load resistance value is crucial for the vibration reduction process.

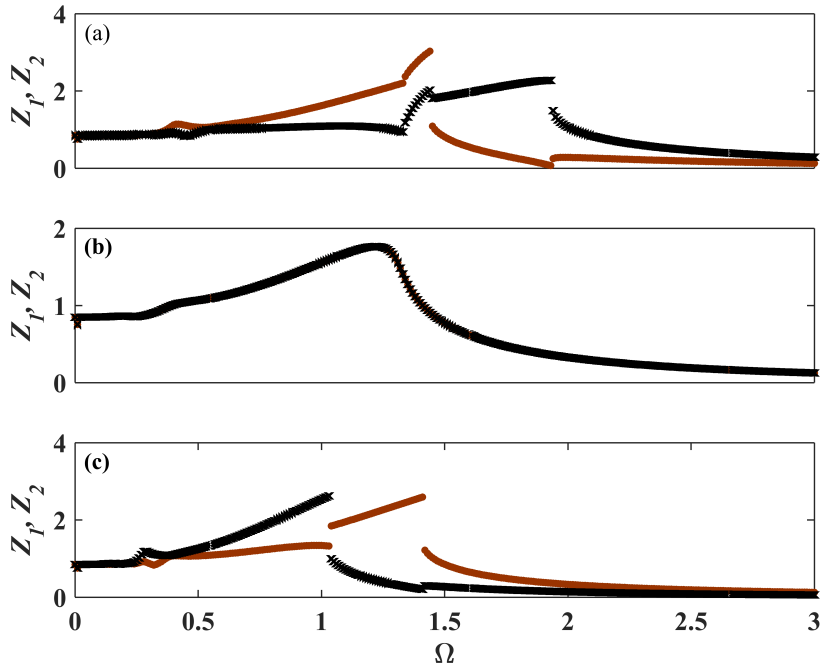

FIGURE 19 – *Amplitude response curves of Z_1 (brown dot) and Z_2 (black star) as function of frequency external excitation* Ω*, with (a)* $\mu = 0.5$*, (b)* $\mu = 1.0$*, (c)* $\mu = 2.0$*. Showing the effects of the shift mass parameter on vibration amplitude of both beams, for* $F_0 = 5.0$*,* $E_0 = 0.0$*,* $\chi = 0.003$*.*

3.3 Dynamical clustering, synchronization and strong amplitude reduction state investigation in a network of Euler's beams coupled via a dynamic environment

In this section, by varying the number of beams as well as the coupling strength, we explore the system dynamics. In particular, we analyse the synchronization state and the appearance of strong amplitude reduction phenomenon in a network of beams indirectly coupled through a dynamic environment (electrical part). In our previous study, the occurrence of strong amplitude reduction phenomenon was found in a system of two indirectly coupled Euler's beams via an electromechanical system consisting of piezoelectric patches. An extension of this study is presented here in order to investigate the effects of the network-size as well as the electromechanical coupling parameter. A high-dimensional

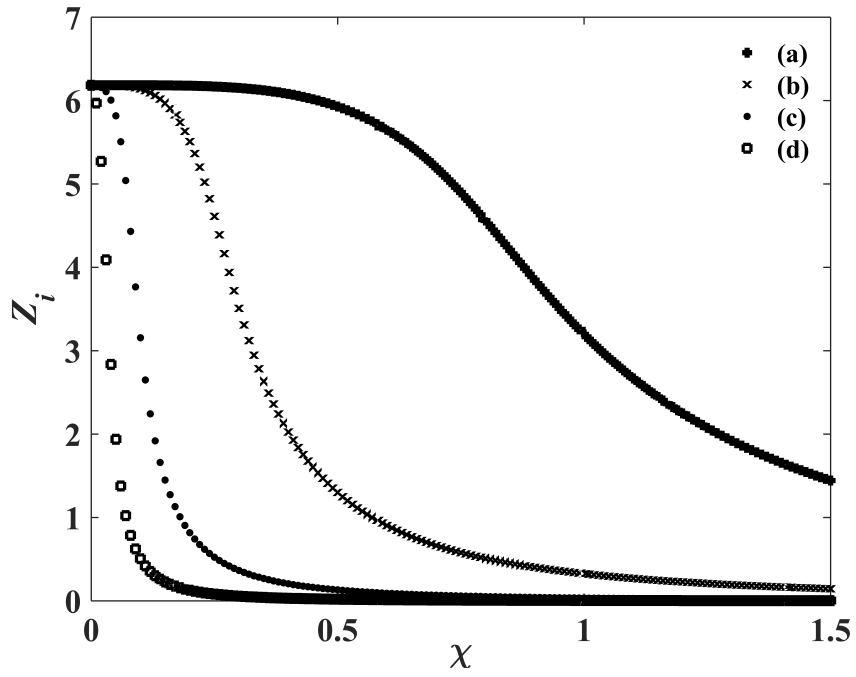

FIGURE 20 – *Vibration amplitude Z_i of both beams as function of the electromechanical coupling parameter χ,with parameters of Fig. 19 and (a) $R_p = 29.3 \times 10^2\ \Omega$, (b) $R_p = 29.3 \times 10^3\ \Omega$, (c) $R_p = 29.3 \times 10^4\ \Omega$, (d) $R_p = 29.3 \times 10^5\ \Omega$.*

nonlinear system of Eqs. (53a) and (53b) is numerically integrated, using the fourth-order Runge-Kutta scheme. In our numerical simulations, the parameters of the beam were as follows : length $l = 10\ m$, the width $b = 0.05\ m$, the height $h = 0.03\ m$, the density of material $\rho = 7850\ kg.m^{-3}$, the Young's modulus $E = 2 \times 10^{11}\ N.m^{-2}$, the damping coefficient $\delta = 0.1\ N.s/m$ and the reference voltage $V_0 = 2\ V$. In addition, the initial conditions for the displacement of each beam were randomly distributed with uniform probability on the interval $[-5,5]$.

3.3.1 Synchronization state

Our goal here, is to examine the synchronization state of the system of Eqs. (53a) and (53b) and to determine the range of parameters for which all the beams exhibit collective dynamics. The synchronization state is numerically characterized by the asymptotic time-average $\langle \eta(t) \rangle$ of the instantaneous root mean square function $\eta(t)$ of the distribution of

displacements and velocities of the beams [114], given by :

$$\eta(t) = \left[\frac{1}{N}\sum_{i=1}^{N}\left(Z_i^2 + \dot{Z}_i^2\right)\right]^{1/2} (i = 1, 2, \cdots, N). \tag{59}$$

Global synchronization of the whole system which describes the collective dynamics is attained when $\langle\eta(t)\rangle = 0$. Fig. 21 shows the time-average root mean square $\langle\eta(t)\rangle$ as function of the coupling strength χ for all the beams interacting indirectly with an environment for different network-sizes. It is found that with the increase of the coupling strength and for $N = 2$, $\langle\eta(t)\rangle$ decreases slowly and the beams do not completely synchronize. For $N = 10$, $\langle\eta(t)\rangle$ decreases more rapidly but the beams do not globally synchronize. However, when $N \geq 50$, the curve presents an abrupt slope, with global network synchronization taking place for strong coupling strength.

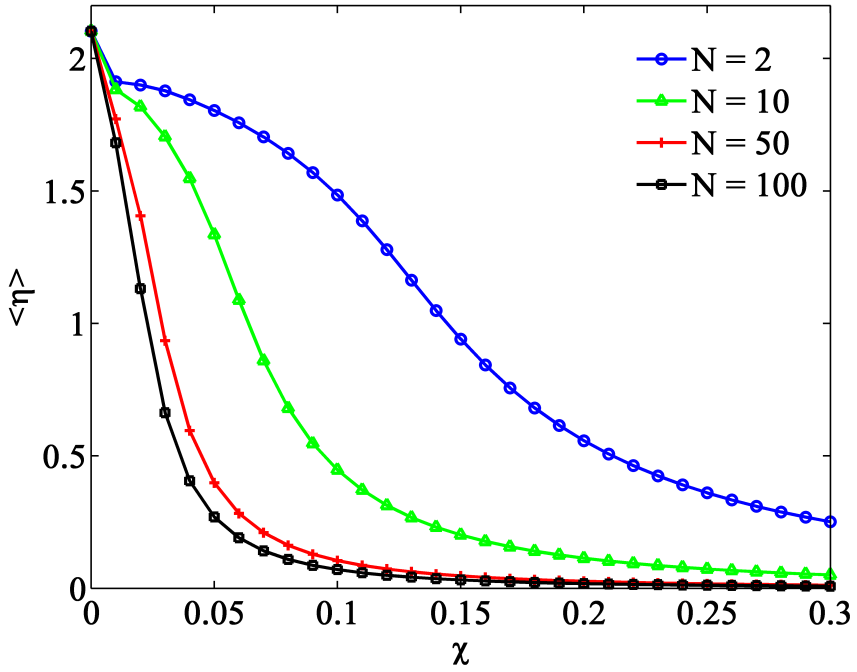

FIGURE 21 – *Time-average of root mean square $\langle\eta(t)\rangle$ of a distribution of a network of beams as function of the coupling parameter χ, for network-sizes $N = 2$, 10, 50, 100. Other parameters are : $F_0 = 5.0$, $\Omega = 0.3$ and $R_p = 29.3$ $k\Omega$.*

Furthermore, for a given coupling parameter χ, $\langle\eta(t)\rangle$ is plotted as function of the network-size, N. This is illustrated in Fig. 22. In this case, the whole system does not synchronize

when $\chi \leq 0.01$; whereas when the strength of the coupling parameter χ increases ($\chi \geq 0.1$), the system approaches global synchronization for large network-sizes.

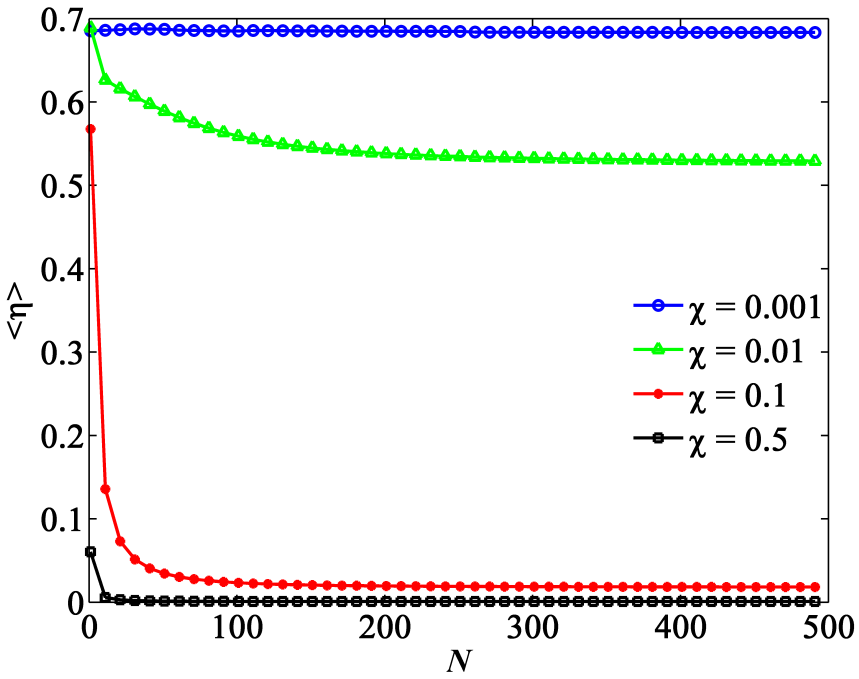

FIGURE 22 – *Time-average of root mean square* $\langle \eta(t) \rangle$ *of a distribution of a network of beams as function of the number of interacting beams* N*, for coupling parameters* $\chi = 0.001$, 0.01, 0.1, 0.5. *Other parameters are defined in Fig. 21.*

A global view of the synchronization state can be obtained by scanning different values of the network-sizes, N and coupling parameter, χ (Fig. 23). We calculate the time-average *rms* $\langle \eta(t) \rangle$ in the parameter space $N - \chi$, and we do this for different values of the load resistance R_p, which is an intrinsic damping of the environment. Note that $\langle \eta(t) \rangle$ is associated with the colorbar in the four panels showing different synchronization states. Figure 23 provides the variation of time-average *rms* $\langle \eta(t) \rangle$ from minimum (blue) to maximum (red) showing the effect of the environment on the global state of synchronization in the network. Blue colours indicate the regions where the whole system exhibit global synchronization, while red colours denote the regions where the whole system is assumed to be de-synchronized. Elsewhere in the colorbars and halfway between the blue and red ones, the whole system is assumed to be either weakly synchronized or completely de-synchronized. As the load resistance increases, the de-synchronized and weak synchronized regions di-

minish while the synchronized ones increase from right to the left.

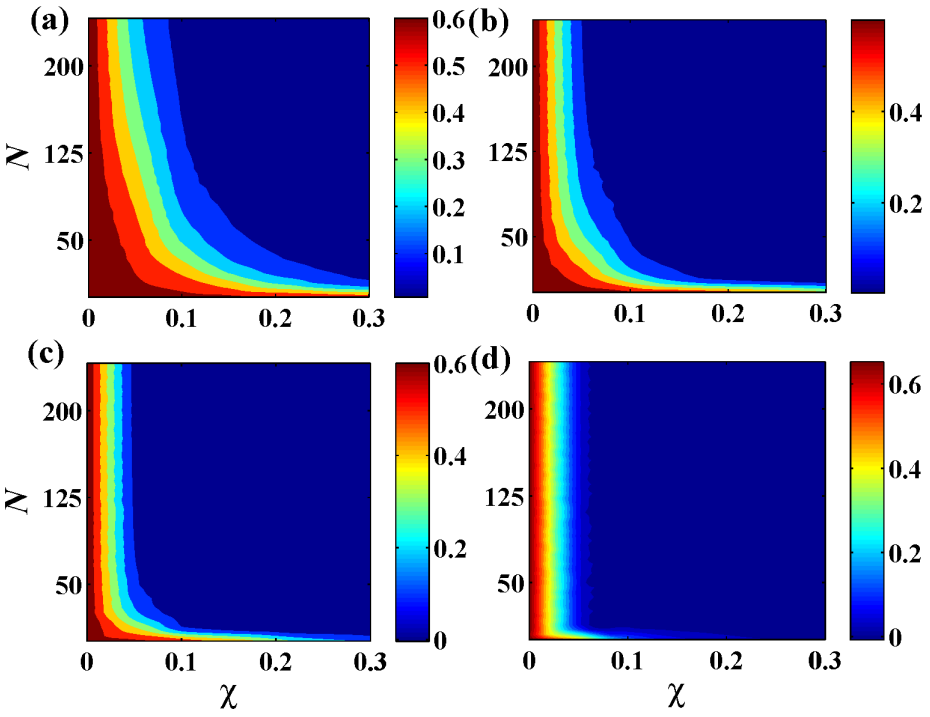

FIGURE 23 – 2 – *D parameter plot of time-average root mean square* $\langle \eta(t) \rangle$ *as function of the number of interacting beams N and coupling parameter* χ *for load resistance values (a)* $R_p = 2.93$ *k*Ω*, (b)* $R_p = 10.0$ *k*Ω*, (c)* $R_p = 29.3$ *k*Ω *and (d)* $R_p = 293$ *k*Ω*. Other parameters are defined in Fig. 21.*

The synchronization feature of the network can be better understood by numerically computing the probability distribution function [115], defined in a subset by generating M realizations of X_i, and counting the number of observable outcomes in the interval and divide by M. This approach was recently employed by Palazzi and Cosenza [91]. Fig. 24 shows the probability distribution of displacement Z_i for different coupling parameter with a network-size $N = 200$, at an asymptotic dimensionless time ; illustrating the synchronization state for different values of coupling strength. At weak coupling ($\chi \leq 0.01$), two clusters are formed as shown in Fig. 24(a-b). This phenomenon described as dynamical clustering or cluster synchronization usually occurs when an ensemble of coupled oscillators splits into groups of synchronized elements [41, 44]. In this system, the dynamical clustering has almost vanished for the coupling parameter ($\chi = 0.01$), and in Figs. 24(c-d) where the coupling parameter $\chi \geq 0.1$, we observe the complete disappearance of the dynamical cluste-

ring and the emergence of global synchronization.

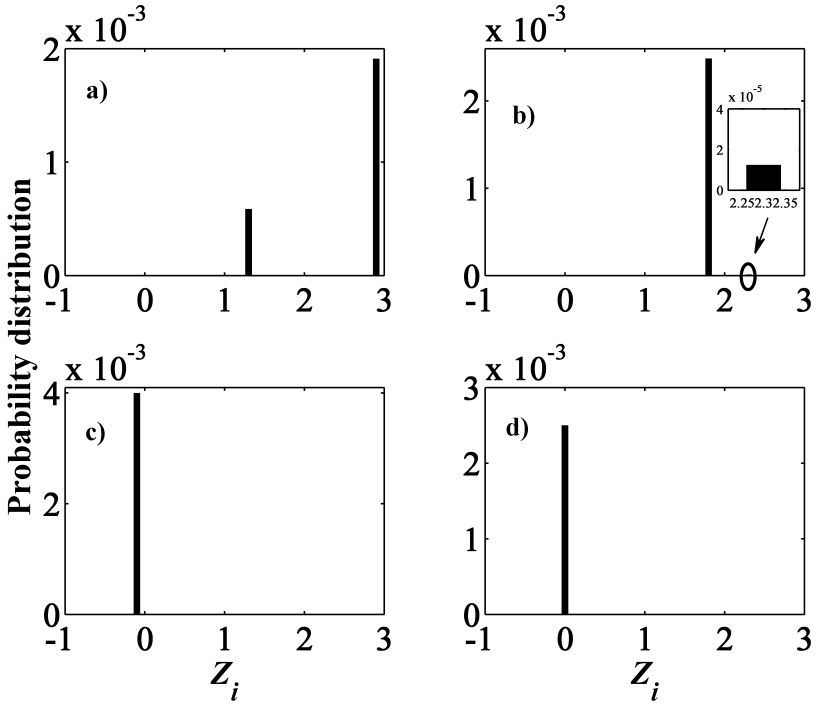

FIGURE 24 – *Probability distribution of the displacement showing the transition to synchronization via dynamical clustering in the system for different coupling parameters at the dimensionless time* $\tau = 8000$ *: (a)* $\chi = 0.001$*, (b)* $\chi = 0.01$*, (c)* $\chi = 0.1$*, (d)* $\chi = 0.5$*. The parameters used are defined in Fig. 21 and* $N = 200$

Zooming on the weak coupling parameter regime ($\chi \leq 0.01$) where the formation of clusters is observed, we illustrate in Fig. 25 the probability distribution for a very weak coupling parameter ($\chi = 0.001$) ; wherein the clusters remain in existence for all values of network-size. For $N = 2$, the clusters are separated in two orbits and the probability distribution are the same. However, by increasing the network-size, the two groups do not have the same size, showing that the beams vibrate in different states. In Fig. 26, we plot the probability distribution of displacement Z_i for different network-sizes and with fixed value of the coupling parameter ($\chi = 0.1$), and at an asymptotic dimensionless time. For any network-size, we observe a global synchronization in the system. The results of Figs. 24 and 25 agree with different synchronization regions obtained with time-average root mean square function in the parameter space $N - \chi$ in Fig. 23(c).

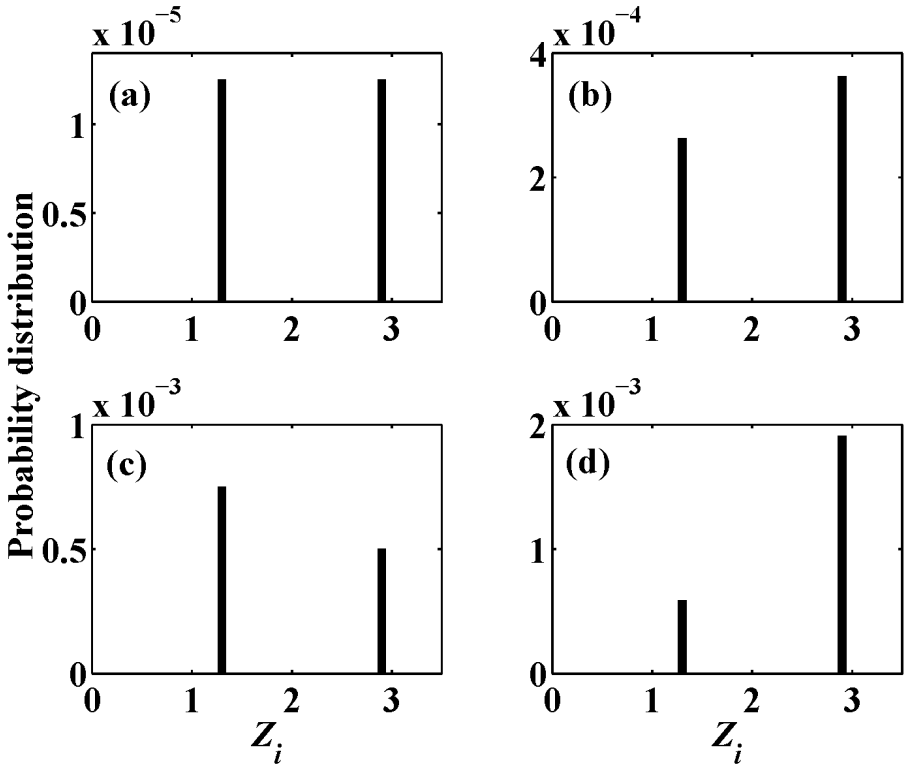

FIGURE 25 – *Probability distribution of the displacement showing dynamical clustering in the system for different network-sizes at the dimensionless time* $\tau = 8000$ *: (a)* $N = 2$*, (b)* $N = 50$*, (c)* $N = 100$*, (d)* $N = 200$*. The parameters used are defined in Fig. 21 and* $\chi = 0.001$

3.3.2 Effect of the network-size on the amplitude response curves

Furthermore, we observe that the increase of the network-size and the coupling parameter leads to the reduction of vibration amplitude in the system of global synchronized beams (Fig. 26). Here, we further investigate the influence of network-size on the vibration amplitude of any beam in the system. By varying the frequency of the external excitation, we provide in Fig. 27 the frequency-response curves of the first beam for different network-sizes. The curves show the resonance peaks, the sub-harmonic resonance, amplitude jump phenomenon for certain values of number of coupled beams N. They show that the amplitude of vibration of the first beam decreases as the number of coupled beams increases. We also observe the disappearance of the sub-harmonic peak and the leakage of the amplitude jump with the increase of the number of coupled beams N in the network.

In Fig. 28, we plot the amplitude of vibration of the first beam as function of the am-

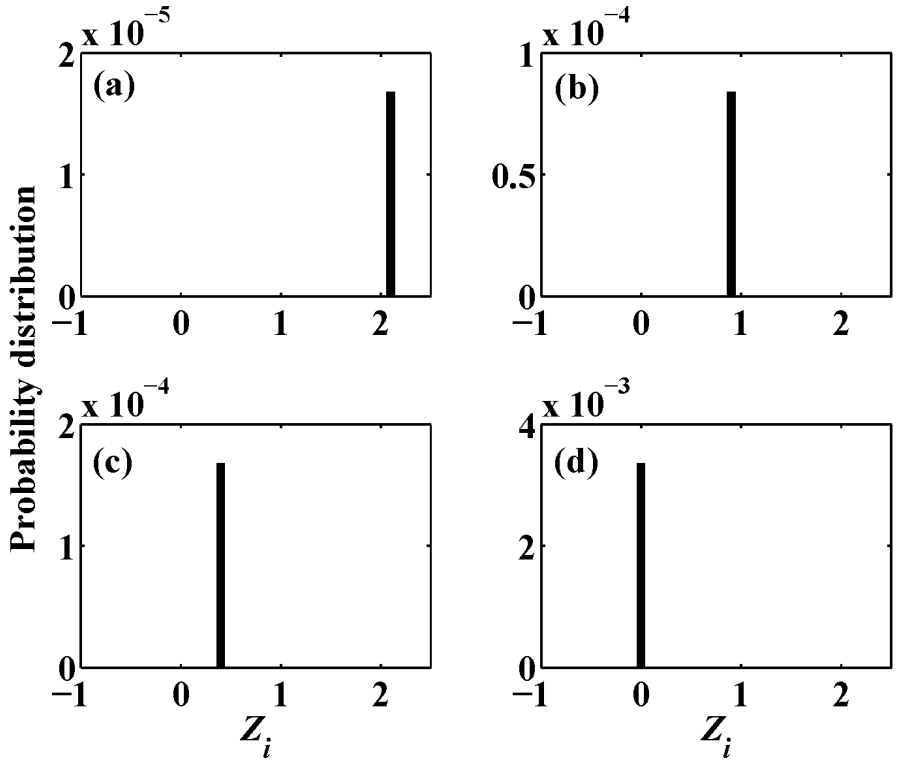

FIGURE 26 – *Probability distribution of the displacement in the system for different network-sizes at the dimensionless time* $\tau = 5950$ *: (a)* $N = 1$*, (b)* $N = 5$*, (c)* $N = 10$*, (d)* $N = 200$*. The parameters used are defined in Fig. 21 and* $\chi = 0.1$

plitude of the external excitation for different values of number of coupled beams. For the case of two indirectly coupled beams, the amplitude-response curve presents a jump phenomenon, which disappears with the increase of the number of coupled beams. Figs. 27 and 28 permit to conclude that the jump phenomenon disappears and the amplitude of vibrations of the beams decreases considerably with an increase of the number of coupled beams.

3.3.3 Strong reduction of amplitude : effects of Euler's beams network-size

Fig. 29 shows the bifurcation diagrams of the first beam as function of the electromechanical coupling parameter for different values of network-size. For a small network-size (Fig. 29(a)), the increase of the coupling parameter leads to the suppression of period$-nT$

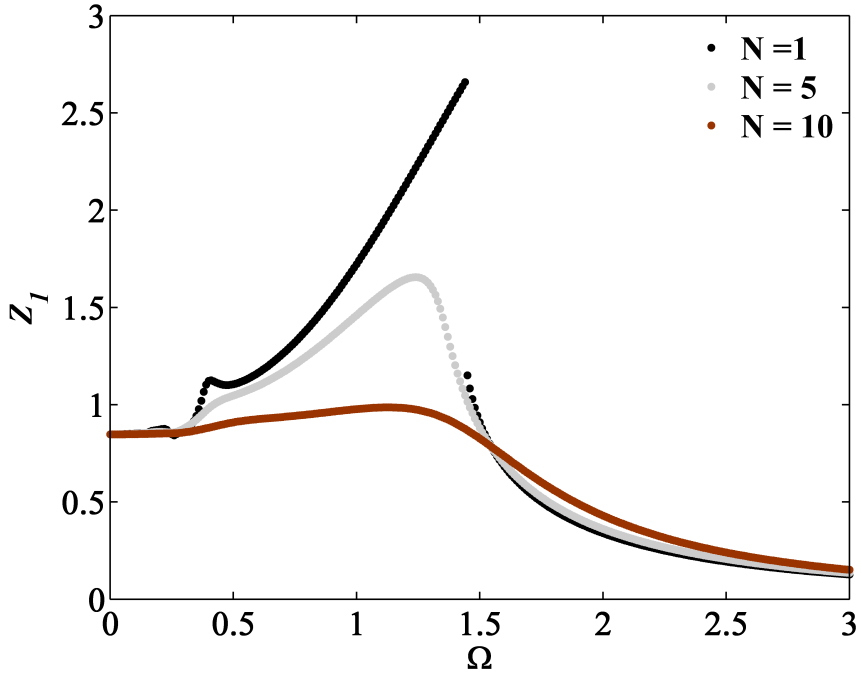

FIGURE 27 – *Effects of the numbers of coupled beams on the amplitude-response curves for the first beam as function the frequency of the external excitation* Ω. *The parameters used are :* $\chi = 0.02$, $F_0 = 1.0$ *and* $R_p = 29.3\ k\Omega$.

(n being an integer) oscillations, but we observe a very low decrease of vibration amplitude. By increasing the network-size (Figs. 29(b-d)), the areas of period$-nT$ oscillations are more and more reduced, and we observe that vibration amplitude decreases gradually reaching to very small amplitude for large network-sizes (Figs. 29(c-d)). It is also found that the parameters space $N-\chi$ for which the strong reduction of amplitude phenomenon is achieved, correspond to the parameters in the global synchronized domain (Fig. 23(c)). This result shows that for a network of beams indirectly coupled through an electrical circuit with a relative weak coupling parameter, strong reduction of amplitude can be obtained by increasing the number of coupled beams in the system.

To complete the picture, we present a further confirmation of SAR by plotting the time series of displacement of the first beam Z_1 in Fig. 30 as the network-size N increases. It is observed in Fig. 30(a) that, as the network-size increases, the amplitude of oscillations of the first beam decreases. For large network-size, the vibration amplitude of the first beam approaches very small values. In Fig. 30(a), a phase shift is also observed as the network-

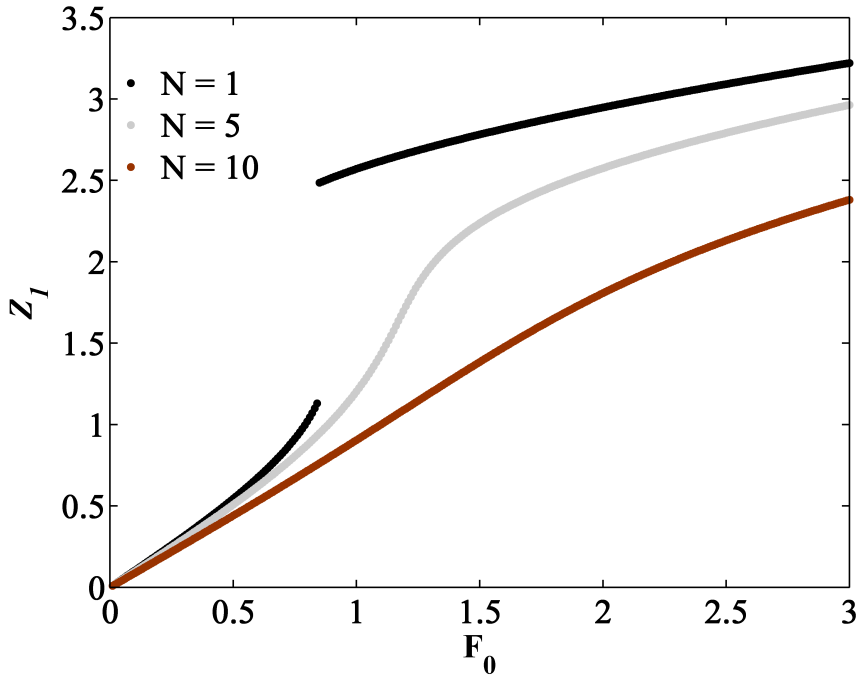

FIGURE 28 – *Effects of the numbers of coupled beams on the amplitude-response curves for the first beam as function the amplitude of the external excitation* F_0. *The parameters used are :* $\chi = 0.02$, $\Omega = 1.4$ *and* $R_p = 29.3\ k\Omega$.

size of Euler's beams increase. Fig. 30(b) shows the time series for a fixed network-size of Euler's beams as the coupling parameter χ increases, in a suppression of period $-nT$ oscillations and the state of strong amplitude reduction is attained by increasing the coupling parameter.

3.4 Delay-induced synchronization on a network of Euler's beams indirectly interconnected via piezoelectric patches

3.4.1 Linear stability analysis

To study the local stability of the equilibrium point $(0,0,0)$, the amplitude of the external excitation is set to be $f_0 = 0.0$. The overall network of coupled beams are assumed to be in

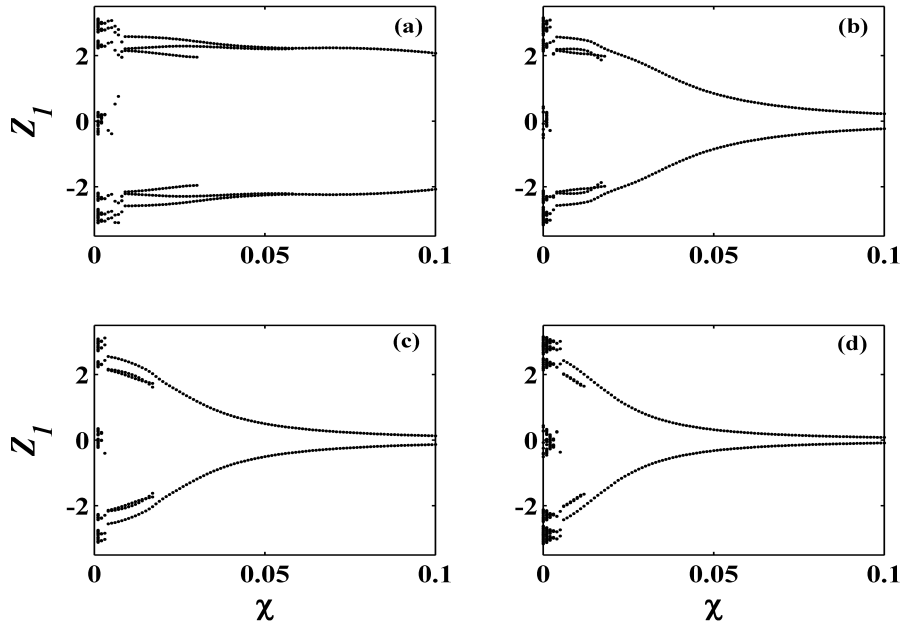

FIGURE 29 – Bifurcation diagram of the displacement of the first beam of the system as function of the coupling parameter χ, for $\Omega = 0.3$, $F_0 = 5.0$ and $R_p = 29.3\ k\Omega$: (a) $N = 2$, (b) $N = 30$, (c) $N = 60$, (d) $N = 200$.

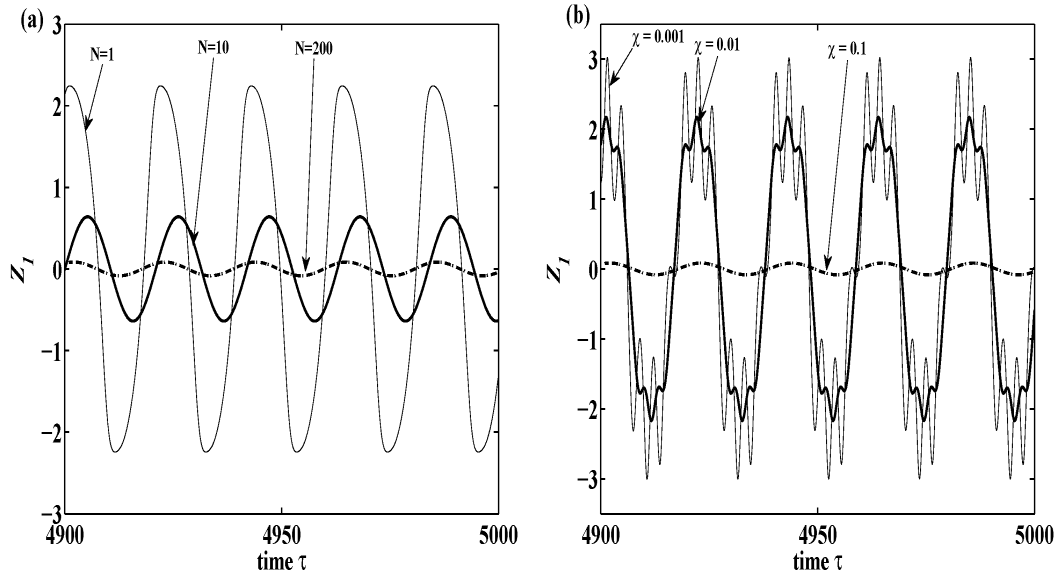

FIGURE 30 – Times series of the first beam for (a) different values of Euler's beams network-sizes, $\chi = 0.1$; (b) different values of the coupling parameter, $N = 200$. Other parameters are defined in Fig. 29.

a synchronized state. Thus, equation (55) can be recast in the following linearized form :

$$\begin{cases} \frac{dz_i}{dt} = y_i \\ \\ \frac{dy_i}{dt} = -\lambda y_i - z_i - \chi V \\ \\ \frac{dv}{dt} = -\beta v + a\chi N y_i\left(t-\tau\right) \end{cases} \tag{60}$$

We set the Lyapunov concept by applying the fundamental solution e^{st} [101, 116]. The characteristic equation related to the fixed point $(0,0,0)$ is given in the following form :

$$s^3 + \left(\beta+\lambda\right)s^2 + \left(1+\lambda\beta+aN\chi^2 e^{-s\tau}\right)s + \beta = 0 \tag{61}$$

To obtain the stability boundary in the control parameter space $\left(\chi,\beta\right)$, we use the D-subdivision method [102, 117]. According to this method, the stability boundary in the space of control parameters $\left(\chi,\beta\right)$ is determined by the points that lead either to a root $s=0$, or a pair of pure imaginary roots of Eq. (61).

Substituting $s=0$ into Eq. (61) yields :

$$\beta = 0 \tag{62}$$

Setting $s = ib$ (where b is a real parameter) into the characteristic equation (61), one finds the following system of equations :

$$\begin{cases} aN\chi^2\left(b\sin\left(b\tau\right)\right) + \left(1-b^2\right)\beta = \lambda b^2 \\ \\ aN\chi^2\cos\left(b\tau\right) + \lambda\beta = b^2 - 1 \end{cases} \tag{63}$$

Equation (63) leads to

$$\beta = \frac{\big(\sin(b\tau)b^2 - \cos(b\tau)b\lambda - \sin(b\tau)\big)b}{\sin(b\tau)b\lambda + \cos(b\tau)b^2 - \cos(b\tau)}$$

$$\chi^2 = \frac{b^4 + b^2\lambda^2 - 2b^2 + 1}{Na\big(\sin(b\tau)b\lambda + \cos(b\tau)b^2 - \cos(b\tau)\big)} \tag{64}$$

The bifurcation curve in plane (χ, β) delimiting the stability boundary can be found from the parametric equations (64) where b is varying, while assuming that the conditions $\chi \geq 0$ and $\beta \geq 0$ are verified. Figure 31 shows the stability boundary in the parameter space $\chi - \beta$ for different values of the time delay. The white colour indicates the region where the whole system is stable, whereas the black colour represents the region where the system is unstable. As the time delay increases, the stable region is reduced. Thus, we lead to the conclusion that the control parameters along with the time delay have an important effect on the stability and the efficiency of the control process.

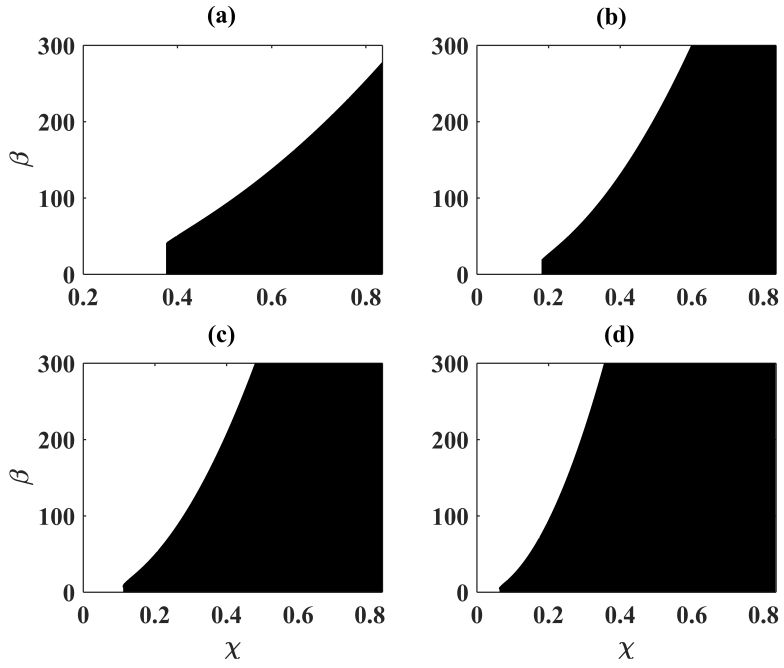

FIGURE 31 – Stability boundary in the parameter space $\chi - \beta$: showing the reduction of the stable region in the system for different values of the time delay : (a) $\tau = 0.1$, (b) $\tau = 0.2$, (c) $\tau = 0.3$, (d) $\tau = 0.5$.

3.4.2 Effect of time delay on the general behavior of the network of indirectly coupled beams

a. On the stability of the network

Bifurcation diagrams are plotted in order to complement the results obtained from the stability analysis. We observe the effect of the delay on the generalized behavior of the network of coupled systems as the coupling parameter increases. Figure 32 shows the bifurcation diagrams of the displacement of the first beam Z_1 as function of the electromechanical coupling parameter χ for different values of the time delay τ. According to the time delay, the trajectory of the beams increases and diverges from the equilibrium point of the network of coupled beams $\left(y_e, z_e\right) = (0,0)$ as the electromechanical coupling parameter increases. Moreover complex motions are observed in the network with a certain range of the coupling parameter. Nevertheless, as the coupling parameter reaches a certain value, the trajectories of all beams in the network diverge towards infinity and whole system exhibits unstable motion.

Some representative time series of the displacement Z_i, phase portrait and amplitude of Fourier spectra of responses of any beam in the system are shown in figure 33 for $\tau = 0.1$ and different values of the electromechanical coupling parameter χ. As the coupling parameter χ increases, the amplitude of vibrations also increases and the periodic oscillations observed for $\chi = 0.1$ involve to a period doubling motion for $\chi = 0.45$ and finally a quasiperiodic motion is observed for $\chi = 0.55$. Correspondingly, the Fourier spectra have been drawn corresponding to the time series in figures 33 (a3)-(b3)-(c3). The increase of χ generates several harmonics and enlarges the range of frequencies in the network. The consideration of the time delay on the feedback control of the network of beams leads to the disappearance of the strong amplitude reduction observed in the case without delay shown in the previous section and brings out disturbance and instability around the system.

Nevertheless, the appearance of harmful effects due to the delay in the network can be

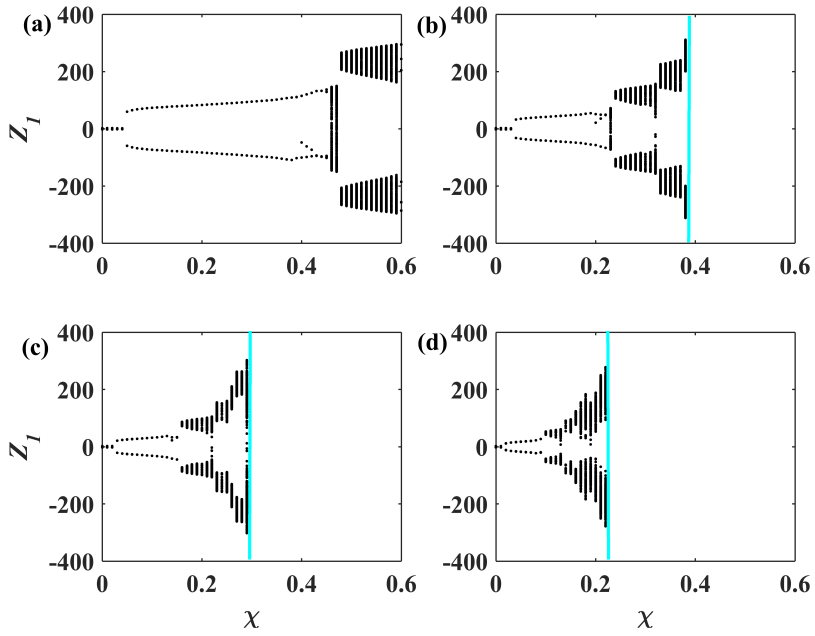

FIGURE 32 – Bifurcation diagrams of the network of coupled beams (Eqs. (55)) depicting the local maxima of the first beam as χ increases : showing the effect of the delay τ on the occurrence of unstable motion on the system with different values of τ : (a) $\tau = 0.1$, (b) $\tau = 0.2$, (c) $\tau = 0.3$, (d) $\tau = 0.5$.

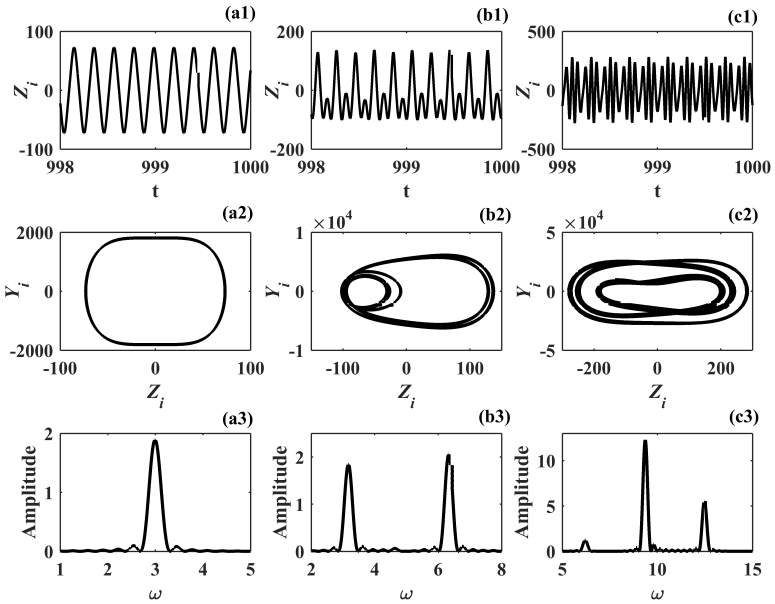

FIGURE 33 – Time series, phase portrait and Fourier spectra of any beam in the network with $\tau = 0.1$ and (a) $\chi = 0.1$, (b) $\chi = 0.45$, (c) $\chi = 0.55$.

pushed towards larger values of the coupling parameter by increasing the value of the dissipative parameter β of the electrical part. Thus, we observe in figure 34 that the increase of the dissipative parameter with the coupling parameter bounded in a certain area, leads to the suppression of the complex dynamics for the case $\tau = 0.1$ in favor of periodic dynamics. This numerical result is in agreement with the analytical study of the stability of the system made in Fig. 31, which shows that the increase of the dissipative coefficient β of the electrical part leads to enlarge the stable domain of the system.

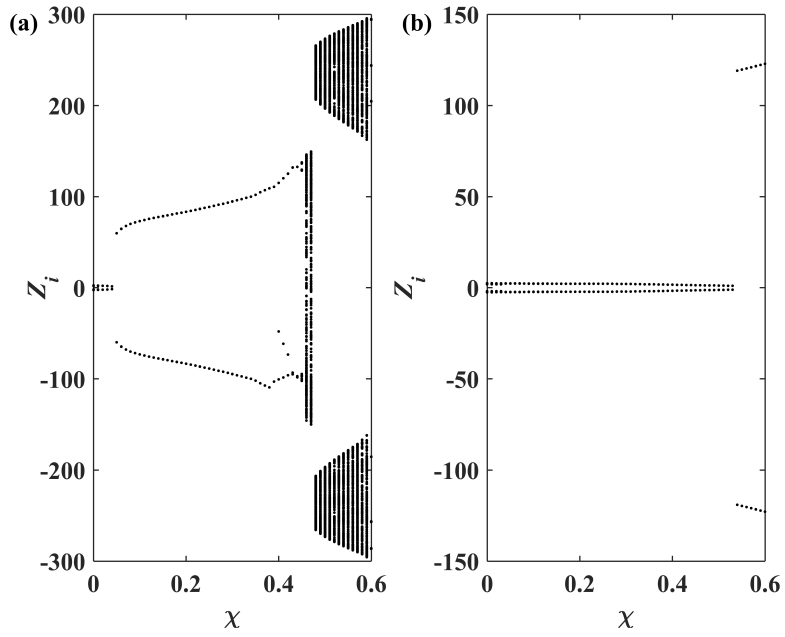

FIGURE 34 – Bifurcation diagrams of the network of coupled beams (Eqs. (55)) depicting the local maxima of the displacement of the beam Z_i as function of the coupling parameter χ for : (a) $\beta = 1.24$ and (b) $\beta = 124.15$.

Now considering both the coupling coefficient χ and the time delay τ, we have numerically developed a stability chart which provides different domains of control parameters where the trajectories of indirectly coupled beams converge. In figure 35, we increase the coupling parameters with a step of 10^{-2} for the coupling parameter and 10^{-3} for the time delay in a fixed time interval, those that lead to unstable trajectories are saved and plotted. The parametric domain spanned both by the coupling coefficient and the time delay is partitioned by the unstable motion area depicted with the black colour and the stable motion area depicted with the white colour. We notice the appearance of a small island of

instability for very low values of the delay. On the other island of instability which is more broader, we observe that the increase of the delay enlarges the unstable area.

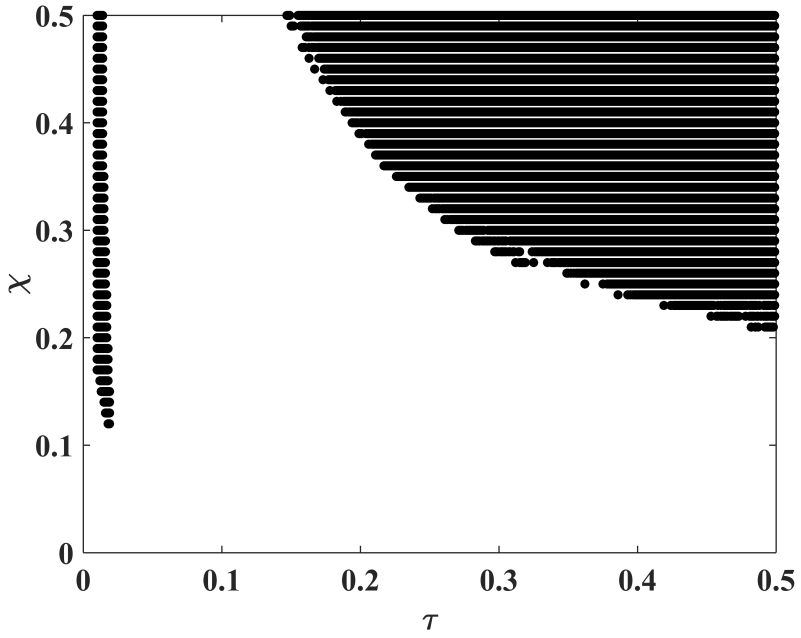

FIGURE 35 – Chart of stability in the $(\tau - \chi)$ parameter space. In the black region, the motion is unstable while in the white region there is stable dynamical motion.

b. On the synchronization and strong amplitude state

In order to characterize the collective behavior of the network of coupled beams and show the effect of the time delay on the strong amplitude reduction (SAR) state, we introduce the following approaches.

On one hand, the occurrence of the global synchronization in the overall system of coupled beams can be numerically investigated through the asymptotic time-average $\langle\sigma\rangle$ of the instantaneous standard deviations of the distributions of state variables related to the beams [50, 91], defined as

$$\langle\sigma\rangle = \frac{1}{T-\tau}\sum_{t=\tau}^{T}\sigma(t), \tag{65}$$

$$\sigma(t) = \left[\frac{1}{N} \sum_{i=1}^{N} \left(Z_i - \overline{Z} \right)^2 + \left(\dot{Z}_i - \overline{\dot{Z}} \right)^2 \right]^{1/2}, \tag{66}$$

where τ is the transient time, and the mean values are defined as

$$\overline{Z}(t) = \frac{1}{N} \sum_{i=1}^{N} Z_i(t), \tag{67}$$

$$\overline{\dot{Z}}(t) = \frac{1}{N} \sum_{i=1}^{N} \dot{Z}_i(t), \tag{68}$$

Global synchronization which describes a collective dynamic of the system of coupled beams, corresponds to the value $\langle \sigma \rangle = 0$. Numerically, we consider that synchronization state is obtained as $\langle \sigma \rangle < 10^{-7}$.

On the other hand, the strong amplitude reduction phenomenon is characterized with the time-average amplitude $\langle A \rangle$ of the displacement variables. $\langle A \rangle$ is calculated by the average difference between the global maximum and global minimum values of the time series of each beam of the system over a sufficient long time [118]. The average amplitude $\langle A \rangle$ is then written as,

$$\langle A \rangle = \frac{1}{N} \sum_{i=1}^{N} \left[\left\langle Z_{i,\max} \right\rangle - \left\langle Z_{i,\min} \right\rangle \right] \tag{69}$$

The case where $\langle A \rangle \sim 0$ is considered as strong amplitude reduction state. Thus, the average amplitude parameter can be useful to identify the coupling parameter regions for which the vibration control strategy is highly efficient.

Figure 36 shows the time-average standard deviation $\langle \sigma \rangle$ of a network of indirectly coupled beams as function of the coupling strength χ for different network-sizes and with a time-delay $\tau = 0.001$. It is found that the network of coupled beams remain in a synchronization state over the coupling parameter range for small values of network-size ($N \leq 15$). As the number of coupled beams is more increased ($N \geq 25$), the synchronization state is lost for large values of the coupling strength.

Furthermore, in figure 37, the variation of the average amplitude $\langle A \rangle$ of the network of

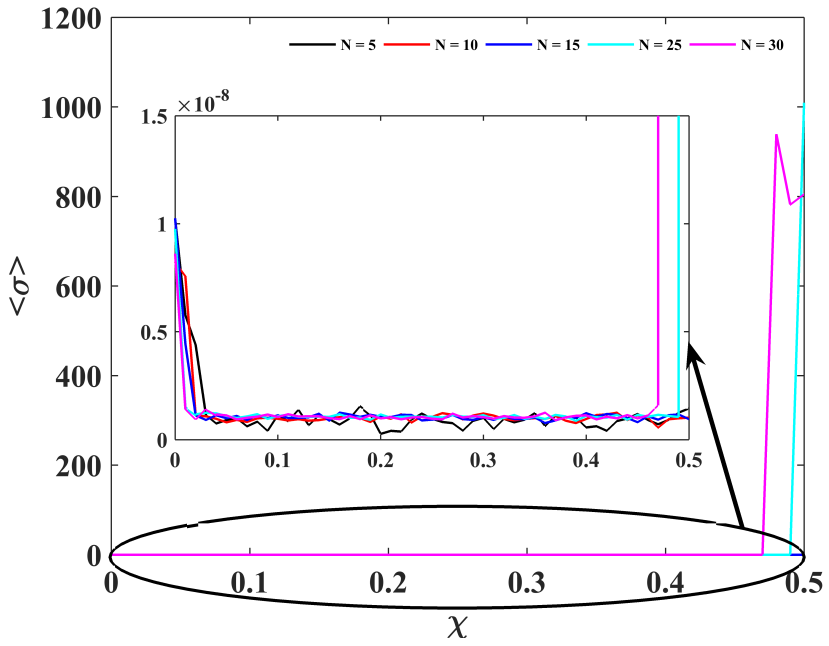

FIGURE 36 – Time-average standard deviation $\langle\sigma\rangle$ of a network of indirectly coupled beams, under the variation of the coupling strength χ, for network-sizes $N = 5, 10, 15, 25, 30$. With $\tau = 0.001$ and other parameters defined above.

coupled beams, with the coupling strength χ, for different network-sizes is investigated. For small values of the network-size ($N \leq 15$), first we observe that the vibration state of the global network of coupled structures increases for small values of the coupling strength. After a threshold value of the coupling parameter, a continuous vibration reduction is observed which leads to a strong amplitude reduction state for large values of the coupling strength. Amplitude reduction is more important when the number of coupled systems increases. When the number of coupled systems grows more ($N \geq 25$), we observe at first the same behavior as in the case of small network-sizes. But for large coupling values, the average amplitude of the system increases abruptly, which means that the system becomes unstable for these values of the coupling parameter. This finding coincides with that made in figure 36, reflecting the fact that the strong amplitude reduction state is only reached when the network of coupled beams is in a synchronization state.

A global representation of the synchronization state and the average amplitude can be obtained by scanning different values of the network-sizes, N and coupling strength, χ. The time-average standard deviation $\langle\sigma\rangle$ and the average amplitude $\langle A\rangle$ are evaluated for

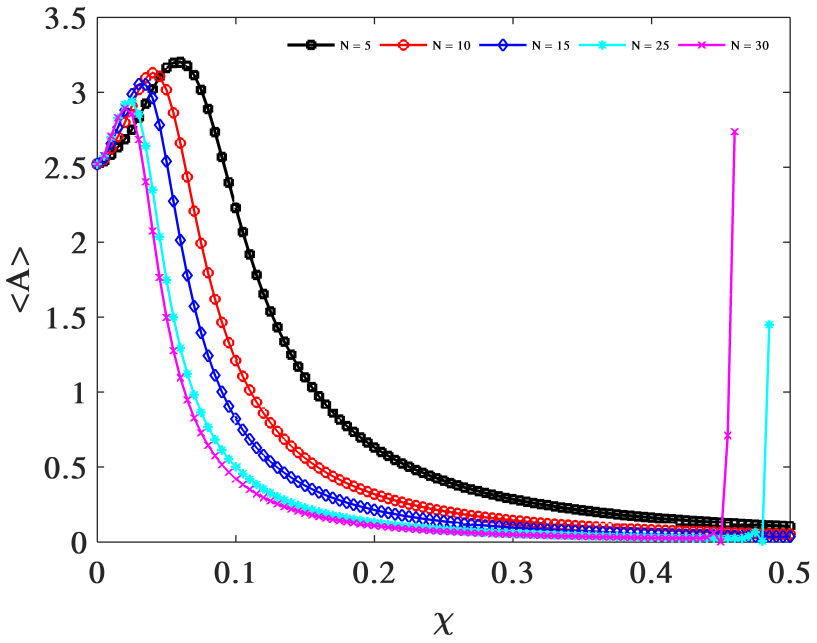

FIGURE 37 – Time-average amplitude $\langle A \rangle$ of a network of indirectly coupled beams, under the variation of the coupling strength χ, for network-sizes $N = 5, 10, 15, 25, 30$. With $\tau = 0.001$ and other parameters defined above.

different values of the time-delay. We note that these quantities are associated in each panel to the colour bars which represent the synchronization state and the global vibration state of the network of coupled beams, respectively. Figure 38 shows that the region of the global synchronization state of the network of coupled beams decreases with the increase of the delay and the number of coupled beams.

Figure 39 shows the variation of the average amplitude of the network with the increase of the delay. The dynamical states observed in figure 39 (a) and (b) coincide nearly with the synchronization state of the network of coupled beams showed in 38 (a) and (b). The strong amplitude reduction state is represented as a part of the region in blue colours and this state is followed by an abrupt increase of vibratory state in the overall network. For value of the time-delay $\tau = 0.1$, the strong amplitude reduction state is almost missed as showed in figure 39 (c). In this case, the large region of synchronization state observes in figure 38 (c) can be explained by the fact the beams are driven by the same external excitation.

Taking into account that in a real environment, the excitation force can fluctuate from one structure to another. Thus, it seems interesting to investigate the effects of time delay

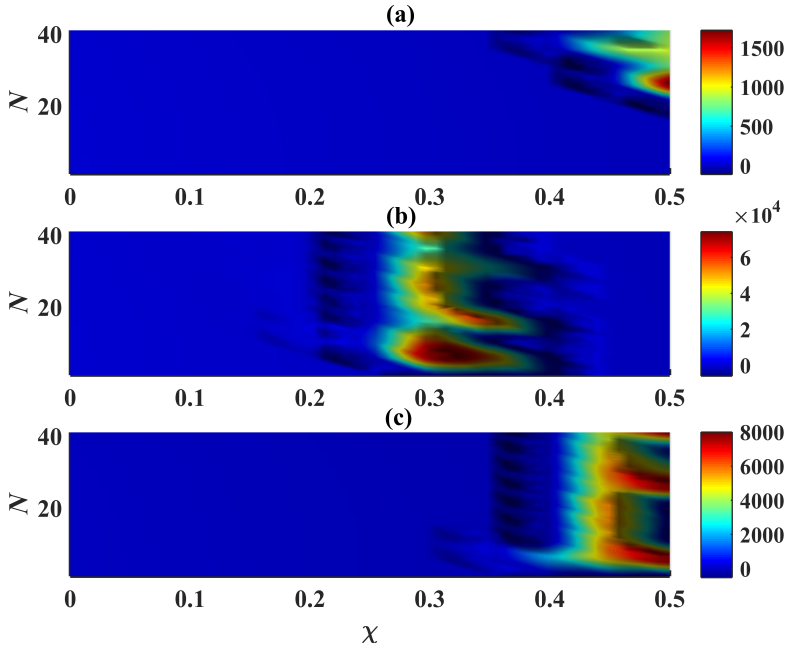

FIGURE 38 – The schematic phase diagram of the time-average standard deviation $\langle\sigma\rangle$ in parameter space (χ, N) for different values of the delay. (a) $\tau = 0.001$, (b) $\tau = 0.01$, (c) $\tau = 0.1$ and the other parameters are defined above.

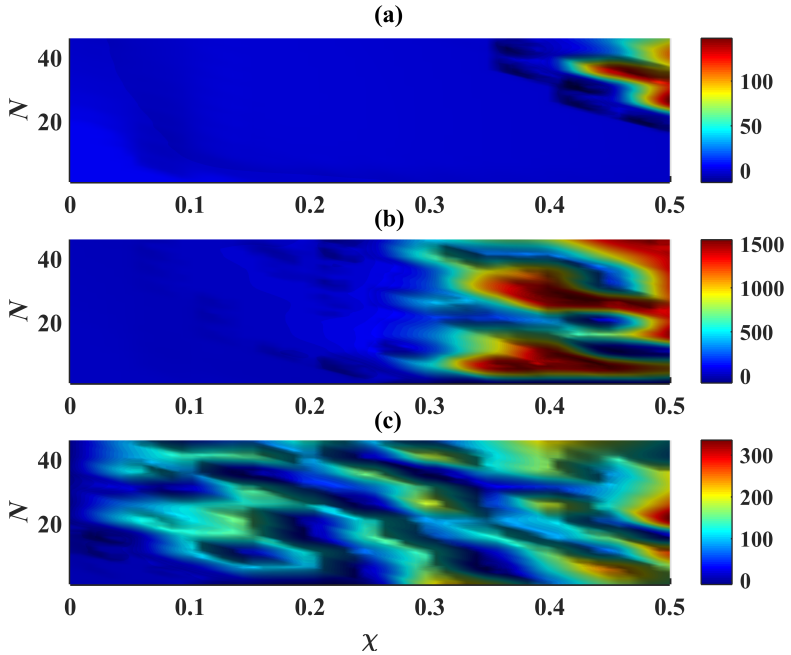

FIGURE 39 – The schematic phase diagram of the average amplitude of the network of coupled beams $\langle A\rangle$ in parameter space (χ, N) for different values of the delay. (a) $\tau = 0.001$, (b) $\tau = 0.01$, (c) $\tau = 0.1$ and the other parameters are defined above.

on a network of coupled beams excited by heterogeneous loads. The case where the beams are excited by external loads with the same amplitude and randomly distributed frequencies such as $\omega_i \in [0, 0.5)$ is investigated.

Figure 40 shows the effects of time delay both on the synchronization and the SAR state of a network of indirectly coupled beams, with randomly distributed external frequencies for different network-sizes and coupling strength. Both the case without delay and the with delay are considered. Thus, the network of coupled beams does not synchronized in the case without delay whereas a synchronization state appears on a certain range of coupling strength in the case with delay as shown in figure 40 (a) and (b), respectively. The strong amplitude reduction state is also lost on both cases as shown in figure 40 (c) and (d).

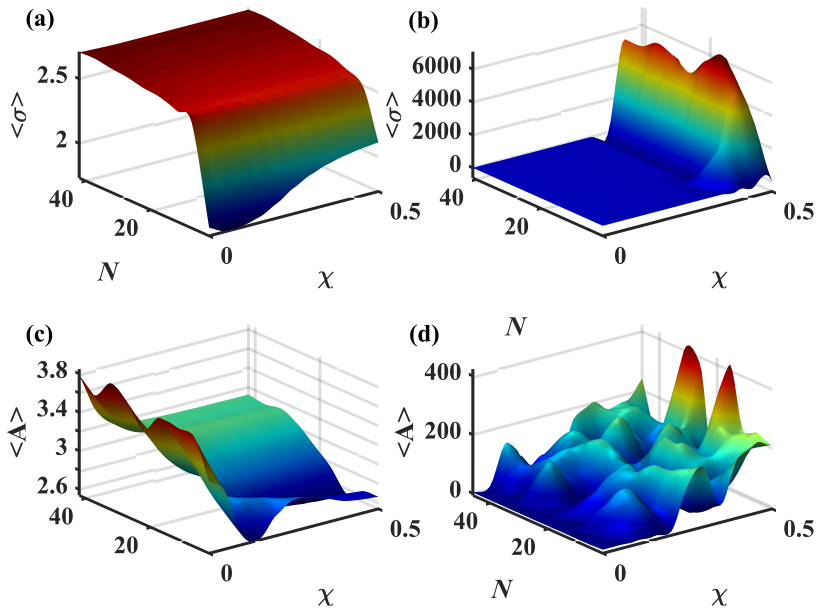

FIGURE 40 – The schematic phase diagram of the time-average standard deviation $\langle\sigma\rangle$ for (a) $\tau = 0.0$, (b) $\tau = 0.1$, and the average amplitude of the network of coupled beams $\langle A\rangle$ for (c) $\tau = 0.0$, (d) $\tau = 0.1$ in parameter space (χ, N). With $f_0 = 10.0$ and the other parameters defined above.

In order to confirm previous observations, some representative time series of the displacement Z_i of a network of $N = 10$ indirectly coupled beams are shown in figure 41 for the case without delay ($\tau = 0.0$) and the case with delay ($\tau = 0.1$). So, the network is in desynchronization state of the case without delay (figure 41 (a)) while a synchronization state

is observed for the case delay (figure 41 (b)). In the last case it can be seen that the presence of the delay in the system contributes to the suppression of the complex dynamics of the network and to a strong increase of the vibrations amplitude of the beams.

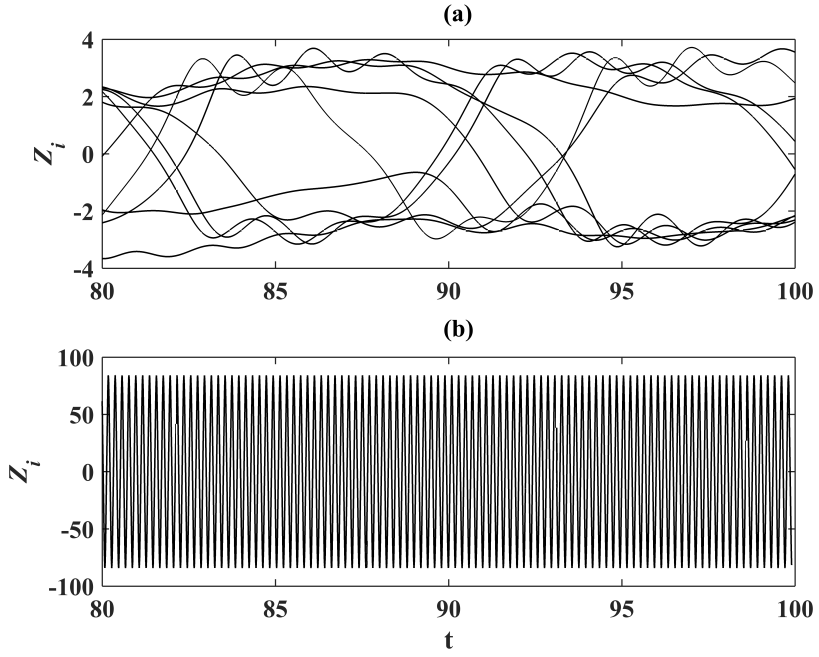

FIGURE 41 – Time series of a network of N coupled beams for (a) $\tau = 0.0$ and (b) $\tau = 0.1$. With $N = 10$, $\chi = 0.2$, $f_0 = 10.0$ and the other parameters defined above.

3.5 Conclusion

In this chapter, we have done a presentation and a discussion of the results from mathematical analysis and numerical simulations. We started by a mathematical modelling and the analysis of a strong amplitude reduction phenomenon taking into account two indirectly coupled Euler's beams through a dynamic environment. An extension of the number of coupled structures allowed to explore the occurrence of strong amplitude reduction phenomenon and synchronization on the network of indirectly coupled Euler's beams through a dynamic environment. At end, we have investigated the effect of the delay on a network of indirectly coupled Euler's beams through an electrical environment.

General conclusion

Through this thesis work, the issue was to analyze the dynamic behavior of a network of beams coupled indirectly through piezoelectric patches, in order to reduce the level of vibrations absorbed by these beams and thus reach the state of strong amplitude reduction. The essential results of this research may thus be useful at different levels of vibration control of mechanical and civil structures such as civil engineering, mechanical engineering, aeronautics, robotics, industry and others where the superstructure is generally constituted by an assembly of several structural elements (beams, plates, and so on).

Thus, in the first chapter of this thesis, we have presented a literature review of the key concepts explored throughout our work. An overview on the generalities concerning the vibrations and the effects induced by those vibrations mainly on human body and also on civil and mechanical structures. The different approaches used to control these vibrations were also presented as well as some limitations observed in each of them. Then, an introduction to the complex network dynamics has been done. Different network topologies have been highlighted and the rich dynamic phenomena exhibited by those network have been discussed, especially the synchronization state and amplitude death. The generalities on the time delay effect on a network of coupled systems have been also described. At end, the problem of this thesis has been stated.

In the second chapter, the mathematical formalisms and numerical methods used to solve the problem of this thesis have been described. A presentation of the Galerkin decomposition method used to transform a problem of the partial differential equations into a set of ordinary differential equations. As analytical method used to solve the nonlinear ordinary differential equations obtained, the harmonic balance method has been employed in order to investigate the amplitude of the harmonic oscillatory states. Taking into account

the effect of the time delay, stability for delayed nonlinear equations near their steady-state solutions or fixed points have been investigated through linear stability of delay differential equations and D-subdivision approach. The numerical procedure used was the fourth order Runge-Kutta method to approximate the solution of the system of ordinary differential equations and also for delay differential equations. Then, we have provided to the readers the tools that will be used for characterization of the dynamical and synchronization states of dynamical systems under consideration in this thesis. Whole mathematical models used to get different results of the thesis have been also presented.

The third chapter was devoted to the presentation and discussion about the results obtained from mathematical analysis and numerical simulations.

- Therefore at first, the analysis of a strong amplitude reduction phenomenon taking into account two indirectly coupled Euler's beams through a dynamic environment (constituted of piezoelectric patches shunted through a simple load resistance) was considered. Through the dimensionless equations of indirectly coupled beams, we have studied numerically the effect of the electromechanical coupling parameter on the amplitude response of both beams, it has been founded that as its strength increases the vibration amplitudes of both beams are considerably reduced. Taking into account this remark, we studied the global effect of the coupling parameter through the amplitude response curves and bifurcation diagrams, it has been found that the vibration amplitude of both beams are strongly reduced for a certain range of the coupling parameter. Using this approach to reduce vibrations on mechanical and civil structures allows to obtain a very low level of vibration amplitude around the fixed point of each structure reflecting a strong reduction amplitude state. The effect of others parameters of the system on the occurrence of strong amplitude reduction were also discussed. It has been shown that the load resistance also plays an important role in the strong dissipation of mechanical energy. As it allows a more or less rapid reduction of vibrations on the structures.
- An extension of the number of coupled structures allowed to explore the occurrence of strong amplitude reduction phenomenon and synchronization in the network. De-

pending on the network-size and the coupling strength, it has been found that the coupled beams exhibit different kinds of synchronization. Specifically, for small values of the load resistance, the state of global synchronization was found when the network-size was large ; whereas with increase in the load resistance, global synchronization takes place with smaller network-size. The occurrence of global synchronization, which was preceded by dynamical clustering. Furthermore, it has been found that the occurrence of strong amplitude reduction phenomenon in this system coincides with the global synchronization state of all beams ; meaning that all the beams attain very small amplitude in a synchronized way. The results further showed that the strong amplitude reduction state can be observed for relatively very weak coupling strength and large system-size.

– Finally, we have investigated the effect of the delay on a network of indirectly coupled Euler's beams through an electrical environment. The generation of the delay in a vibration control strategy can give birth to diverse rich dynamical states. An analytical analysis of stability of the overall system has been done and it has been shown that the increase of the time delay reduces the area of stable motion of the system. The vibratory state and the collective dynamics of the network coupled beams have been characterized using the average amplitude function and the time-average standard deviation. It has been shown that the variation of the time-delay affects both the synchronization state and the strong amplitude reduction of the network of coupled beams as the coupling strength and the number of coupled structures increase. It has been observed that the large values of the delay leads the suppression of the SAR state with the increase of the coupling parameter. Although, we have also shown that the delay could be beneficial to the synchronization state of coupled systems.

This thesis work has also opened interesting perspectives for future researches and the main ones are stated as follows :

– It will certainly be interesting at first to identify and study other configurations of control strategies of mechanical systems able to reach to the strong amplitude state, in which other types of coupling can be exploited as magnetic coupling, electrostatic

coupling or magnetoresistive coupling for example. This is to extend the field of application of the strong amplitude reduction control to the micro-electromechanical and nano-electromechanical systems.

– In a real world, the mechanical and civil structures are not submitted in general to deterministic excitations but rather stochastic ones. It will therefore be interesting to take into account the effect of noise on the appearance of the phenomenon of strong amplitude reduction on a network of coupled structures.
– Over the last decades, tremendous investigations have been done to provide a better understanding of the concept of fractional-order derivative and integral in various branches of science. So, we shall intend to show the effect of fractional-order derivative on the occurrence of the strong amplitude reduction and the synchronization phenomenon of a network of indirectly coupled beams.

Bibliographie

[1] Denys J Mead and DJ Meador. *Passive vibration control*. Wiley Chichester, 1998.

[2] Giancarlo Genta. *Vibration dynamics and control*. Springer, 2009.

[3] André Preumont. *Vibration control of active structures : an introduction*, volume 246. Springer, 2018.

[4] Jacob Pieter Den Hartog. *Mechanical vibrations*. Courier Corporation, 1985.

[5] SM Han, H Benaroya, T Wei. Dynamics of transversely vibrating beams using four engineering theories. *Journal of Sound and vibration*, 225(5) :935-988, 1999.

[6] Ali H Nayfeh and Dean T Mook. *Nonlinear oscillations*. John Wiley & Sons, 2008.

[7] Richard Evelyn Donohue Bishop. *Vibration*. CUP Archive, 1979.

[8] MR Svinkin. Minimizing construction vibration effects. *Practice periodical on structural design and construction*, 9(2) :108-115, 2004.

[9] M Abdel-Rohman, MJ John. Control of wind-induced nonlinear oscillations in suspension bridges using multiple semi-active tuned mass dampers. *Journal of Vibration and Control*, 12(9) :1011-1046, 2006.

[10] H Bachmann, WJ Ammann, F Deischl, JE isenmann, I Floegl, GH Hirsch, ... and H Nussbaumer. *Vibration problems in structures : practical guidelines*. Birkhäuser, 2012.

[11] David Wagg and SA Neild. *Nonlinear vibration with control*. Springer, 2016.

[12] L. A. ; Caughey T. K. ; Chassiakos A. G. ; Claus R. O. ; Masri S. F. ; Skelton R. E. ; Soong T. T. ; Spencer B. F. ; Yao J. T. P. Housner, G. W. ; Bergman. Structural control : Past, present, and future. *Journal of Engineering Mechanics*, 123, 09 1997.

[13] P Watts. On a method of reducing the rolling of ships at sea. *Transactions of the Institution of Naval Architects*, 24 :165–190, 1883.

[14] F Sakai, S Takaeda, and T Tamaki. Tuned liquid column dampers (tlcd) for cable-stayed bridges. In *Proc. Specialty Conf. Innovation in Cable-Stayed Bridges*, pages 197–205, 1991.

[15] KM Shum. Closed form optimal solution of a tuned liquid column damper for suppressing harmonic vibration of structures. *Engineering Structures*, 31(1) :84–92, 2009.

[16] Yasser Bigdeli and Dookie Kim. Damping effects of the passive control devices on structural vibration control : Tmd, tlc and tlcd for varying total masses. *KSCE Journal of Civil Engineering*, 20(1) :301–308, 2016.

[17] A Di Matteo, F Lo Iacono, G Navarra, and A Pirrotta. Direct evaluation of the equivalent linear damping for tlcd systems in random vibration for pre-design purposes. *International Journal of Non-Linear Mechanics*, 63 :19–30, 2014.

[18] H Frahm. Device for damping vibrations of bodies, 1909. US Patent US989,958.

[19] J Ormondroyd. The theory of the dynamic vibration absorber. *Trans., ASME, Applied Mechanics*, 50 :9–22, 1928.

[20] AA Nanha Djanan, BR Nana Nbendjo, and P Woafo. Electromechanical control of vibration on a plate submitted to a non-ideal excitation. *Mechanics Research Communications*, 54 :72–82, 2013.

[21] CA Kitio Kwuimy, BR Nana Nbendjo, and P Woafo. Optimization of electromechanical control of beam dynamics : Analytical method and finite differences simulation. *Journal of Sound and Vibration*, 298(1-2) :180–193, 2006.

[22] PR Nwagoum Tuwa and P Woafo. Electromechanical control of the dynamics of a thin elasticplate : Analytical method and finite differences simulation. *Mechanics Research Communications*, 61 :19–26, 2014.

[23] BR Nana Nbendjo. Amplitude control on hinged–hinged beam using piezoelectric absorber : Analytical and numerical explanation. *International Journal of Non-Linear Mechanics*, 44(6) :704–708, 2009.

[24] AA Nanha Djanan, BR Nana Nbendjo, and P Woafo. Control of vibration on a hinged-hinged beam under a non-ideal excitation using rlc circuit with variable capacitance. *Nonlinear Dynamics*, 63(3) :477–489, 2011.

[25] BP Ndemanou, J Metsebo, BR Nana Nbendjo, and P Woafo. Dynamics and magneto-rheological control of vibration of cantilever timoshenko beam under earthquake loads. *Nonlinear Dynamics*, 78(1) :163–171, 2014.

[26] GS Mbouna Ngueuteu, R Yamapi, and P Woafo. Effects of higher nonlinearity on the dynamics and synchronization of two coupled electromechanical devices. *Communications in Nonlinear Science and Numerical Simulation*, 13(7) :1213–1240, 2008.

[27] DO Tcheutchoua Fossi and P Woafo. Generation of complex phenomena in a simple electromechanical system using the feedback control. *Communications in Nonlinear Science and Numerical Simulation*, 18(1) :209–218, 2013.

[28] RL Harne and KW Wang. A review of the recent research on vibration energy harvesting via bistable systems. *Smart materials and structures*, 22(2) :023001, 2013.

[29] G Litak, MI Friswell, and S Adhikari. Magnetopiezoelastic energy harvesting driven by random excitations. *Applied Physics Letters*, 96(21) :214103, 2010.

[30] R Yamapi, FM Moukam Kakmeni, and JB Chabi Orou. Nonlinear dynamics and synchronization of coupled electromechanical systems with multiple functions. *Communications in Nonlinear Science and Numerical Simulation*, 12(4) :543–567, 2007.

[31] Vicky Y. Taffoti Yolong. *Dynamics of network of nonlinear electromechanical systems with rigid and flexible arms*. PhD thesis, University of Yaounde I, 2009.

[32] G. T. Oumbé Tékam, C. A. Kitio Kwuimy, and P. Woafo. Analysis of tristable energy harvesting system having fractional order viscoelastic material. *Chaos : An Interdisciplinary Journal of Nonlinear Science*, 25(1) :013112, 2015.

[33] Murielle Vanessa Tchakui and Paul Woafo. Dynamics of three unidirectionally coupled autonomous duffing oscillators and application to inchworm piezoelectric motors : Effects of the coupling coefficient and delay. *Chaos : An Interdisciplinary Journal of Nonlinear Science*, 26(11) :113108, 2016.

[34] Tobias Hemsel and Wallaschek Jörg. Survey of the present state of the art of piezoelectric linear motors. *Ultrasonics*, 38(1) :37 – 40, 2000.

[35] T. Bailey and J. E. Hubbard. Distributed piezoelectric-polymer active vibration control of a cantilever beam. *Journal of Guidance, Control, and Dynamics*, 8(5) :605–611, 1985.

[36] K. W. Morgan, R. A. ; Wang. An active-passive piezoelectric absorber for structural vibration control under harmonic excitations with time-varying frequency, part 1 : Algorithm development and analysis. *Journal of Vibration Acoustics Stress and Reliability in Design*, 124, 2002.

[37] K. W. Morgan, R. A. ; Wang. An active-passive piezoelectric absorber for structural vibration control under harmonic excitations with time-varying frequency, part 2 : Experimental validation and parametric study. *Journal of Vibration Acoustics Stress and Reliability in Design*, 124, 2002.

[38] G Caruso. A critical analysis of electric shunt circuits employed in piezoelectric passive vibration damping. *Smart materials and structures*, 10(5) :1059, 2001.

[39] Judith Lehnert. *Controlling Synchronization Patterns in Complex Networks*. PhD thesis, Technische Universität Berlin, 2015.

[40] S Boccaletti, V Latora, Y Moreno, M Chavez, and DU Hwang. Complex networks : structure and dynamics. *Physics Reports*, 424 :175, 2006.

[41] Arkady Pikovsky, Michael Rosenblum, and Jürgen Kurths. *Synchronization : a universal concept in nonlinear sciences*, volume 12. Cambridge university press, 2003.

[42] K. Kaneko. *Theory and applications of coupled map lattices*. Wiley, 1993.

[43] Edward Ott, Celso Grebogi, and James A Yorke. Controlling chaos. *Physical Review Letters*, 64 :1196, 1990.

[44] G. Osipov, J. Kurths, and Ch. Zhou. *Synchronization in Oscillatory Networks*. Springer Series in Synergetics. Springer, Berlin, 2007.

[45] U. E. Vincent, B. R. Nana Nbendjo, and P. V. E. McClintock. Collective dynamics of a network of ratchets coupled via a stochastic dynamical environment. *Physical Review E*, 87 :022913, Feb 2013.

[46] R. Gutiérrez, R. Sevilla-Escoboza, P. Piedrahita, C. Finke, U. Feudel, J. M. Buldú, G. Huerta-Cuellar, R. Jaimes-Reátegui, Y. Moreno, and S. Boccaletti. Generalized synchronization in relay systems with instantaneous coupling. *Physical Review E*, 88 :052908, Nov 2013.

[47] Erika Camacho, Richard Rand, and Howard Howland. Dynamics of two van der pol oscillators coupled via a bath. *International Journal of Solids and Structures*, 41(8) :2133 – 2143, 2004.

[48] AM Wickenheiser and E Garcia. Broadband vibration-based energy harvesting improvement through frequency up-conversion by magnetic excitation. *Smart Materials and Structures*, 19(6) :065020, 2010.

[49] V. Resmi, G. Ambika, and R. E. Amritkar. General mechanism for amplitude death in coupled systems. *Physical Review E*, 84 :046212, Oct 2011.

[50] C. Quintero-Quiroz and M.G. Cosenza. Collective behavior of chaotic oscillators with environmental coupling. *Chaos, Solitons & Fractals*, 71 :41 – 45, 2015.

[51] Amit Sharma, Pooja Rani Sharma, and Manish Dev Shrimali. Amplitude death in nonlinear oscillators with indirect coupling. *Physics Letters A*, 376(18) :1562 – 1566, 2012.

[52] Alex Arenas, Albert Díaz-Guilera, Jurgen Kurths, Yamir Moreno, and Changsong Zhou. Synchronization in complex networks. *Physics Reports*, 469(3) :93–153, 2008.

[53] T Kapitaniak and J Kurths. Synchronized pendula : From huygens' clocks to chimera states, 2014.

[54] A Chéagé Chamgoué, R Yamapi, and P Woafo. Dynamics of a biological system with time-delayed noise. *The European Physical Journal Plus*, 127(5) :59, 2012.

[55] Herve Germain Enjieu Kadji. Effects of a locally injected signal on phase synchronization in a network of self-excited cells. *The European Physical Journal B*, 86(4) :181, 2013.

[56] FM Moukam Kakmeni and VM Nguemaha. Enhancement of synchronization in inter–intra-connected neuronal networks. *Physics Letters A*, 380(1-2) :200–206, 2016.

[57] Louis M Pecora and Thomas L Carroll. Synchronization in chaotic systems. *Physical review letters*, 64(8) :821, 1990.

[58] Y Chembo Kouomou and P Woafo. Cluster synchronization in coupled chaotic semiconductor lasers and application to switching in chaos-secured communication networks. *Optics communications*, 223(4-6) :283–293, 2003.

[59] Adilson E Motter, Seth A Myers, Marian Anghel, and Takashi Nishikawa. Spontaneous synchrony in power-grid networks. *Nature Physics*, 9(3) :191, 2013.

[60] Eric Donald Dongmo and Paul Woafo. Effects of asymmetry, transmission delay and noises on the stability of an elementary electricity network. *The European Physical Journal B*, 88(7) :170, 2015.

[61] Takashi Nishikawa and Adilson E Motter. Comparative analysis of existing models for power-grid synchronization. *New Journal of Physics*, 17(1) :015012, 2015.

[62] K Fukui and S Nogi. Mode analytical study of cylindrical cavity power combiners. *IEEE transactions on microwave theory and techniques*, 34(9) :943–951, 1986.

[63] VY Taffoti Yolong and P Woafo. Synchronization in a ring of mutually coupled electromechanical devices. *Physica Scripta*, 74(5) :591, 2006.

[64] R Yamapi and P Woafo. Dynamics and synchronization of coupled self-sustained electromechanical devices. *Journal of Sound and Vibration*, 285(4-5) :1151–1170, 2005.

[65] R Yamapi and P Woafo. Dynamics and synchronization of coupled self-sustained electromechanical devices. *Journal of Sound and Vibration*, 285(4-5) :1151–1170, 2005.

[66] K Bar-Eli. Coupling of chemical oscillators. *The Journal of Physical Chemistry*, 88(16) :3616–3622, 1984.

[67] Haicheng Zhang, Daolin Xu, Chao Lu, Enrong Qi, Jiajun Hu, and Youshen Wu. Amplitude death of a multi-module floating airport. *Nonlinear Dynamics*, 79(4) :2385–2394, 2015.

[68] SY Xia, DL Xu, HC Zhang, ER Qi, JJ Hu, and YS Wu. On retaining a multi-module floating structure in an amplitude death state. *Ocean Engineering*, 121 :134–142, 2016.

[69] Aleš Tondl. *Quenching of self-excited vibrations.* Academia, Prague, 1991.

[70] KR Asfar. Quenching of self-excited vibrations. *ASME, Transactions, Journal of Vibration, Acoustics, Stress, and Reliability in Design*, 111 :130–133, 1989.

[71] Miguel A Barron, Isaias Hilerio, and Gabriel Plascencia. Numerical analysis of oscillation death in coupled self-excited elastic beams. *Advances in Mechanical Engineering*, 4 :746537, 2012.

[72] Ekkehard Ullner, Alexei Zaikin, Evgenii I Volkov, and Jordi García-Ojalvo. Multistability and clustering in a population of synthetic genetic oscillators via phase-repulsive cell-to-cell communication. *Physical Review Letters*, 99(14) :148103, 2007.

[73] Aneta Koseska, Evgenij Volkov, and Juergen Kurths. Detuning-dependent dominance of oscillation death in globally coupled synthetic genetic oscillators. *EPL (Europhysics Letters)*, 85(2) :28002, 2009.

[74] Min-Young Kim, Rajarshi Roy, Joan L Aron, Thomas W Carr, and Ira B Schwartz. Scaling behavior of laser population dynamics with time-delayed coupling : theory and experiment. *Physical Review Letters*, 94(8) :088101, 2005.

[75] Awadhesh Prasad, Ying-Cheng Lai, Athanasios Gavrielides, and Vassilios Kovanis. Amplitude modulation in a pair of time-delay coupled external-cavity semiconductor lasers. *Physics Letters A*, 318(1-2) :71–77, 2003.

[76] Donald G Aronson, G Bard Ermentrout, and Nancy Kopell. Amplitude response of coupled oscillators. *Physica D : Nonlinear Phenomena*, 41(3) :403–449, 1990.

[77] Renato E Mirollo and Steven H Strogatz. Synchronization of pulse-coupled biological oscillators. *SIAM Journal on Applied Mathematics*, 50(6) :1645–1662, 1990.

[78] G Bard Ermentrout. Oscillator death in populations of "all to all" coupled nonlinear oscillators. *Physica D : Nonlinear Phenomena*, 41(2) :219–231, 1990.

[79] DV Ramana Reddy, Abhijit Sen, and George L Johnston. Time delay induced death in coupled limit cycle oscillators. *Physical Review Letters*, 80(23) :5109, 1998.

[80] Rajat Karnatak, Ram Ramaswamy, and Awadhesh Prasad. Amplitude death in the absence of time delays in identical coupled oscillators. *Physical Review E*, 76(3) :035201, 2007.

[81] Keiji Konishi. Amplitude death induced by dynamic coupling. *Physical Review E*, 68(6) :067202, 2003.

[82] Awadhesh Prasad, Mukeshwar Dhamala, Bhim Mani Adhikari, and Ramakrishna Ramaswamy. Amplitude death in nonlinear oscillators with nonlinear coupling. *Physical Review E*, 81(2) :027201, 2010.

[83] Minoru Yoshimoto, Kenichi Yoshikawa, and Yoshihito Mori. Coupling among three chemical oscillators : synchronization, phase death, and frustration. *Physical Review E*, 47(2) :864, 1993.

[84] Pooja Rani Sharma, Amit Sharma, Manish Dev Shrimali, and Awadhesh Prasad. Targeting fixed-point solutions in nonlinear oscillators through linear augmentation. *Physical Review E*, 83(6) :067201, 2011.

[85] Chen Hai-Ling and Yang Jun-Zhong. Transition to amplitude death in coupled system with small number of nonlinear oscillators. *Communications in Theoretical Physics*, 51(3) :460, 2009.

[86] DL Xu, HC Zhang, C Lu, ER Qi, C Tian, and YS Wu. Analytical criterion for amplitude death in nonautonomous systems with piecewise nonlinear coupling. *Physical Review E*, 89(4) :042906, 2014.

[87] AN Pisarchik. Oscillation death in coupled nonautonomous systems with parametrical modulation. *Physics Letters A*, 318(1-2) :65–70, 2003.

[88] Munehisa Sekikawa, Kuniyasu Shimizu, Naohiko Inaba, Hiroki Kita, Tetsuro Endo, Ken'ichi Fujimoto, Tetsuya Yoshinaga, and Kazuyuki Aihara. Sudden change from chaos to oscillation death in the bonhoeffer–van der pol oscillator under weak periodic perturbation. *Physical Review E*, 84 :056209, Nov 2011.

[89] René Yamapi. Dynamics of an electromechanical damping device with magnetic coupling. *Communications in Nonlinear Science and Numerical Simulation*, 11(8) :907–921, 2006.

[90] Weiqing Liu, Guibao Xiao, Yun Zhu, Meng Zhan, Jinghua Xiao, and Jürgen Kurths. Oscillator death induced by amplitude-dependent coupling in repulsively coupled oscillators. *Physical Review E*, 91(5) :052902, 2015.

[91] M. J. Palazzi and M. G. Cosenza. Amplitude death in coupled robust-chaos oscillators. *The European Physical Journal Special Topics*, 223 :2831–2836, December 2014.

[92] Paul C. Matthews and Steven H. Strogatz. Phase diagram for the collective behavior of limit-cycle oscillators. *Physical Review Letters*, 65 :1701–1704, Oct 1990.

[93] Zhonghuai Hou and Houwen Xin. Oscillator death on small-world networks. *Physical Review E*, 68 :055103, Nov 2003.

[94] Keiji Konishi. Amplitude death in oscillators coupled by a one-way ring time-delay connection. *Physical Review E*, 70 :066201, Dec 2004.

[95] Weiqing Liu, Xingang Wang, Shuguang Guan, and Choy-Heng Lai. Transition to amplitude death in scale-free networks. *New Journal of Physics*, 11(9) :093016, 2009.

[96] Fatihcan M Atay. *Complex time-delay systems : theory and applications*. Springer, 2010.

[97] C Jeevarathinam, S Rajasekar, and MAF Sanjuan. Effect of multiple time-delay on vibrational resonance. *Chaos : An Interdisciplinary Journal of Nonlinear Science*, 23(1) :013136, 2013.

[98] Rafal Rusinek, Andrzej Weremczuk, Krzysztof Kecik, and Jerzy Warminski. Dynamics of a time delayed duffing oscillator. *International Journal of Non-Linear Mechanics*, 65 :98–106, 2014.

[99] MV Tchakui, VY Taffoti Fondjo, and P Woafo. Bifurcation structures in three unidirectionally coupled electromechanical systems with no external signal and with regenerative process. *Nonlinear Dynamics*, 84(4) :1961–1972, 2016.

[100] Gautam C Sethia, Abhijit Sen, and Fatihcan M Atay. Clustered chimera states in delay-coupled oscillator systems. *Physical Review Letters*, 100(14) :144102, 2008.

[101] BR Nana Nbendjo and P Woafo. Active control with delay of horseshoes chaos using piezoelectric absorber on a buckled beam under parametric excitation. *Chaos, Solitons & Fractals*, 32(1) :73–79, 2007.

[102] L. Zhang, C. Y. Yang, M. J. Chajes, and A. H. D. Cheng. Stability of active tendon structural control with time delay. *Journal of Engineering Mechanics*, 119(5) :1017–1024, 1993.

[103] Angelo Luongo, Daniele,Zulli. Parametric,external and self-excitation of a tower under turbulent wind flow. *Journal of Sound and Vibration*, 330 :3057–3069, 2011.

[104] Jon Juel Thomsen. *Vibrations and stability : advanced theory, analysis, and tools*. Springer Science & Business Media, 2013.

[105] SP Timoshenko, DH Young, and W Weaver. Vibrations in engineering. *Mashinostroenie, Moscow*, 1967.

[106] Chihiro Hayashi. *Forced oscillations in nonlinear systems*. 1953.

[107] Wim Michiels and Silviu-Iulian Niculescu. *Stability and stabilization of time-delay systems : an eigenvalue-based approach*. SIAM, 2007.

[108] Franck Jedrzejewski. Valeurs et vecteurs propres. *Introduction aux méthodes numériques*, pages 129–140, 2005.

[109] William H Press, Saul A Teukolsky, William T Vetterling, and Brian P Flannery. Numerical recipes in c++. *The art of scientific computing*, 2 :1002, 1992.

[110] Steven H Strogatz. *Nonlinear dynamics and chaos : with applications to physics, biology, chemistry, and engineering*. CRC Press, 2018.

[111] Thomas Erneux. *Applied delay differential equations*, volume 3. Springer Science & Business Media, 2009.

[112] Alfredo Bellen and Marino Zennaro. *Numerical methods for delay differential equations*. Oxford university press, 2013.

[113] SC Mba Feulefack, BR Nana Nbendjo, UE Vincent, and P Woafo. Dynamical clustering, synchronization and strong amplitude reduction in a network of euler's beams coupled via a dynamic environment. *Nonlinear Dynamics*, 88(1) :455–464, 2017.

[114] Anders Nordenfelt, Alexandre Wagemakers, and Miguel A. F. Sanjuán. Frequency dispersion in the time-delayed kuramoto model. *Physical Review E*, 89 :032905, Mar 2014.

[115] Steven M. Kay. *Intuitive probability and random processes using MATLAB*. Springer, New York, 2006.

[116] PR Nwagoum Tuwa and P Woafo. Analysis of an electrostatically actuated microplate subject to proportional-derivative controllers. *Journal of Vibration and Control*, DOI : 1077546316674609, 2016.

[117] Vladimir Borisovich Kolmanovskii and Valerij Romanovič Nosov. *Stability of functional differential equations*, volume 180. Elsevier, 1986.

[118] Umesh Kumar Verma, Neeraj Kumar Kamal, and Manish Dev Shrimali. Co-existence of in-phase oscillations and oscillation death in environmentally coupled limit cycle oscillators. *Chaos, Solitons & Fractals*, 110 :55 – 63, 2018.

List of Publications

1. **S.C. Mba Feulefack**, B.R. Nana Nbendjo, U.E. Vincent, P. Woafo. Dynamical clustering, synchronization and strong amplitude reduction in a network of Euler's beams coupled via a dynamic environment. *Nonlinear Dynamics*, 88(1) :455-464, 2017.

Nonlinear Dyn
DOI 10.1007/s11071-016-3252-9

ORIGINAL PAPER

Dynamical clustering, synchronization and strong amplitude reduction in a network of Euler's beams coupled via a dynamic environment

S. C. Mba Feulefack · B. R. Nana Nbendjo · U. E. Vincent · P. Woafo

Received: 6 April 2016 / Accepted: 24 November 2016

Abstract In this paper, strong amplitude reduction (SAR) phenomenon is reported in a network of Euler's beams indirectly coupled via an electrical circuit consisting of piezoelectric patches. SAR phenomenon appears in this system when global synchronization of all beams takes place. The occurrence of global synchronization, which was preceded by dynamical clustering, is dependent on the size of the network as well as on the load resistance of the electrical circuit which indirectly interacts with all the beams. The results further show that the SAR state can be observed for relatively very weak coupling strength and large system-size.

Keywords Strong amplitude reduction · Synchronization state · Network · Euler's beams

S. C. Mba Feulefack · B. R. Nana Nbendjo (✉) · P. Woafo
Laboratory of Modelling and Simulation in Engineering, Biomimetics and Prototypes and TWAS Research Unit, Faculty of Sciences, University of Yaounde I, PO Box 812, Yaoundé, Cameroon
e-mail: nananbendjo@yahoo.com

U. E. Vincent
Department of Physical Sciences, Redeemer's University, Ede, Nigeria

U. E. Vincent
Department of Physics, Lancaster University, Lancaster LA1 4YB, UK

1 Introduction

Most systems in the nature exhibit very complex dynamics, owing to the fact they could be regarded as many subsystems interacting with each other. The collective dynamical behaviours of such interacting or coupled nonlinear systems have attracted great attention of researchers from various scientific fields such as: physics; chemistry; biology and social sciences. The interaction between the subsystems may exhibit rich forms of emergent phenomena such as: synchronization; hysteresis; phase locking; riddling; and oscillation quenching [1–3]. Recently, quenching of dynamics has been widely studied in many theoretical and experimental models due to its relevance in many real-world applications such as: chemical reactions; biological oscillators; coupled laser systems; relativistic magnetron; and synthetic genetic networks [4]. Quenching phenomenon refers to the suppression of oscillation under various types of interaction or intentional control. There are two distinct types which are amplitude death (AD) and oscillation death (OD) [6]. In AD, coupled oscillators arrive at a common stable steady state. Although most research reports on quenching phenomenon in coupled systems have been mainly focused on the suppression of the dynamics of two interacting oscillators using different coupling processes [4,6], quenching of oscillations has been investigated in a large number of coupled robust-chaos oscillators [7], in which globally coupled systems exhibit amplitude

Published online: 07 December 2016

death beyond a threshold of the coupling parameter. Moreover, the introduction of heterogeneity in the local parameters of coupled oscillators could drive the system to oscillation death state, with coexisting clusters of oscillators in different steady states. In addition, quenching phenomenon in a variety of network topologies, such as global connection topology [8,9]; networks with complex topologies for instance small-world networks [10]; the ring topology [11]; and scale-free networks [12], had been investigated and reported. However, all these works have investigated quenching phenomena in self-oscillatory (autonomous) case, but recently researchers have introduced AD in non-autonomous coupled systems [3–5].

In this paper, we investigate the occurrence of strong amplitude reduction phenomenon and synchronization in a network of Euler's beams indirectly coupled through an external electrical circuit consisting of piezoelectric patches. Here, indirect coupling implies that the beams are not interacting with each other but with the piezoelectric patches, while the piezoelectric patches in turn influence the dynamics of each beam. This kind of scenario was considered in Refs. [13–16] from different perspectives. The control strategy presented by indirect coupling can be applied to the elements of beams of a skyscraper, when the whole structure is subjected to an environmental excitation such as the wind or an earthquake.

The rest of the paper is organized as follows: In Sect. 2, we describe the network of beams indirectly coupled via the piezoelectric patches and proceed with the modelling. In Sect. 3, we numerically analyse the modal equations and investigate the dynamics vis-a-vis the synchronization state, using the root-mean-square (rms) function and probability distribution of the vibratory state of beams in the network and also point out the condition for the appearance of strong amplitude reduction phenomenon. The work is then summarized in Sect. 4.

2 Model description of a network of coupled Euler's beams

2.1 Model description

Figure 1 shows a system of N number of hinged-hinged Euler's beams and the electrical circuit which is consisting of piezoelectric patches. The piezoelectric patches

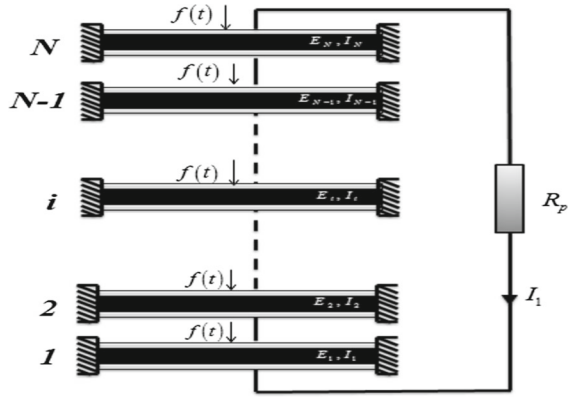

Fig. 1 Schematic of a network of N hinged-hinged beams indirectly coupled via piezoelectric patches

are laminated on both sides of each beam; they are all mounted together in parallel with a resistance load. In this coupling configuration, the electrical part is kept active by feedback from the vibrations of each beam and mutually, the state of electrical part influences or regulates the dynamics of each beam. This kind of coupling configuration is known in the literature as indirect coupling [13] or environmental coupling [14] or relay coupling [15] or bath coupling [16]. In this paper, we assume that in the network, the beams are identical Euler's beams with length l and excited by a common force of amplitude f_0 and frequency ω. The model equation of the network is then given by:

$$m\frac{\partial^2 w_i}{\partial t^2} + \delta\frac{\partial w_i}{\partial t} + EI\frac{\partial^4 w_i}{\partial x^4} - EA\left[\frac{1}{2l}\int_0^l \left(\frac{\partial w_i}{\partial x}\right)^2 dx\right]\frac{\partial^2 w_i}{\partial x^2} + \tilde{\alpha}v(t) = f_0\cos\omega t \tag{1a}$$

$$C_p\frac{dv}{dt} + \frac{v}{R_p} = -\tilde{\alpha}\sum_{i=1}^{N}\int_0^l \frac{\partial^3 w_i}{\partial x^2 \partial t} \tag{1b}$$

where in Eq. (1a), $w_i(t)$ represents transversal displacement of the beam i ($i = 1, 2, \ldots, N$) at time t; $v(t)$ is the voltage across the resistance load; $\tilde{\alpha}$ is the electromechanical coupling parameter, measuring the strength of the global coupling between piezoelectric patches and beams. m, E, I, and δ are the mass per unit length, Young's modulus, quadratic moment, and transversal damping coefficient of each beam, respectively. The equation of the electrical part can

be obtained applying Kirchhoff's laws to all the coupled piezoelectric patches; it is given by Eq. (1b), with $C_p = \sum_{i=1}^{N} c_{p_i}$ and R_p which are the resultant capacitance of the piezoelectric patches and load resistance, respectively. The capacitance of a unit pair of piezoelectric layers is defined by $c_{p_i} = 2\varepsilon_{33}^{S} bl/t_p$, where ε_{33}^{S} is the permittivity, t_p is the thickness of piezoelectric [17]. The term on the right-hand side of the electrical equation represents the influence of the motion of each beam on the electrical part, and mutually the resultant voltage $v\,(t)$ from this electrical part influences the dynamics of each beam.

2.2 Modal equations of the system

In order to proceed with numerical analysis of the system of Eqs. (1a) and (1b), we first introduce the following dimensionless variables:

$$W_i = \frac{w_i}{r};\ X = \frac{x}{l};\ \tau = \frac{t}{T};\ V = \frac{v}{V_0} \tag{2}$$

where $r = \sqrt{I/A}$ is the radius of gyration of the cross section A, T is a dimensionless time variable, and V_0 is a reference voltage. The value of T will be given later. It is convenient to transform the dimensionless partial differential equations into ordinary differential equations by using the Galerkin decomposition method [18]. According to the boundary conditions of a hinged-hinged beam defined by Eq. (3):

$$W_i|_{X=0,1} = 0 \text{ and } \left.\frac{\partial^2 W_i}{\partial X^2}\right|_{X=0,1} = 0, \tag{3}$$

the transversal displacement of the ith beam is defined as follows:

$$W_i\,(X,\tau) = \sum_n Z_{ni}\,(\tau)\,\Phi_n\,(X) \tag{4}$$

where $Z_{ni}\,(\tau)$ is the time-dependent function of the mode n for each beam i, and $\Phi_n\,(X) = \sin\,(n\pi X)$ is the shape function. After some mathematical manipulations, we obtain the following modal equations:

$$\frac{d^2 Z_{ni}}{d\tau^2} + \lambda\frac{dZ_{ni}}{d\tau} + Z_{ni} + \frac{1}{4}Z_{ni}^3 + \chi V = F_0\cos\,(\Omega\tau) \tag{5a}$$

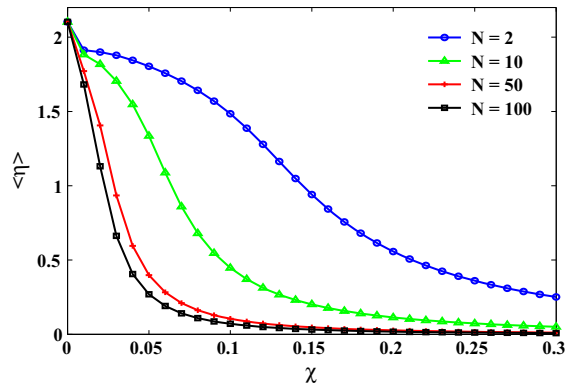

Fig. 2 Time-average of root-mean-square $\langle\eta(t)\rangle$ of a distribution of a network of beams as function of the coupling parameter χ, for network-sizes $N = 2,\ 10,\ 50,\ 100$. Other parameters are: $F_0 = 5.0$, $\Omega = 0.3$ and $R_p = 29.3\,\mathrm{k}\Omega$

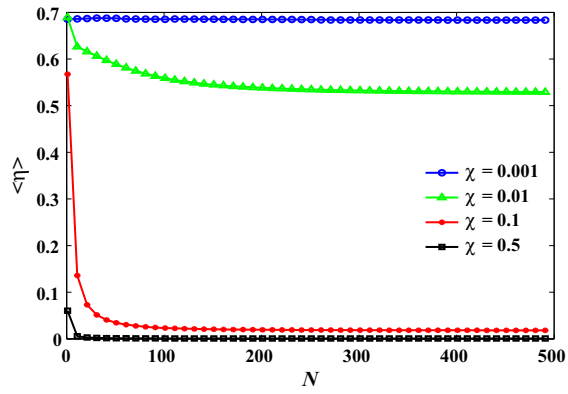

Fig. 3 Time-average of root-mean-square $\langle\eta(t)\rangle$ of a distribution of a network of beams as function of the number of interacting beams N, for coupling parameters $\chi = 0.001,\ 0.01,\ 0.1,\ 0.5$. Other parameters are defined in Fig. 2

$$\frac{dV}{d\tau} + \beta V = a\chi\sum_{i=1}^{N}\frac{dZ_{ni}}{d\tau} \tag{5b}$$

with

$$\lambda = \left(\frac{l}{n\pi}\right)^2\frac{\delta}{\sqrt{E\mathrm{Im}}};\ \chi = \frac{2\tilde{\alpha}V_0 l^4}{EIr(n\pi)^5}\left(1-(-1)^n\right);$$
$$F_0 = \frac{2f_0 l^4}{EIr(n\pi)^5}\left(1-(-1)^n\right)$$
$$T = \left(\frac{l}{n\pi}\right)^2\sqrt{\frac{m}{EI}};\ \Omega = \omega T;\ \beta = \frac{T}{R_p C_p};$$
$$a = \frac{EIr^2(n\pi)^6}{2C_p V_0^2 l^5} \tag{6}$$

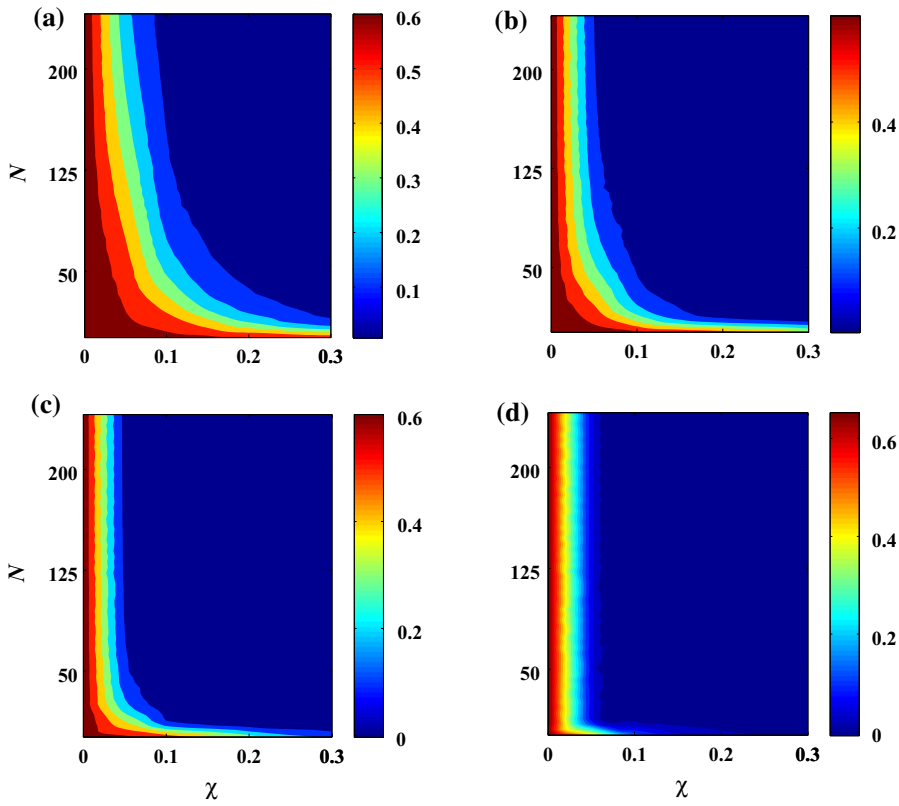

Fig. 4 2-D parameter plot of time-average root-mean-square $\langle \eta(t) \rangle$ as function of the number of interacting beams N and coupling parameter χ for load resistance values. **a** $R_p = 2.93\,\mathrm{k\Omega}$, **b** $R_p = 10.0\,\mathrm{k\Omega}$, **c** $R_p = 29.3\,\mathrm{k\Omega}$ and **d** $R_p = 293\,\mathrm{k\Omega}$. Other parameters are defined in Fig. 2

3 Dynamical analysis

In this section, by varying the number of beams as well as the coupling strength, we explore the system dynamics. In particular, we analyse the synchronization state and the appearance of strong amplitude reduction phenomenon in a network of beams indirectly coupled through a dynamic environment (electrical part). In our previous study, the occurrence of strong amplitude reduction phenomenon was found in a system of two indirectly coupled Euler's beams via an electromechanical system consisting of piezoelectric patches. We have numerically integrated the high-dimensional nonlinear system of Eqs. (5a) and (5b), using the fourth-order Runge–Kutta scheme. In our numerical simulations, the parameters of the beam were as follows: length $l = 10\,\mathrm{m}$, the width $b = 0.05\,\mathrm{m}$, the height $h = 0.03\,\mathrm{m}$, the density of material $\rho = 7850\ \mathrm{kg\,m^{-3}}$, the Young's modulus $E = 2 \times 10^{11}\,\mathrm{N\,m^{-2}}$, the damping coefficient $\delta = 0.1\,\mathrm{N\,s\,m^{-1}}$, and the reference voltage $V_0 = 2\,\mathrm{V}$. In addition, the initial conditions for the displacement of each beam were randomly distributed with uniform probability on the interval $[-5, 5]$.

3.1 Synchronization state

Our aim here is to examine the synchronization state of the system of Eqs. (5a) and (5b) and to determine the range of parameters for which all the beams exhibit collective dynamics. The synchronization state is numerically characterized by the asymptotic time-average $\langle \eta(t) \rangle$ of the instantaneous root-mean-square function $\eta(t)$ of the distribution of displacements and velocities of the beams [19], given by:

$$\eta\,(t) = \left[\frac{1}{N} \sum_{i=1}^{N} \left(Z_i^2 + \dot{Z}_i^2 \right) \right]^{1/2} \qquad (i = 1, 2, \ldots, N). \tag{7}$$

Global synchronization of the whole system which describes the collective dynamics is attained when $\langle \eta(t) \rangle = 0$. Figure 2 shows the time-average root-mean-square $\langle \eta(t) \rangle$ as function of the coupling strength χ for all the beams interacting indirectly with an environment for different network-sizes. It is found that with the increase in the coupling strength and for

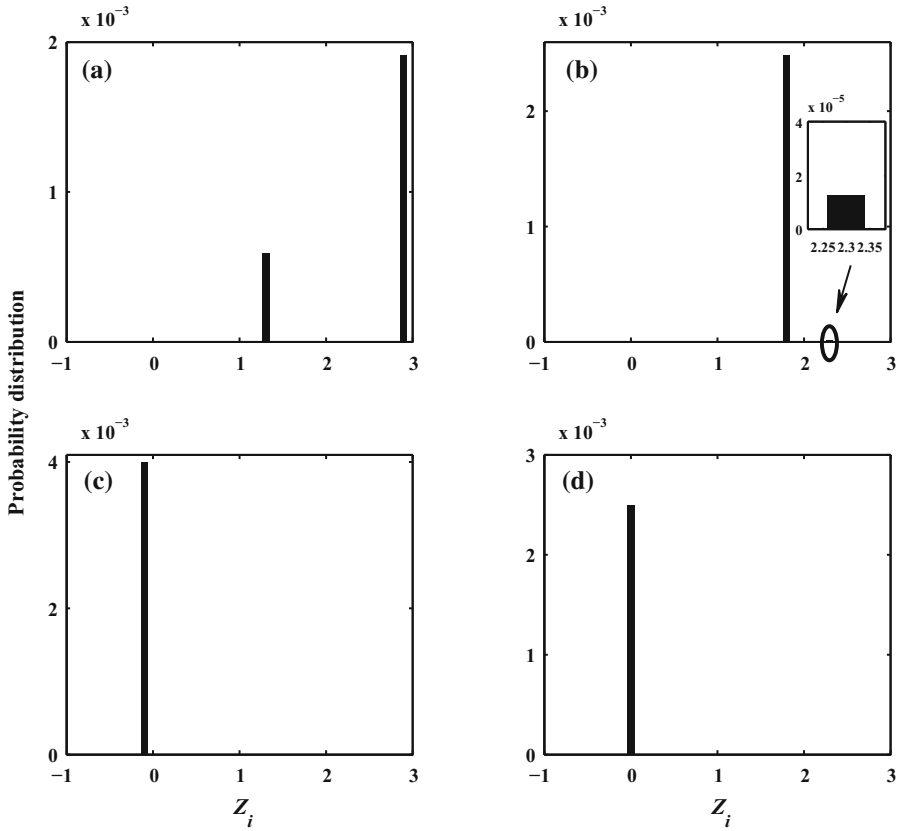

Fig. 5 Probability distribution of the displacement showing the transition to synchronization via dynamical clustering in the system for different coupling parameters at the dimensionless time $\tau = 8000$: **a** $\chi = 0.001$, **b** $\chi = 0.01$, **c** $\chi = 0.1$, **d** $\chi = 0.5$. The parameters used are defined in Fig. 2 and $N = 200$

$N = 2$, $\langle \eta(t) \rangle$ decreases slowly and the beams do not completely synchronize. For $N = 10$, $\langle \eta(t) \rangle$ decreases more rapidly but the beams do not globally synchronize. However, when $N \geq 50$, the curve presents an abrupt slope, with global network synchronization taking place for strong coupling strength.

Furthermore, for a given coupling parameter χ, $\langle \eta(t) \rangle$ is plotted as function of the network-size, N. This is illustrated in Fig. 3. In this case, the whole system does not synchronize when $\chi \leq 0.01$, whereas when the strength of the coupling parameter χ increases ($\chi \geq 0.1$), the system approaches global synchronization for large network-sizes.

A global view of the synchronization state can be obtained by scanning different values of the network-sizes, N and coupling parameter, χ. We calculate the time-average *rms* $\langle \eta(t) \rangle$ in the parameter space $N - \chi$, and we do this for different values of the load resistance R_p, which is an intrinsic damping of the environment. Note that $\langle \eta(t) \rangle$ is associated with the colour bar in the four panels showing different synchronization states. Figure 4 provides the variation of time-average *rms* $\langle \eta(t) \rangle$ from minimum (blue) to maximum (red) showing the effect of the environment on the global state of synchronization in the network. Blue colours indicate the regions where the whole system exhibits global synchronization, while red colours denote the regions where the whole system is assumed to be de-synchronized. Elsewhere in the colour bars and halfway between the blue and red ones, the whole system is assumed to be either weakly synchronized or completely de-synchronized. As the load resistance increases, the de-synchronized and weak synchronized regions diminish while the synchronized ones increase from right to the left.

The synchronization feature of the network can be better understood by numerically computing the probability distribution function [20], defined in a subset by generating M realizations of X_i, and counting the number of observable outcomes in the interval and divide by M. This approach was recently employed by Palazzi and Cosenza [7]. Figure 5 shows the probability distribution of displacement Z_i for different coupling parameter with a network-size $N = 200$, at an asymp-

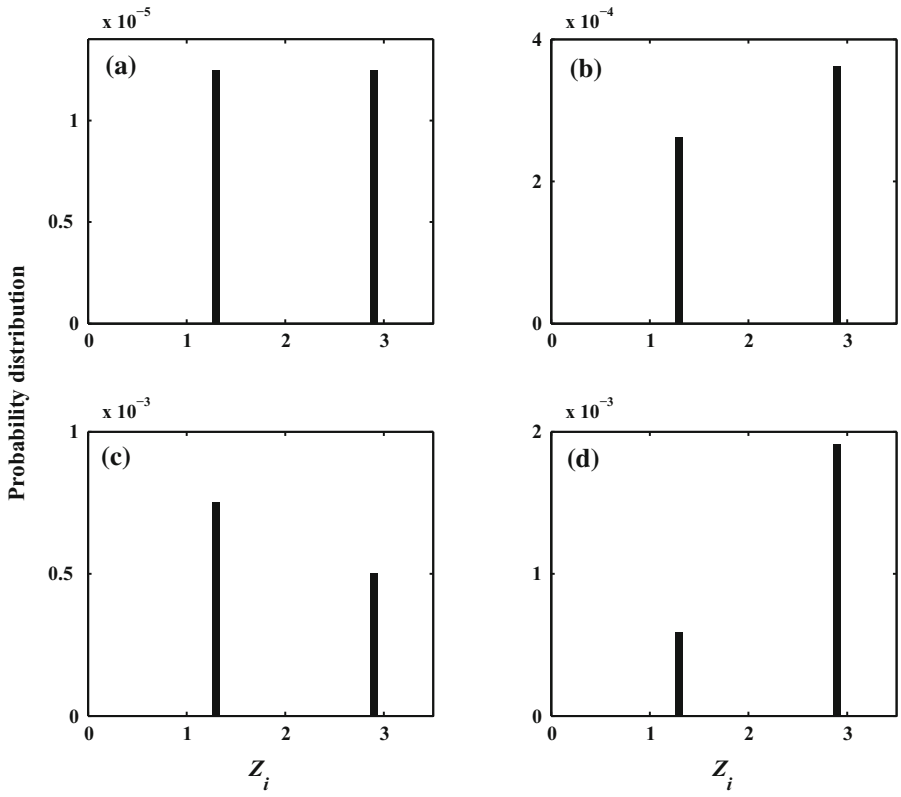

Fig. 6 Probability distribution of the displacement showing dynamical clustering in the system for different network-sizes at the dimensionless time $\tau = 8000$: **a** $N = 2$, **b** $N = 50$, **c** $N = 100$, **d** $N = 200$. The parameters used are defined in Fig. 2 and $\chi = 0.001$

totic dimensionless time, illustrating the synchronization state for different values of coupling strength. At weak coupling ($\chi \leq 0.01$), two clusters are formed as shown in Fig. 5a, b. This phenomenon described as dynamical clustering or cluster synchronization usually occurs when an ensemble of coupled oscillators splits into groups of synchronized elements [1,21]. In this system, the dynamical clustering has almost vanished for the coupling parameter ($\chi = 0.01$), and in Fig. 5c, d where the coupling parameter $\chi \geq 0.1$, we observe the complete disappearance of the dynamical clustering and the emergence of global synchronization.

Zooming on the weak coupling parameter regime ($\chi \leq 0.01$) where the formation of clusters is observed, we illustrate in Fig. 6 the probability distribution for a very weak coupling parameter ($\chi = 0.001$); wherein the clusters remain in existence for all values of network-size. For $N = 2$, the clusters are separated in two orbits, and the probability distribution are the same. However, by increasing the network-size, the two groups do not have the same size, showing that the beams vibrate in different states. In Fig. 7, we plot the probability distribution of displacement Z_i for different network-sizes and with fixed value of the coupling parameter ($\chi = 0.1$), and at an asymptotic dimensionless time. For any network-size, we observe a global synchronization in the system. The results of Figs. 5 and 6 agree with different synchronization regions obtained with time-average root-mean-square function in the parameter space $N - \chi$ in Fig. 4c.

3.2 Effect of the network-size on the amplitude–response curves

Furthermore, we observe that the increase in the network-size and the coupling parameter leads to the reduction in vibration amplitude in the system of global synchronized beams. Here, we further investigate the influence of network-size on the vibration amplitude of any beam in the system. By varying the frequency of the external excitation, we provide the frequency–response curves of the first beam for different network-sizes in Fig. 8. The curves show the resonance peaks, the subharmonic resonance, amplitude jump phenomenon for certain values of number of coupled beams N. They show that the amplitude of vibration of the first beam

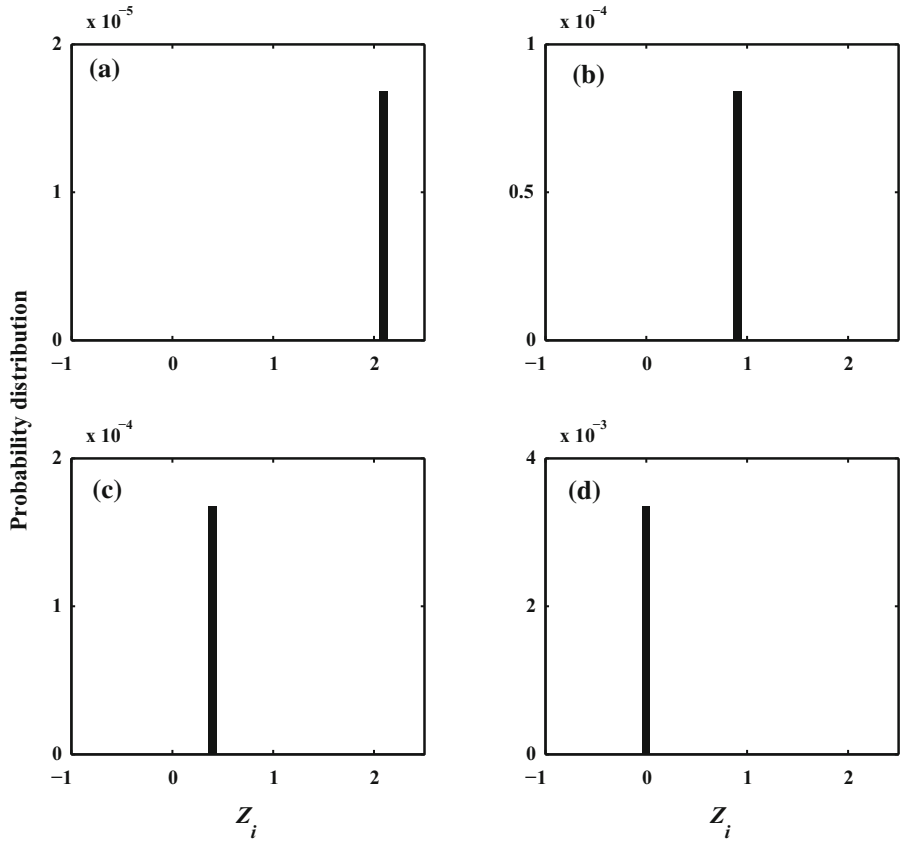

Fig. 7 Probability distribution of the displacement in the system for different network-sizes at the dimensionless time $\tau = 5950$: **a** $N = 1$, **b** $N = 5$, **c** $N = 10$, **d** $N = 200$. The parameters used are defined in Fig. 2 and $\chi = 0.1$

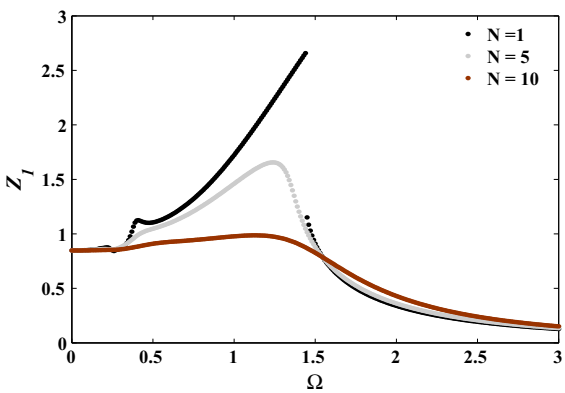

Fig. 8 Effects of the numbers of coupled beams on the amplitude–response curves for the first beam as function the frequency of the external excitation Ω. The parameters used are: $\chi = 0.02$, $F_0 = 1.0$ and $R_p = 29.3\,\mathrm{k}\Omega$

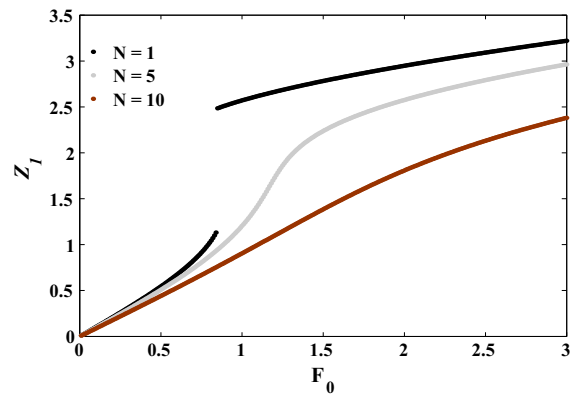

Fig. 9 Effects of the numbers of coupled beams on the amplitude–response curves for the first beam as function the amplitude of the external excitation F_0. The parameters used are: $\chi = 0.02$, $\Omega = 1.4$ and $R_p = 29.3\,\mathrm{k}\Omega$

decreases as the number of coupled beams increases. We also observe the disappearance of the sub-harmonic peak and the leakage of the amplitude jump with the increase in the number of coupled beams N in the network.

In Fig. 9, we plot the amplitude of vibration of the first beam as function of the amplitude of the external excitation for different values of number of coupled beams. For the case of two indirectly coupled beams, the amplitude–response curve presents a jump phe-

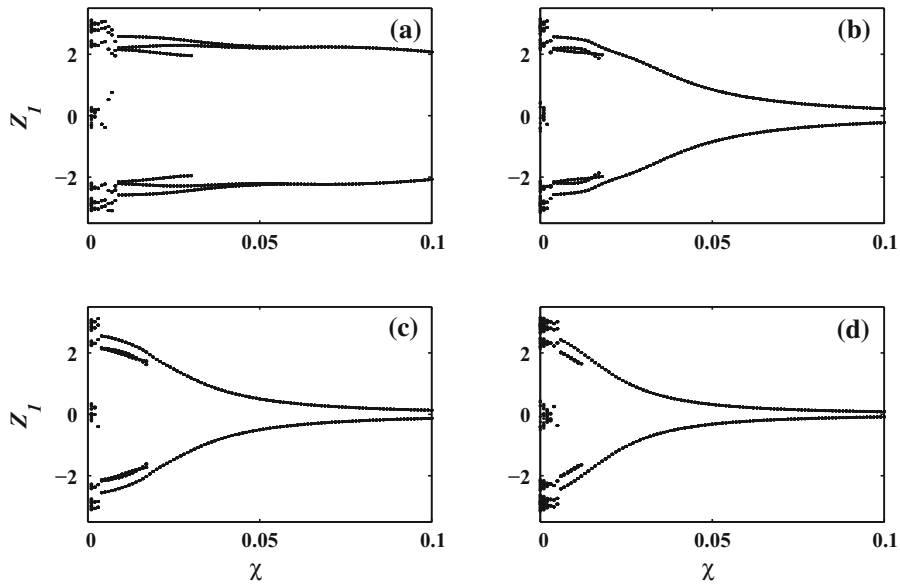

Fig. 10 Bifurcation diagram of the displacement of the first beam of the system as function of the coupling parameter χ, for $\Omega = 0.3$, $F_0 = 5.0$ and $R_p = 29.3\,\mathrm{k}\Omega$: **a** $N = 2$, **b** $N = 30$, **c** $N = 60$, **d** $N = 200$

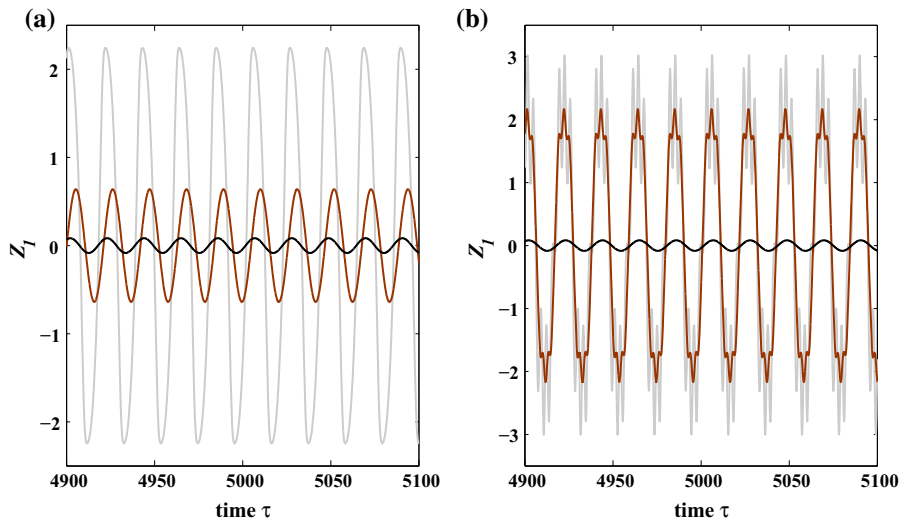

Fig. 11 Times series of the first beam for **a** different values of Euler's beams network-sizes, $\chi = 0.1$; **b** different values of the coupling parameter, $N = 200$. Other parameters are defined in Fig. 10

nomenon, which disappears with the increase in the number of coupled beams. Figures 8 and 9 permit to conclude that the jump phenomenon disappears and the amplitude of vibrations of the beams decreases considerably with an increase in the number of coupled beams.

3.3 Strong reduction in amplitude: effects of Euler's beams network-size

Figure 10 shows the bifurcation diagrams of the first beam as function of the electromechanical coupling parameter for different values of network-size. For a small network-size (Fig. 10a), the increase in the coupling parameter leads to the suppression of period—nT (n being an integer) oscillations, but we observe a very low decrease in vibration amplitude. By increasing the network-size (Fig. 10b–d), the areas of period−nT oscillations are more and more reduced, and we observe that vibration amplitude decreases gradually reaching to very small amplitude for large network-sizes (Fig. 10c, d). It is also found that the parameters space $N - \chi$ for which the strong reduction in amplitude phenomenon is achieved, corresponding to the parameters in the global synchronized domain (Fig. 4c). This

result shows that for a network of beams indirectly coupled through an electrical circuit with a weak coupling parameter, strong reduction in amplitude can be obtained by increasing the number of coupled systems.

To complete the picture, we present a further confirmation of SAR by plotting the time series of displacement of the first beam Z_1 in Fig. 11 as the network-size N increases. It is observed in Fig. 11a that, as the network-size increases, the amplitude of oscillations of the first beam decreases. For large network-size, the vibration amplitude of the first beam approaches very small values. In Fig. 11a, a phase shift is also observed as the network-size of Euler's beams increase. Figure 11b shows the time series for a fixed network-size of Euler's beams as the coupling parameter χ increases, in a suppression of period—nT oscillations—and the state of strong amplitude reduction is attained by increasing the coupling parameter.

4 Conclusion

We have examined the dynamics of a system of coupled hinged-hinged Euler's beams, indirectly interacting with an electrical circuit consisting of piezoelectric patches. Depending on the network-size and the coupling strength, it has been found that the coupled beams exhibit different kinds of synchronization. Specifically, for small values of the load resistance, the state of global synchronization was found when the network-size was large, whereas with increase in the load resistance, global synchronization takes place with smaller network-size. Furthermore, we found that the increase in the network-size leads to the decrease in vibration amplitude of the beam as well as the disappearance of the jump phenomenon and sub-harmonic resonance on the amplitude–response curve. Using the bifurcation diagram based on the vibration amplitude of displacement of the first beam, we have found that the increase in the number of coupled beams leads to the reduction in the regimes of period—nT oscillations and to the appearance of a strong amplitude reduction state. Indeed, this amplitude reduction state could be reached with relatively small values of the coupling strength, and this was observed as the network-size increases. The parameter space $N - \chi$ which corresponds to strong amplitude reduction state was found to coincide with those of the global synchronization state, meaning that all the beams attain very small amplitude in a synchronized way.

Acknowledgements UEV is supported by the Royal Society of London, through their Newton International Fellowship Alumni scheme. Part of this work was completed during a research visit of Dr. Nana Nbendjo at the University of Kassel in Germany. He is grateful to the Alexander von Humboldt Foundation for financial support within the Georg Forster Fellowship.

References

1. Pikovsky, A., Rosenblum, M., Kurths, J.: Synchronization: A Universal Concept in Nonlinear Sciences. Cambridge University Press, Cambridge (2001)
2. Kaneko, K.: Theory and Applications of Coupled Map Lattices. Wiley, New York (1993)
3. Zhang, H., Xu, D., Lu, C., Qi, E., Hu, J., Wu, Y.: Amplitude death of a multi-module floating airport. Nonlinear Dyn. **79**(4), 2385–2394 (2015)
4. Resmi, V., Ambika, G., Amritkar, R.E.: General mechanism for amplitude death in coupled systems. Phys. Rev. E **84**, 046212 (2011)
5. Pisarchik, A.N.: Oscillation death in coupled nonautonomous systems with parametrical modulation. Phys. Lett. A **318**(1), 65–70 (2003)
6. Liu, W., Xiao, G., Zhu, Y., Zhan, M., Xiao, J., Kurths, J.: Oscillator death induced by amplitude-dependent coupling in repulsively coupled oscillators. Phys. Rev. E **91**, 052902 (2015)
7. Palazzi, M.J., Cosenza, M.G.: Amplitude death in coupled robust-chaos oscillators. Eur. Phys. J. Spec. Top. **223**, 2831–2836 (2014)
8. Matthews, P.C., Strogatz, S.H.: Phase diagram for the collective behavior of limit-cycle oscillators. Phys. Rev. Lett. **65**, 1701–1704 (1990)
9. Ermentrout, G.: Oscillator death in populations of all to all coupled nonlinear oscillators. Phys. D Nonlinear Phenom. **41**, 219–231 (1990)
10. Hou, Z., Xin, H.: Oscillator death on small-world networks. Phys. Rev. E **68**, 055103 (2003)
11. Konishi, K.: Amplitude death in oscillators coupled by a one-way ring time-delay connection. Phys. Rev. E **70**, 066201 (2004)
12. Liu, W., Wang, X., Guan, S., Lai, C.H.: Transition to amplitude death in scale-free networks. New J. Phys. **11**(9), 093016 (2009)
13. Sharma, A., Sharma, P.R., Shrimali, M.D.: Amplitude death in nonlinear oscillators with indirect coupling. Phys. Lett. A **376**(18), 1562–1566 (2012)
14. Vincent, U.E., Nana Nbendjo, B.R., McClintock, P.V.E.: Collective dynamics of a network of ratchets coupled via a stochastic dynamical environment. Phys. Rev. E **87**, 022913 (2013)
15. Gutiérrez, R., Sevilla-Escoboza, R., Piedrahita, P., Finke, C., Feudel, U., Buldú, J.M., Huerta-Cuellar, G., Jaimes-Reátegui, R., Moreno, Y., Boccaletti, S.: Generalized synchronization in relay systems with instantaneous coupling. Phys. Rev. E **88**, 052908 (2013)

16. Camacho, E., Rand, R., Howland, H.: Dynamics of two van der Pol oscillators coupled via a bath. Int. J. Solids Struct. **41**(8), 2133–2143 (2004)
17. Wickenheiser, A.M., Garcia, E.: Broadband vibration-based energy harvesting improvement through frequency up-conversion by magnetic excitation. Smart Mater. Struct. **19**(6), 065020 (2010)
18. Nana Nbendjo, B.R.: Amplitude control on hinged-hinged beam using piezoelectric absorber: analytical and numerical explanation. Int. J. Non Linear Mech. **44**(6), 704–708 (2009)
19. Nordenfelt, A., Wagemakers, A., Sanjuán, M.A.F.: Frequency dispersion in the time-delayed Kuramoto model. Phys. Rev. E **89**, 032905 (2014)
20. Kay, S.M.: Intuitive Probability and Random Processes Using MATLAB. Springer, New York (2006)
21. Osipov, G., Kurths, J., Zhou, C.: Synchronization in Oscillatory Networks. Springer, Berlin (2007)